(2)

RESEARCH TRIANGLE INSTITUTE

RTI/5294/92-Quarterly

November 1992

HETEROEPITAXIAL DIAMOND GROWTH

Quarterly Report -- First Quarter
16 April 1992 - 30 June 1992

R. J. Markunas
R. A. Rudder
R. E. Thomas
J. B. Posthill
G. C. Hudson

STRATEGIC DEFENSE INITIATIVE ORGANIZATION
Innovative Science and Technology Office

Office of Naval Research
Program No.
N00014-92-C-0081

POST OFFICE BOX 12194 RESEARCH TRIANGLE PARK, NORTH CAROLINA 27709-2194

REPORT DOCUMENT PAGE

Form Approved
OMB No 0704-0188

1. AGENCY USE ONLY *(Leave blank)*	2. REPORT DATE	3. REPORT TYPE AND DATES COVERED
	November 1, 1992	Quarterly Report April 16, 1992 -- June 30, 1992

4. TITLE AND SUBTITLE

Heteroepitaxial Diamond Growth

5. FUNDING NUMBERS

N00014-92-C-0081

6. AUTHOR(S)

R. J. Markunas, R. A. Rudder, J. B. Posthill, R. E. Thomas, G. Hudson

7. PERFORMING ORGANIZATION NAME(S) AND ADDRESS(ES)

Research Triangle Institute
P. O. Box 12194
Research Triangle Park, NC 27709

8. PERFORMING ORGANIZATION REPORT NUMBER

83U-5294

9. SPONSORING/MONITORING AGENCY NAME(S) AND ADDRESSES(ES)

Office of Naval Research
800 N. Quincy Street
Arlington, VA 22217-5000

10. SPONSORING/MONITORING AGENCY REPORT NUMBER

11. SUPPLEMENTARY NOTES

12a. DISTRIBUTION/AVAILABILITY STATEMENT

Approved for public release; unlimited distribution

12b. DISTRIBUTION CODE

13. ABSTRACT

Work at Research Triangle Institute during this quarter concentrated on establishing directions and meaningful collaborations through which progress towards large-area, single-crystal diamond could be obtained. Three formal subcontracts with Jerry Whitten (NCSU), Max Swanson (UNC), and Robert Nemanich (NCSU) on the RTI prime have been established to pursue *ab initio* diamond surface kinetics, ion implantation studies, and atomic scale characterization of diamond respectively. The program here at RTI has adopted two approaches to pursue large-area, single crystal diamond:

1. heteroepitaxial diamond growth
2. diamond bonding, consolidation, and lift-off

These two approaches have dictated the experimented directions for the program. The formal collaboration with Jerry Whitten and informal collaborations with Michael Frenklach now add theoretical capability to the RTI diamond program.

14. SUBJECT TERMS

15. NUMBER OF PAGES

16. PRICE CODE

17. SECURITY CLASSIFICATION OF REPORT	18. SECURITY CLASSIFICATION OF THIS PAGE	19. SECURITY CLASSIFICATION OF ABSTRACT	20. LIMITATION OF ABSTRACT
UNCLASSIFIED	UNCLASSIFIED	UNCLASSIFIED	

TABLE OF CONTENTS

1.0 PROGRAM ACTIVITY

This period of the Research Triangle Institute diamond program while representing a new program start continues the development of diamond technologies at RTI which had been previously supported by SDIO/IST through ONR Contract N00014-86-C-0460. Along with the new program start, came new responsibilities for the diamond program at RTI. Besides support of work at RTI, the new contract included subcontracts to three university groups:

Jerry Whitten North Carolina State University,
Max Swanson University of North Carolina,
Bob Nemanich North Carolina State University.

Work with these three university groups was designed to be and has become highly interactive. Staff at Research Triangle Institute have held round-table discussions with each of the three groups to define specific goals and directions for the subcontracts that will allow their subcontractual work to impact the goals of the RTI prime contract in a timely fashion. As part of this process, new work statements were received from these groups which better reflect the direction of their work during the first year. A synopsis of those work statements is included in Section 2.0.

Besides highly formalized collaborative relations, RTI began to establish informal relationships with others in the country who are actively involved in diamond research. We sought to establish natural relationships which would permit complementary work between RTI and outside parties. Perhaps, the relationship (established during the last contractual period) which best typifies this informal, active collaboration is the relationship between RTI and Michael Frenklach at Penn State University. More about the nature of this relationship and the focus of this relationship is contained in section 3.0. Other activities at fostering scientific collaboration have included oral and poster presentations at the Diamond Gordon Conference in New Hampshire in June, personal

visitations by RTI staff to Linares Management Associates, Advanced Technology Materials, Raytheon, Lincoln Laboratories, Penn State University, and JPL. These activities at a minimum allowed fellow scientist in the diamond community to become intimately familiar with the technologies and capabilities available at RTI. In some instances, the visits by RTI personnel to these institutions were reciprocated.

Work during this quarter of the diamond program focused on the development of technologies for large-area, single-crystal diamond fabrication. The program undertook the evaluation of two approaches to achieve this goal:

1) heteroepitaxial diamond growth,
2) diamond bonding, consolidation, and liftoff.

Both these approaches have each required that a specific set of issues be addressed and that solutions be found.

Diamond heteroepitaxy has been addressed by collaborative work involving experimentation at RTI and by theoretical calculations outside RTI. Specifically, the subcontractual work with Jerry Whitten (NCSU) has provided new direction to Ni heteroepitaxy by expounding the role of subsurface C on the bond strengths of adatom species. This work suggests that heteroepitaxy on Ni must occur on surfaces which do not have subsurface carbon contamination. Rather, heteroepitaxy may be assisted if the subsurface contains electropositive elements such as H, Li, or Na. Keeping these elements near the surface and excluding C from the subsurface requires low temperature diamond deposition. Water-based diamond growth techniques invented during the last contractual period at RTI now permit extremely low temperature diamond growth (250 - 300°C). Another example of where low temperature processing would be indispensable would be for metastable carbides grown explicitly on the nickel (111) surface. Experimentally, we find that these carbides convert the surface from the hexagonal

structure to a cubic structure which may be more amenable to diamond nucleation. However, the cubic phase is only stable up to ≈ 300°C, which would require a low temperature process to preserve the cubic carbide and propagate the diamond. It is now clearly evident that water plays a pivotal role in low temperature diamond growth. Other workers have also enhanced low temperature diamond growth through addition of O_2 to the plasma gas. Both H_2O and O_2 undoubtedly provide elemental oxygen to the growth surface. RTI has devoted considerable effort to expound the role of oxygen on the diamond (100) surface. We have developed models for the role of oxygen on the diamond surface. These models have been formulated with considerable input and assistance from Michael Frenklach at Penn State University.

Besides the homoepitaxial approach to large-area single crystal diamond, we are developing techniques for diamond bonding, consolidation, and lift-off. Diamond bonding, consolidation, and liftoff represent a new programmatic effort. Development of these technologies has been a highly collaborative effort between the staff at UNC (Nalin Parikh and Max Swanson) and the staff at RTI. Experiments during this phase addressed ion implantation techniques for the separation of thin diamond layers from a parent crystal. Preliminary results appear to be very encouraging. C^+ and O^+ high energy implants (performed at Oak Ridge National Laboratory at no charge to the diamond program) have proven capable of creating a buried damage layer in diamond single crystals which can be separated by proper annealing. Details of that process are found in Section 4.0. This technology in conjunction with high-quality homoepitaxy could form the basis for large-area diamond electronics wherein the active devices are contained within each single crystal area.

2.0 FORMAL COLLABORATIONS

2.1 Dr. Jerry Whitten: North Carolina State University, School of Physical and Mathematical Sciences.

During this phase of the project Dr. Whitten has calculated the effect of subsurface interstitial atoms on the bonding of methyl radicals to a nickel (111) surface. The detailed results are contained in an attached copy of a recently published journal article, "Effects of subsurface Na, H and CH_3 adsorption on Ni (111)". Briefly, Dr. Whitten finds that both subsurface Na and H considerably enhance bonding of methyl radicals to the nickel surface. These two subsurface species also serve to maintain the methyl radicals in a configuration with more sp^3 like bonding. In contrast, subsurface C reduces the bond energy of methyl radicals to the nickel surface. For those radicals which do bond, the C-H bonds assume a more planar configuration, i.e., more sp^2 bonding. Work on ab initio calculations is expanding during this phase of the project to address the bonding of more complex hydrocarbons to the nickel surface.

2.2 Dr. Robert Nemanich: North Carolina State University, Department of Physics.

Work continues on the development of in situ atomic resolution STM and eventually AFM capability. The system is on site and currently undergoing testing and fitting to the UHV system. Once the capability for in situ analysis is brought online, STM studies of nucleation surface structures on Si structures will commence. Having STM in situ will allow complementary studies with Angle Resolved Ultraviolet Photoelectron Spectroscopy (ARUPS) to be performed. Detailed comparisons will then be performed on diamond growth surfaces using both hydrogen-based and water-based diamond deposition chemistries. Work is underway to compare surface structures of the

hydrogen terminated diamond (100) surface and the oxygen terminated diamond (100) surface using both STM and ARUPS. Dr. Nemanich continues to supply routine Raman analysis of samples for RTI.

2.3 Dr. Max Swanson: University of North Carolina, Department of Physics and Astronomy.

There are two major thrust areas in the work at UNC. Work continues, stimulated in part by the results of Dr. Whitten's group, on implants into candidate heteroepitaxial substrates for nucleation enhancement. For example, Na implants into Ni single crystals are being evaluated for heteroepitaxy. A variety of implanted species and substrates are currently under evaluation. The explicit purpose of these implants is to enhance diamond nucleation on surfaces which otherwise would not even nucleate diamond. The second area of research is devoted to the development of implant and annealing techniques for the separation of thin single crystal diamond sheets which could serve as templates for future homoepitaxy or which could be potentially used for discrete diamond devices. Section 4.0 highlights specifically the progress in diamond lift-off.

3.0 INFORMAL COLLABORATIONS

Recent experimental results at RTI involving oxygen interactions with diamond single crystals have prompted a continuation of the collaboration between the surface studies at RTI and the theoretical work by Michael Frenklach at Penn State. In a previous collaboration, Michael's calculations were invaluable in explaining results of hydrogen dosing of diamond surfaces. Experimental results indicated that the dimmer bond on the diamond 2x1 surface was very resistant to attack by atomic hydrogen. Calculations indicated that there was in fact a barrier of approximately 50 kcal/mole for the addition of a hydrogen atom to the dimmer bond.(Journal of Chemical Vapor Deposition, (1), 1 (1992)).

In contrast to hydrogen, we have found that oxygen has the ability to convert the 2x1 diamond surface back to the 1x1 configuration. This is potentially quite important in explaining one role oxygen might play in diamond growth. The 2x1 diamond surface is not thought to be a preferred configuration for subsequent carbon addition during the growth process. Oxygen may readily convert the 2x1 surface states to 1x1. In addition, we find that the 1x1 surface is stabilized by filling as little as 20% of the available surface sites with oxygen. The remaining sites are open and potentially available for carbon addition. Thermal desorption from oxygen covered surfaces indicates that the primary product from the surface is CO and that it is desorbed from the surface from a variety of sites with different bonding energies. Removal of a carbon atom from the (100) surface creates a "diradical" site. Addition of hydrocarbon species to diradical sites should be extremely easy.

Based on these current results, Penn State will be running a series of calculations to address a number of specific questions.

1. What are the possible bonding configurations for oxygen on the surface and what are the binding energies?

2. How does oxygen stabilize the 1x1 configuration on the (100) surface? What coverage of oxygen is required?

3. If possible, use molecular dynamics to simulate thermal desorption from different oxygenated sites on the diamond surface.

In other related work, informal collaborations are now underway between JPL and RTI. JPL is developing a variety of techniques for TEM diamond sample preparation. The goal of this collaboration is to develop techniques which will routinely and readily provide TEM analysis for diamond epitaxial films. RTI diamond films have been supplied to JPL during this program phase.

4.0 DIAMOND BONDING, CONSOLIDATION, AND LIFTOFF

Recent developments in ion implantation/lift-off at UNC and RTI allow us to propose a novel technique for the creation of a large-area diamond single crystal wherein small natural diamond crystals are overgrown for consolidation. From that parent substrate, ion-implantation lift-off will be used to duplicate the large-area template for subsequent substrate growth. Shown below is one possible fabrication process for the proposed large-area diamond crystal. The strategy for development of a large-area diamond crystal is to fabricate a template by consolidating individual crystals into a continuous crystal. *(Step 1)* Single crystals are bonded in close proximity to each other on a flat plate. (Details of the bonding are critical to this process and are considered RTI proprietary.) *(Step 2)* Epitaxial overgrowth consolidates the isolated crystals producing a large-area template. For proof-of-concept, two edge polished 2 × 2 mm type IA diamonds have been overgrown. Figure 2 shows the join-line between these crystals. In this experiment, the crystals were not perfectly coplanar. Figure 2 shows two regions where, with one crystal higher than the other, the overgrowth shows a stepped join-line. Figure 2 also shows a region where, with the crystals, originally at the same height, the overgrown solidified with no apparent join-line. *(Step 3)* Ion implantation creates a buried layer in the diamond crystal. *(Step 4)* The implanted layer is bonded to a flat plate prior to vacuum annealing. *(Step 5)* Vacuum annealing is used to chemically activate the O^+ implant, providing release. Coworkers at UNC have used ion implantation to define a buried O layer which upon simple vacuum anneal allows the top-most diamond layer to be released from the host crystal (patent disclosure forthcoming). Figure 3 shows SEM micrographs taken from a Type IA crystal following the 5 MeV O^+ implant and a 950°C vacuum anneal. The majority of the layer released after the 950 °C anneal. The micrograph shows platelets on the surface which did not release. Higher magnification shows that the base of these platelets as well as the surrounding diamond was etched by

the O^+ implant/anneal. It is evident that diamond layers can be separated from a parent crystal using a high energy O^+ implantation/anneal without using liquid or gaseous etchants to undercut the platelets. Technologically, this represents a major accomplishment. This accomplishment now allows one to lift thin epitaxial diamond films over large areas without having to chemically undercut the film. (In subsequent experiments, a diamond layer was deposited on the ion implanted surface prior to annealing. The researchers at UNC were able to release the entire 2×2 mm implanted area intact by annealing at ~ 600 °C). *(Step 6)* Subsequent homoepitaxial growth on the released template duplicates the original 4×4" template without the need to perform another tiling process.

There are a number of critical steps to the large-area substrate fabrication. As proof-of-concept, RTI and UNC have collaborated to demonstrate some of these critical steps. RTI in collaboration with UNC has demonstrated (1) CVD consolidation, (2) MeV ion implantation to define a chemically separable layer, and (3) severance of the top-most layer without chemical undercut by a gaseous or liquid etchant. Epitaxial growths on the implanted layers have been undertaken. SEM micrographs of diamond growth on an O^+ implanted/annealed platelet showed a highly mottled, morphology resembling one morphology produced from the consolidation experiment (Figure 2). Raman results from the consolidation experiment showed a small amorphous carbon component along with a dominant 1332 cm^{-1} line (FWHM 4.3 cm^{-1}). Previous homoepitaxial films deposited at RTI showed no amorphous component and FWHM's of < 3.0 cm^{-1}. We are confident that, given better water/alcohol ratios, successful epitaxial growth on the released layers is possible once the damage layer is chemically or mechanically removed.

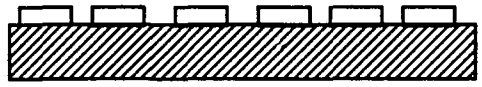

1. Bonding 10 X 10 mm single crystals to flat plate.

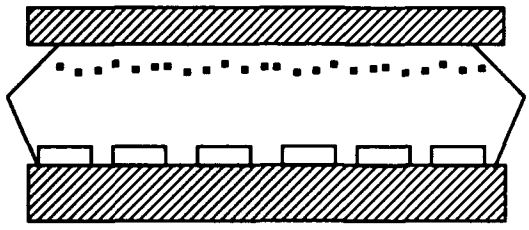

4. Bonding substrate for chemical separation.

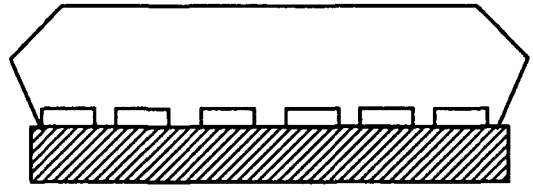

2. Epitaxial overgrowth to solidify crystals into a large area substrate.

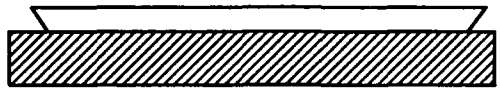

5. Vacuum anneal to release layer.

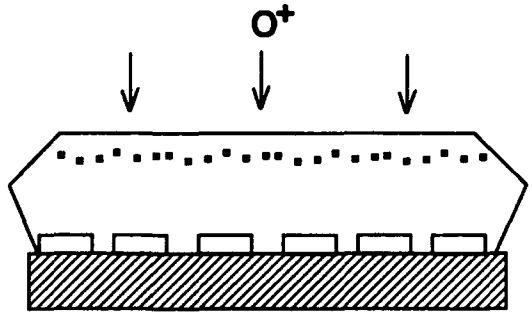

3. Ion implantation to define buried separable layer.

6. Subsequent homoepitaxy to duplicate the large area template.

Figure 1. Fabrication process for generation of large area tiled substrate.

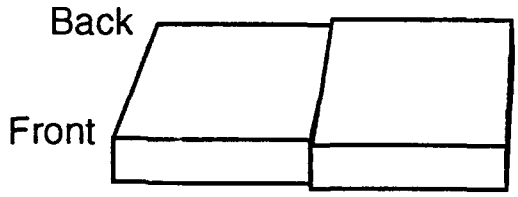

2x2 mm Edge-polished
Diamonds

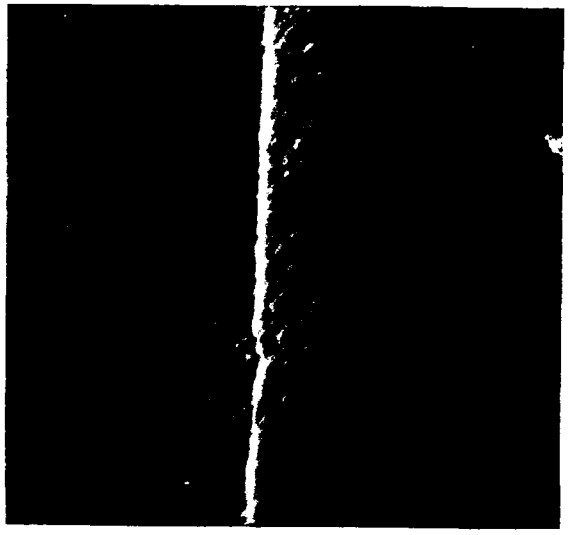

Back

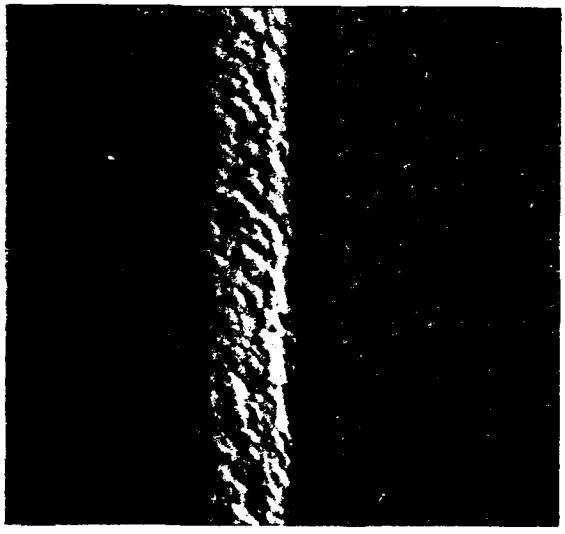

Front

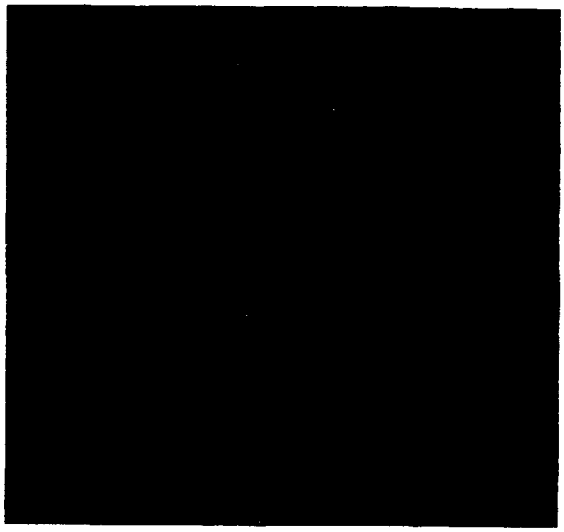

Middle

5.0 μm

SEM micrographs showing join-line between 2 diamond single crystals after CVD growth.

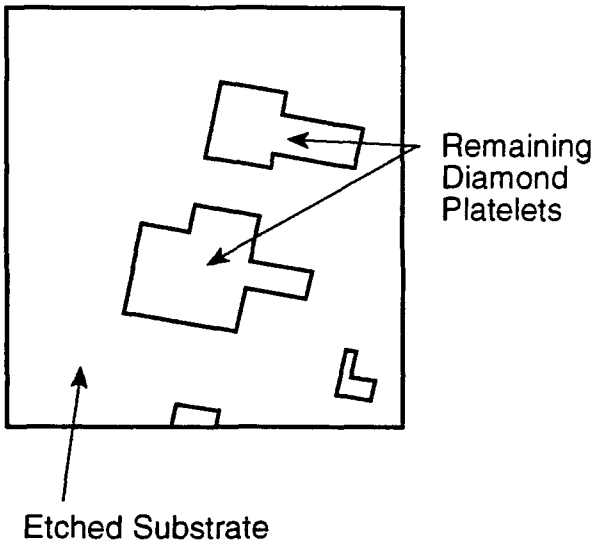
Remaining
Diamond
Platelets
Etched Substrate

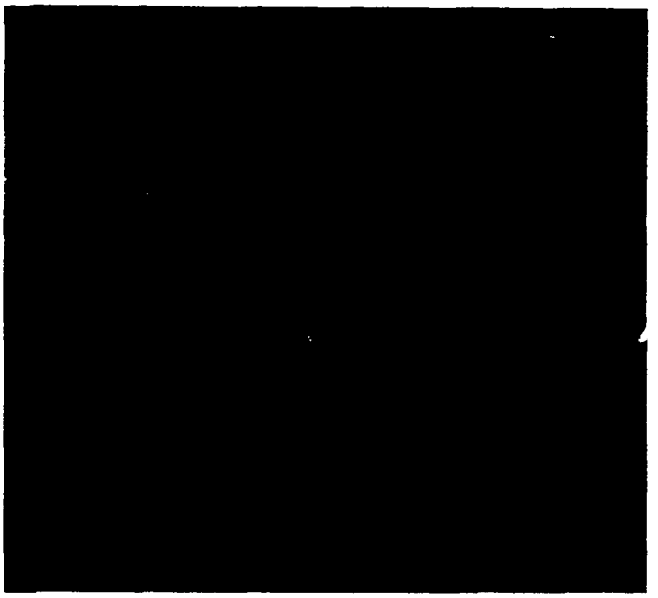
2.50 µm

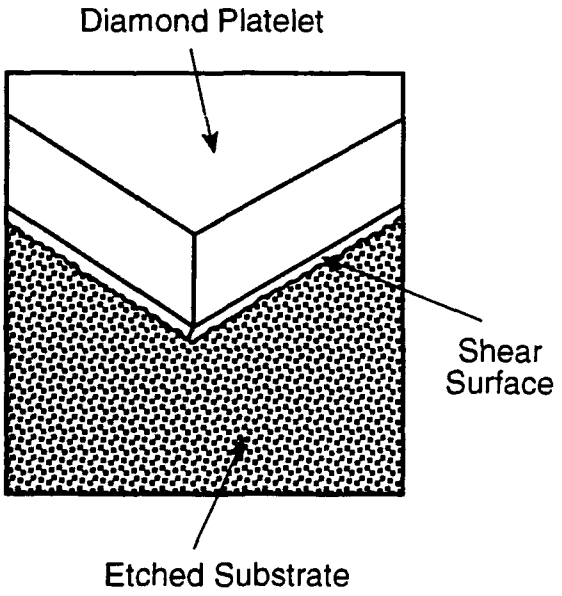
Diamond Platelet
Shear
Surface
Etched Substrate

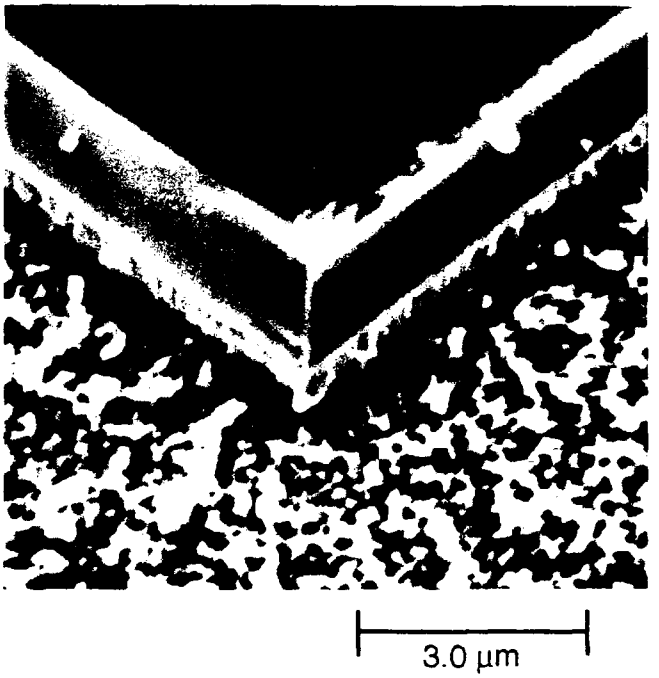
3.0 µm

5.0 PUBLICATIONS AND PRESENTATIONS

1. *Effects of Subsurface Na, H and C on CH_3 Adsorption on Ni(111)*, H. Yang, J.L. Whitten, R.E. Thomas, R.A. Rudder, and R.J. Markunas.

2. *Atomic Hydrogen Adsorption on the Reconstructed Diamond (100)-(2 × 1) Surface*, R.E. Thomas, R.A. Rudder, R.J. Markunas, D. Huang, and M. Frenklach.

3. *Chemical Vapor Deposition of Diamond Films from Water Vapor rf-Plasma Discharges*, R.A. Rudder, G.C. Hudson, J.B. Posthill, R.E. Thomas, R.C. Hendry, D.P. Malta, and R.J. Markunas.

4. *Chemical Vapor Deposition of Diamond Films Using Water:Alcohol:Organic-Acid Solutions*, R.A. Rudder, J.B. Posthill, G.C. Hudson, D.P. Malta, R.E. Thomas, R.J. Markunas, T.P. Humphreys, and R.J. Nemanich.

5. *Chemical Vapor Deposition of Diamond Films from Water-Vapor rf-Plasma Discharges*, R.A. Rudder.

6. *Thermal Desorption from Hydrogenated and Oxygenated Diamond (100) Surfaces*, R.E. Thomas, R.A. Rudder, and R.J. Markunas.

7. *Carbon and Oxygen Removal from Silicon (100) Surfaces by Remote Plasma Cleaning Techniques*, R.E. Thomas, M.J. Mantini, R.A. Rudder, D.P. Malta, S.V. Hattangady, and R.J. Markunas.

8. *Effect of Thin Interfacial SiO_2 on Metal Contacts to B Doped Diamond Films*, V. Venkatesan, K. Das, G.G. Fountain, R.A. Rudder, J.B. Posthill, and R.J. Markunas.

9. *Growth and Characterization of Heteroepitaxial Nickel Films on Diamond Substrates*, T.P. Humphreys, H. Jeon, R.J. Nemanich, J.B. Posthill, R.A. Rudder, D.P. Malta, G.C. Hudson, R.J. Markunas, J.D. Hunn, and N.R. Parikh.

10. *Cathodoluminescence from Diamond Films Grown by Plasma-Enhanced Chemical Vapor Deposition in Dilute CO/H_2, CF_4/H_2, and CH_4/H_2 Mixtures*, R.J. Graham, J.B. Posthill, R.A. Rudder, and R.J. Markunas.

Effects of Subsurface Na, H and C on CH_3 Adsorption on Ni(111)

Hong Yang and Jerry L. Whitten
Department of Chemistry
North Carolina State University
Raleigh, NC 27695-8204, USA

Raymond E. Thomas, Ronald A. Rudder and Robert J. Markunas
Research Triangle Institute,
Research Triangle Park, NC 27709-2194, USA

Abstract

Ab initio valence orbital configuration interaction calculations are used to study the energy effect of Na, H and C atom subsurface species on CH_3 chemisorption at a hollow 3-fold site on Ni(111). The lattice is modeled as an embedded three layer cluster of 41 atoms. Ni 3d orbitals are explicitly included on seven nickel atoms on the surface. The calculated chemisorption energies of pyramidal CH_3 on Ni(111) are 38 for the clean surface and 50, 47, and 17 kcal/mol for the Na, H, and C implants, respectively. The energies required to distort tetrahedral CH_3 into a planar structure are 22 kcal/mol on clean Ni(111), 30 kcal/mol with the Na implant, 24 kcal/mol with the H implant, and 12 kcal/mol with the C implant, respectively. Thus, Na below the surface may stabilize a carbon overlayer to a tetrahedral diamond structure. CH_3-surface distances, C-H stretching and surface-CH_3 vibrational frequencies are also reported.

I. INTRODUCTION

In the past decade, diamond film growth has received a great deal of attention not only due to the pure scientific interest in the low pressure formation of metastable diamond but also due to the many practical applications that exist for diamond films.[1-9] Despite the progress that has been made in developing a variety of techniques for diamond film formation, understanding the mechanisms for diamond formation is still a subject of current debate. Continued progress in diamond film technology will depend in particular on developing a better understanding of diamond heteronucleation and correspondingly heteroepitaxy. Heteroepitaxial growth of diamond on c-BN has been successful, but the availability of c-BN limits the utility of this technology. Epitaxial growth on other closely lattice matched materials such as Ni, Cu, or Co have had only limited success. The formation of aligned diamond crystals in a small local area has been reported for diamond growth on Ni.[10] One difficulty in diamond heteroepitaxy is the poor chemical bonding between adsorbate and substrate. During heteronucleation, adsorbate species such as methyls are receiving substantial fluxes of atomic H. Under this high flux, carbon adsorbates on the surface are gasified, defeating diamond nucleation. As a result, diamond nucleation and growth is sporadic and highly three-dimensional.

In the present studies, *ab initio* cluster model calculations are used to investigate the energy effect of subsurface interstitials such as Na, H, and C on the bonding of a CH_3 radical to a hollow 3-fold site on Ni(111). The calculated results show that the presence of electropositive subsurface species in Ni dramatically increase the bond strength between a CH_3 radical and the Ni surface. Correspondingly, electronegative subsurface species such as C dramatically weaken a CH_3-Ni surface bond. In addition, the energy required to planarize a tetrahedral CH_3 on Ni(111) increases when electropositive species reside interstitially below the Ni surface.

Calculations are performed in the context of a many-electron embedding theory that permits the accurate computation of molecule-solid surface interactions at an *ab initio* configuration interaction level. The CH_3 and local surface region are treated as embedded in a lattice electron distribution which is modeled as a 41-atom, three layer cluster.

The objective of the present paper is to calculate the adsorption energy of CH_3 on Ni(111) with subsurface Na, H, and C implants and then to calculate the energy required to distort the tetrahedral CH_3 into a planar structure on the surface.

II. THEORY AND CALCULATIONS

The purpose of the embedding theory employed in this work is to treat adsorbed species and a surface region of the metal with sufficient accuracy to describe reaction energetics, while at the same time maintaining a proper coupling of the surface region to the bulk.[11-13] The present approach most closely resembles that in Refs. 14 and 15, where the details of the method are discussed. Calculations are performed by first obtaining self-consistent-field (SCF) solutions for the nickel cluster plus adsorbed species. The occupied and virtual orbitals of the SCF solution are then transformed separately to obtain orbitals spatially localized about all the atoms of the cluster except those in the seven-atom surface region shown in Fig. 1. This unitary transformation of orbitals is based upon exchange maximization with the valence orbitals of atoms outside the surface region and is designed to enhance convergence of the configuration interaction (CI) expansion.[11-13]

The CI calculations involve single and double excitations from multiple parent configurations within a 28 or 29-electron subspace to 28 possible localized virtual orbitals. All configurations arising from excitations with an interaction energy greater than $1x10^{-5}$ hartree with the parent SCF configuration are explicitly retained in the expansion; contributions of excluded configurations are estimated using second order perturbation theory. For all geometries calculated, the SCF solution is the dominant configuration. Configurations with coefficients > 0.05 are included as parent configurations. Details of the procedure are given in Ref. 16. Basis superposition contributions to the total energy were taken into account by calculating the energy of the Ni cluster with the adsorbed species' virtual basis present (but not the adsorbate nuclei).

The cluster geometry and local region of the nickel cluster used to model the (111) crystal face of nickel are shown in Fig. 1. The three layer, 88-atom cluster, consists of a surface layer of 37 atoms, a second layer of 30 atoms and a third layer of 21 atoms. Embedding theory is used to reduce the Ni_{88} cluster to the 41-atom model depicted as shaded

atoms: the surface layer of 19 atoms, a second layer of 14 atoms, and a third layer of 8 atoms. For the seven-nickel-atom local surface region, a [1*s*-3*p*] core potential is used; 3d, 4s and 4p orbitals are explicitly included in the valence basis. Other Ni atoms are described by an effective core potential for [1*s*-3*d*] electrons, and a single 4s orbital. For all boundary atoms, and those in the third layer, the core potential is further modified to account for bonding to the bulk region, as described in Refs. 14 and 15. The basis orbitals of Ni, C, and H are the same as used in previous dissociative chemisorption studies of CH_4 on Ni(111).[17] A double zeta *s* and *p* basis for Na is taken from Veillard[18] and augmented with a set of *p* polarization functions (exponent of 0.5).

The Na, H and C interstitials are positioned below a hollow 3-fold site and midway between the first and second layers, as shown in Fig. 2.

III. RESULTS

Fig. 2 shows the geometry of pyramidal CH_3 adsorbed at a hollow 3-fold site, where there is no second layer Ni atom underneath. The interstitial Na, H or C atom is below the hollow 3-fold site, in the interstitial position midway between the first and second layers. In the initial carbon-surface distance optimization, the C-H bond lengths are fixed at 1.08 Å and the HCH angles at 109.5°. Calculated adsorption energies, distances from CH_3 to the surface, and vibrational frequencies are reported in Table I. For CH_3 on clean Ni(111), the computed adsorption energy is 38 kcal/mol with a surface-CH_3 distance of 1.90 Å. These values along with the calculated vibrational frequencies are consistent with our previous calculations of CH_3 on Ni(111), where the lattice was modeled as a 28-atom, three layer cluster.[19,20]

For CH_3 adsorption at the 3-fold site above the interstitial atom, the chemisorption energy increases to 50 and 47 kcal/mol for Na and H subsurface atoms, respectively. However, the energy decreases to 17 kcal/mol in the case of a C subsurface atom. The distances of CH_3 to the surface change only slightly from 1.85 Å to 1.93 Å.

Thus CH_3 adsorption energies are comparable for Na and H interstitials; while the subsurface C significantly weakens the CH_3-surface bond to a value less than one-half that for Ni(111) with no interstitial species. Na is an electron donor and the 3*s* electron is distributed

over the neighboring Ni atoms in the first and second layers. It is therefore easier for CH_3 to receive electronic charge from the surface and form a strong bond. The interstitial H behaves somewhat like the Na interstitial, but its net charge is only +0.09 |e|. On the other hand, Mulliken populations from the SCF calculations show that the C interstitial receives almost 2 electrons.[21] The surface adsorption region becomes electron deficient, and the CH_3-surface bond strength is diminished since it is more difficult for CH_3 to pull electrons from the substrate.

Fig. 3 shows the energy required to distort the tetrahedral CH_3 into a planar structure on Ni(111) with and without the interstitial species. The purpose of these calculations is to determine whether the implants stabilize or destabilize the CH_3 tetrahedral geometry. The figure shows that the energy required to distort tetrahedral CH_3 to a planar sp^2 geometry is 22 kcal/mol on Ni(111), at the surface-CH_3 equilibrium distance of 1.90 Å. For Ni(111) with an interstitial Na atom, this energy increases to 30 kcal/mol, for interstitial H, the value is 24 kcal/mol, and with the C interstitial atom, only 12 kcal/mol is required. The latter value is about one-half that required for distortion of CH_3 on Ni(111) with no implant.

As indicated above, the interstitial atoms are positioned below a hollow 3-fold site and midway between the first and second layers, i.e., at the center of an octahedral hole in the lattice. The smaller, tetrahedral hole (below the filled 3-fold site) was not investigated. The octrahedral hole is not quite large enough to accommodate Na^+ and is much too small for negatively charged carbon. Therefore, we would expect that interstitial species such as Na and C, and to a lesser extent hydrogen, will expand the lattice locally. This in turn will affect some of the properties we have calculated, but the extent is unclear. Further, the implant species are mobile and in the case of H and C may ultimately react with the adsorbed CH_3. Thus, although the large effects found in the present study are intriguing, much more work is needed before a quantitative understanding of accompanying effects will be possible.

IV. CONCLUSIONS

The conclusions of the present study of CH_3 at a hollow 3-fold site on Ni(111) with subsurface Na, H and C interstitials can be summarized as follows.

(1) Tetrahedral CH_3 binds strongly to the Ni(111) when an interstitial Na or H atom implant is present; the adsorption energy is 50 or 47 kcal/mol, respectively, compared to 38 kcal/mol for Ni(111) with no implant. The adsorption energy is only 17 kcal/mol in the presence of a subsurface C implant. The corresponding CH_3-surface distances are 1.85 Å, 1.87 Å, and 1.93 Å for Na, H, and C cases, respectively. With no implant the value is 1.90 Å.

(2) Energies required to distort tetrahedral sp^3 CH_3 into a planar sp^2 structure are 22 kcal/mol on Ni(111), and 30, 24, 12 kcal/mol for Na, H, C implants, respectively.

(3) Calculated C-H stretching frequencies are all around 3150 cm^{-1} with or without the implants. The surface-CH_3 perpendicular stretch vibrational frequencies are 374 cm^{-1} on Ni(111), and 361 cm^{-1}, 340 cm^{-1}, 476 cm^{-1} with the Na, H, C implants, respectively.

(4) The present studies indicate that C below the Ni surface may make it easier for a carbon overlayer to revert to a planar graphite structure, while interstitial Na atoms may stabilize a tetrahedral C sp^3 structure on Ni(111).

Note added: A recent published experimental study by S. T. Ceyer and coworkers [22] has demonstrated that interstitial H is the active species in the hydrogenation of CH_3 on Ni(111). The reaction of surface hydrogen with methyl is inhibited by a substantial energy barrier.[17] The experimental evidence is consistent with H in an octahedral interstitial site reacting with CH_3 adsorbed at the three-fold surface site above H (see Fig. 2c). Our theoretical results suggest that the presence of interstitial H enhances the adsorption energy of CH_3 at this site.

ACKNOWLEDGMENTS

This work was supported by the Office of Naval Research, the Strategic Defense Initiative Organization-Innovative Science and Technology Office. Studies of the clean surface and interstitial H was supported by the U. S. Department of Energy.

REFERENCES

(1) R. Messier, J. T. Glass, J. E. Butler, and R. Roy, eds. "New Diamond Science and Technology", MRS, Pittsburgh, 1991.

(2) R. F. Davis, Z. Sitar, B. E. Williams, H. S. Kong, H. J. Kim, J. W. Palmour, J. A. Edmond, J. Ryu, J. T. Glass, and C. H. Carter, Jr. *Mater. Sci. Eng.* **B1**, 77 (1988).

(3) R. A. Rudder, J. B. Posthill, and R. J. Markunas, *Elect. Letters*. **25**, 1220 (1989).

(4) K. E. Spear, *J. Am. Ceram. Soc.* **72**, 171 (1989).

(5) H. Kawarada, J. S. Ma, T. Yonehara, and A. Hiraki, *Mater. Res. Soc. Symp. Proc.* **162**, 195 (1990).

(6) H. Itoh, T. Nakamura, H. Iwahara, and H. Sakamoto, in "New Diamond Science and Technology", p. 929, eds. R. Messier, J. T. Glass, J. E. Butler, and R. Roy, MRS, Pittsburgh, 1991.

(7) W. A. Yarbrough, *J. Vac. Sci. Technol.* **A9**, 1145 (1991).

(8) J. F. Prins, and H. L. Gaigher, in "New Diamond Science and Technology", p. 561, eds. R. Messier, J. T. Glass, J. E. Butler, and R. Roy, MRS, Pittsburgh, 1991.

(9) J. Narayan, V. P. Godbole, and C. W. White, *Science*, **252**, 416 (1991).

(10) Y. Sato, I. Yashima, H. Fujita, T. Ando, and M. Kamo, in "New Diamond Science and Technology", p. 371, eds. R. Messier, J. T. Glass, J. E. Butler, and R. Roy, MRS, Pittsburgh, 1991.

(11) J. L. Whitten, and T. A. Pakkanen, *Phys. Rev. B.* **21**, 4357 (1980).

(12) J. L. Whitten, *Phys. Rev. B.* **24**, 1810 (1981).

(13) P. Cremaschi, and J. L. Whitten, *Surf. Sci.* **149**, 273 (1985).

(14) J. L. Whitten, *"Theoretical Studies of Surface Reactions on Metals: Cluster and Embedding Theory"* chapter in *Cluster Models for Surface and Bulk Phenomena*, Pacchioni, G and Bagus, P. S. eds., Plenum Press, New York, p. 375 (1992).

(15) P. Cremaschi, and J. L. Whitten, *Theor. Chim. Acta*, **72**, 485 (1987).

(16) P. Madhavan, and J. L. Whitten, *J. Chem. Phys.* **77**, 2673 (1982).

(17) H. Yang, and J. L. Whitten, *J. Chem. Phys.* **96**, 5529 (1992).

(18) A. Veillard, in "Handbook of Gaussian Basis Sets", *Table* 11.9.2., eds. R. Poirier, R. Kari, and I. G. Csizmadia, Elsevier, N.Y. 1985.

(19) H. Yang, and J. L. Whitten, *J. Am. Chem. Soc.* **113**, 6442 (1991).

(20) H. Yang, and J. L. Whitten, *Surf. Sci.* **255**, 193 (1991).

(21) The electron charge ascribed to the C atom (and to H or Na) should not be interpreted strictly as an atomic charge but as a measure of the electron distribution in the vicinity of the interstitial atom.

(22) A. D. Johnson, S. P. Daley, A. L. Utz, and S. T. Ceyer, *Science*, **257**, 223 (10 July, 1992).

Table I.

CH_3 adsorbed at a hollow 3-fold site on Ni(111) with subsurface Na, H and C interstitials. Adsorption energies (E_b), CH_3 distances from C to the surface (R_e), and vibrational frequencies are reported. Results are from configuration interaction calculations and are corrected for basis superposition effects of approximate 3 to 4 kcal/mol.

	Ni(111)	Na Interstitial	H Interstitial	C Interstitial
E_b (Kcal/mol)	38	50	47	17
R_e (Å)	1.90	1.85	1.87	1.93
Ni-CH_3 strech (cm^{-1})	374	361	340	476
C-H stretch (cm^{-1})	3140	3140	3130	3170

FIGURE CAPTIONS

Fig. 1. Cluster geometry and local region of the nickel cluster used to model the (111) crystal face of nickel. The three layer, 88-atom cluster, consists of a surface layer of 37 atoms, a second layer of 30 atoms and a third layer of 21 atoms. Embedding theory is used to reduce the Ni_{88} cluster to a 41 atom model depicted as shaded atoms. Atoms surrounding the seven local region atoms in the surface layer and those surrounding the four central atoms in the second layer are described by effective potentials for $(1s)^2...(3p)^6(3d)^9(4s)^{1/2}$ and $(1s)^2...(3p)^6(3d)^9(4s)^{3/10}$ configurations, respectively. Effective potentials for the shaded atoms in the third layer describe the $(1s)^2...(3p)^6(3d)^9(4s)^{3/4}$ configuration. Unshaded atoms have neutral atom (1s-3p core)$(3d)^9(4s)^1$ potentials. All atoms have Phillips-Kleinman projectors $\Sigma|Q_m><Q_m|(-\epsilon_m)$ for the fixed electronic distribution. The nearest neighbor Ni-Ni distance is 2.48 Å.

Fig. 2. CH_3 geometry and the local region of Ni(111) showing subsurface Na, H and C atoms. The interstitial species are below a hollow 3-fold site, midway between the first and second layers. The vertical distance of the interstitial to the first and second layers is 1.01 Å.

Fig. 3. Tetrahedral and planar CH_3 geometries on Ni(111) with subsurface Na, H and C interstitials (shaded circles). The interstitials are below a hollow 3-fold site, midway between the first and second layers. ΔE is the energy required to distort the tetrahedral geometry of (a) into a planar structure of (b). The CH_3-surface distances (R_e) are listed in Table I.

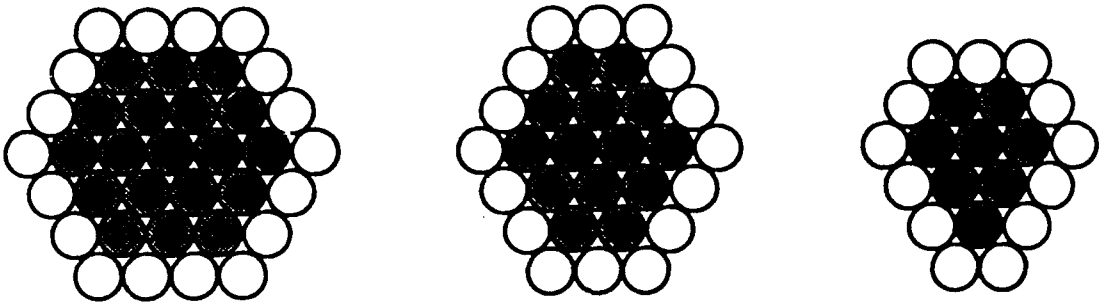

surface layer second layer third layer

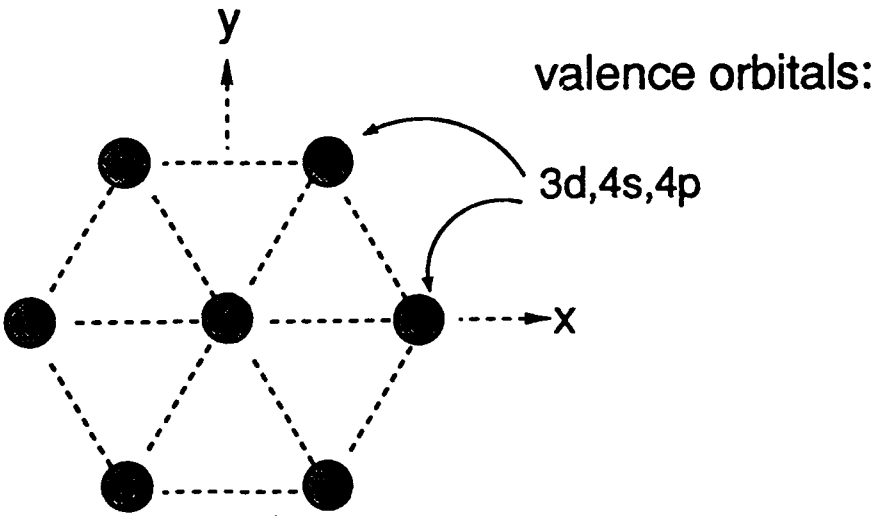

surface layer local region

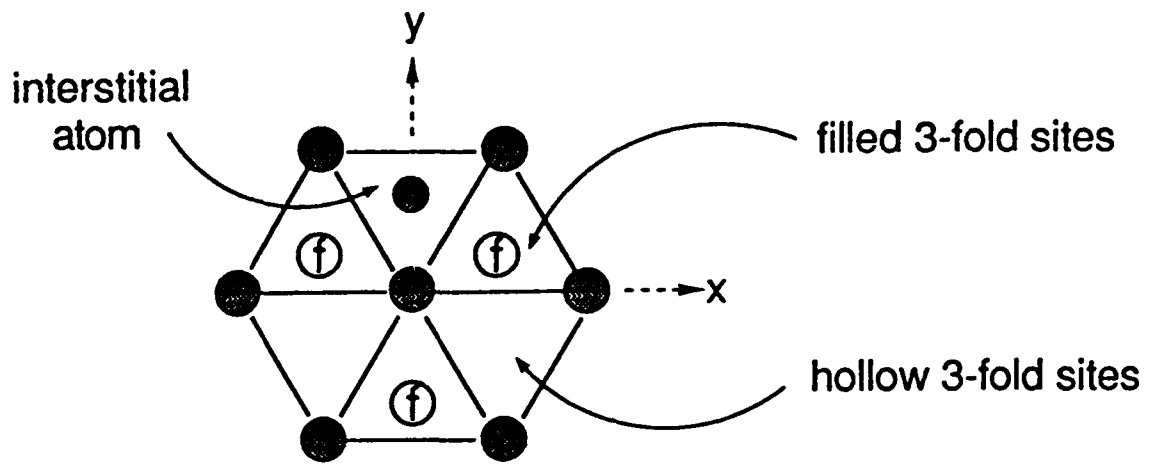

(a)

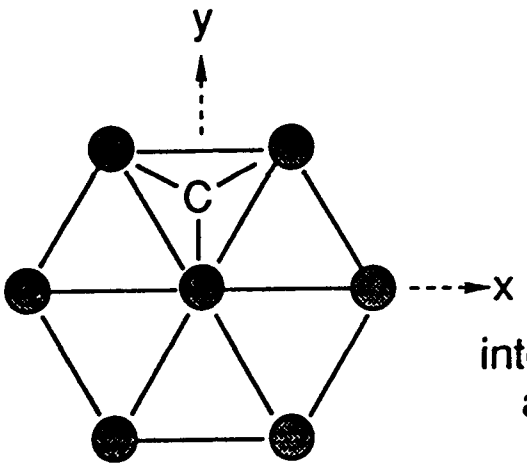

interstitial
atom

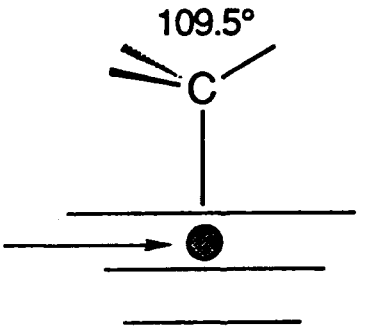

(b)

(c)

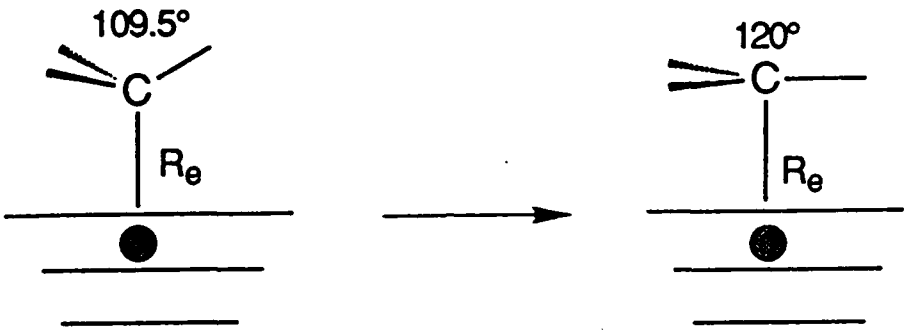

(a) (b)

	Ni(111)	Na Interstitial	H Interstitial	C Interstitial
ΔE (Kcal/mol)	+22	+30	+24	+12

Atomic Hydrogen Adsorption on the Reconstructed Diamond (100)-(2 × 1) Surface

R. E. THOMAS, R. A. RUDDER AND R. J. MARKUNAS
Research Triangle Institute
Research Triangle Park, NC 27709

D. HUANG AND M. FRENKLACH
Department of Materials Science and Engineering
Pennsylvania State University
University Park, PA 16802

(Received December 20, 1991)
(Accepted April 2, 1992)

ABSTRACT: A combination of theoretical and experimental techniques have been used to study atomic hydrogen adsorption on the diamond 2 × 1 surface. Low energy electron diffraction (LEED) has been used to study the effects of atomic and molecular species of hydrogen on the reconstructed 2 × 1 surface. Atomic hydrogen appears relatively inefficient at breaking C—C dimer bonds on the (100)-(2 × 1) surface. LEED patterns show only slight changes even after exposure of the surface to approximately 400 monolayers of atomic hydrogen. Calculations using modified neglect of diatomic overlap (MNDO) were done for two atomic hydrogen insertion reactions: direct attack of the dimer bond and attack of the back bond. Calculations indicate that there are substantial potential energy barriers to both reactions. The barrier to hydrogen addition on the dimer bond was calculated as 48.7 kcal/mol as compared to 76.1 kcal/mol for addition to the dimer back bond. Based on experimental and theoretical results, it appears that exposure of the C(100)-(2 × 1) surface to atomic hydrogen at 25°C does not readily convert the surface to the 1 × 1 state.

1. INTRODUCTION

Hydrogen is an integral constituent in many of the CVD diamond growth processes developed to date [1]. Hydrogen is thought to

1056-7860/92/01 0006-14 $6.00/0

ption on
amond
ace

J. MARKUNAS

09

\CH
ngineering
y

imental techniques have
e diamond 2 × 1 surface.
sed to study the effects of
constructed 2 × 1 surface.
eaking C—C dimer bonds
only slight changes even
ionolayers of atomic hydro-
ic overlap (MNDO) were
irect attack of the dimer
ate that there are substan-
e barrier to hydrogen addi-
/mol as compared to 76.1
on experimental and theo-
)–(2 × 1) surface to atomic
face to the 1 × 1 state.

ny of the CVD diamond
Hydrogen is thought to

DEPOSITION, Vol. 1—*July 1992*

0/0
Co., Inc.

function in the growth process in a number of ways, including maintenance of sp^3 hybridization of carbon atoms at the growth surface. In spite of numerous growth studies, the details of the role of hydrogen in CVD growth environments are still unclear, as are fundamental questions concerning interactions of this gas with the diamond surface.

Although similar in structure to the silicon (100) surface, the diamond (100) surface has not been studied nearly as intensively; there have been only a handful of experimental studies [2–6] and theoretical studies [7–10,13] published to date. Important questions remain concerning the details of the reconstruction and the effect of adsorbates on surface structure. As with silicon (100), the diamond (100) surface reconstructs to a 2 × 1:1 × 2 dimer configuration upon heating [2,4,6]. Due to the higher bond strengths in the carbon system, the reconstruction does not occur until the diamond is annealed to approximately 1000°C as compared to 450°C for silicon. Hydrogen desorption from the diamond (100) surface has been found to occur at approximately 900°C for a heating rate of 20°C/s [4]. Adsorption of atomic hydrogen has been reported to convert the surface back to the 1 × 1 configuration [2]. However, subsequent annealing to 1200°C did not convert the surface back to the 2 × 1 configuration [2]. Recently published theoretical calculations indicate a barrier of 34.1 kcal/mol for the insertion of hydrogen into the C—C dimer bond [10]. In contrast, silicon (100)–(2 × 1) surfaces have been shown to easily convert from the 2 × 1 to the 1 × 1 configuration at room temperature upon exposure to atomic hydrogen doses on the order of 10 monolayers or less [12–14]. From these calculations it appears difficult to form the dihydride from the monohydride by exposure of the surface to atomic hydrogen.

In the present paper we have used low energy electron diffraction (LEED) analysis and modified neglect of diatomic overlap (MNDO) calculations to study the effects of atomic and molecular species of hydrogen on the reconstructed 2 × 1 surface. LEED combined with UHV (ultrahigh vacuum) dosing with atomic hydrogen was chosen in order to reduce extraneous surface interactions. Two atomic hydrogen insertion reactions were studied with MNDO calculations: direct attack of the dimer bond and attack of the dimer back bond. The attack of the dimer bond simulates the conversion of the surface from 2 × 1 to 1 × 1. Studies of hydrogen attack of the dimer back bond were stimulated by recent results of Boland, wherein strained silicon back bonds on the reconstructed silicon (7 × 7) surface were found susceptible to attack by atomic hydrogen [15].

2. METHODS

2.1 Experimental

Atomic hydrogen dosing and LEED observations were performed in a stainless steel UHV system. Turbomolecular pumps were used both on the main chamber and to differentially pump the chamber housing the quadrupole mass spectrometer. Base pressure was 5×10^{-10} Torr for the sample chamber and 1×10^{-10} Torr for the quadrupole chamber. LEED observations were performed with a Princeton Research Instruments reverse view system.

Sample heating was accomplished by clipping the diamond crystals to a 0.25 mm thick molybdenum resistive strip heater. All parts associated with the heater stage, including the clamps and current leads, were manufactured from molybdenum. The sample temperature was measured by a 0.125 mm diameter chromel/alumel thermocouple threaded through a laser-drilled hole in the diamond and held in tension against the crystal. The sample heating was controlled by feedback from the thermocouple, which adjusted a SCR power supply. After an initial warm-up phase, the temperature ramps were linear from approximately 150°C to over 1100°C.

Two type IIa (100), $5 \times 5 \times 0.25$ mm, diamond crystals were used in the course of the present study. Other than thermal cleaning, no technique is available in situ for removing surface contamination from the diamond crystals. Particular attention was, therefore, paid to preparing the diamond surface before entry into the vacuum system. The samples were initially hand polished for 5 minutes with 0.25 μm diamond grit and deionized water on a nylon polishing pad. The samples were then ultrasonically degreased in a series of solvents, trichloroethylene, acetone, methanol, and deionized water. Following the deionized water rinse, the samples were swabbed under DI (deionized) water to remove particles. The samples were rinsed again in the solvent series and then placed in CrO_3/H_2SO_4 (125°C) solution for 20 minutes to remove non-diamond carbon. The samples were rinsed in DI water and then boiled in a 3:1 solution of HCl/HNO_3 for 20 minutes to remove any metals contamination. Finally the samples were rinsed in deionized water and blow-dried with compressed nitrogen. Samples subjected to this cleaning process typically show a good quality 1×1 LEED pattern with no annealing. For the initial thermal cleaning the sample was ramped up in temperature at approximately 10°C/sec until the pressure in the main chamber rose to 5×10^{-8} Torr at which point the power was shut

off and the sample cooled. This cycle was repeated until a maximum temperature of 1150°C was reached.

In all cases atomic hydrogen was generated via a tungsten filament operating at a temperature of approximately 1500°C. The filament temperature was measured with a hand held optical pyrometer. The sample was positioned approximately 2 cm from the filament during dosing. The sample was not actively cooled and at the lowest dosing pressures remained at room temperature. No attempt was made to quantify the percentage of atomic hydrogen generated by the filament. From earlier experiments on silicon (100) substrates, under conditions identical to those used in the present study, we can estimate the degree of molecular hydrogen dissociation. It was found that for unterminated silicon 2 × 1 surfaces, an exposure for 300 seconds at a chamber pressure of 1×10^{-6} Torr was sufficient to convert the surface to the 1 × 1 configuration [14]. Therefore, the surface has been exposed to at least 1 monolayer of atomic hydrogen, and the minimum degree of dissociation is .3%. From dissociation curves for hydrogen we estimated the maximum fractional dissociation at 1500°C was approximately 5% [16]. X-ray photoelectron spectroscopy was done ex situ after extensive dosing with the tungsten filament and no evidence of metal contamination was seen.

2.2 Calculational

The energies were obtained, as in the previous studies [11,17,18], using the MNDO all-valence electron parametrization of the NDDO SCF approximation [19]. Calculations were of restricted Hartree-Fock type with the half-electron method being used for single-radical species [20]. Computations were performed with the AMPAC computer program developed by Dewar and co-workers [21], using an IBM-3090/600S mainframe computer.

The "background" (100) surface element was represented in this study by a $C_{28}H_{46}$ cluster used in the previous study [11]. The cluster, shown in Figure 1, consisted of three layers of carbon atoms. All dangling bonds of these carbon atoms were saturated with hydrogen atoms. For identification purposes, the carbon sites of the first two layers are marked with letters a, b, c, and d in Figure 1. The central C_a—C_a carbon site of the top layer, on which the reaction took place, was a carbon monohydride dimer. It was a product of H_2 elimination from a 1 × 1 surface dihydride, $C_{28}H_{48}$. To simulate the rigidity of the real surface, the dihydride carbons of the top layer (C_b and C_c atoms) were fixed at

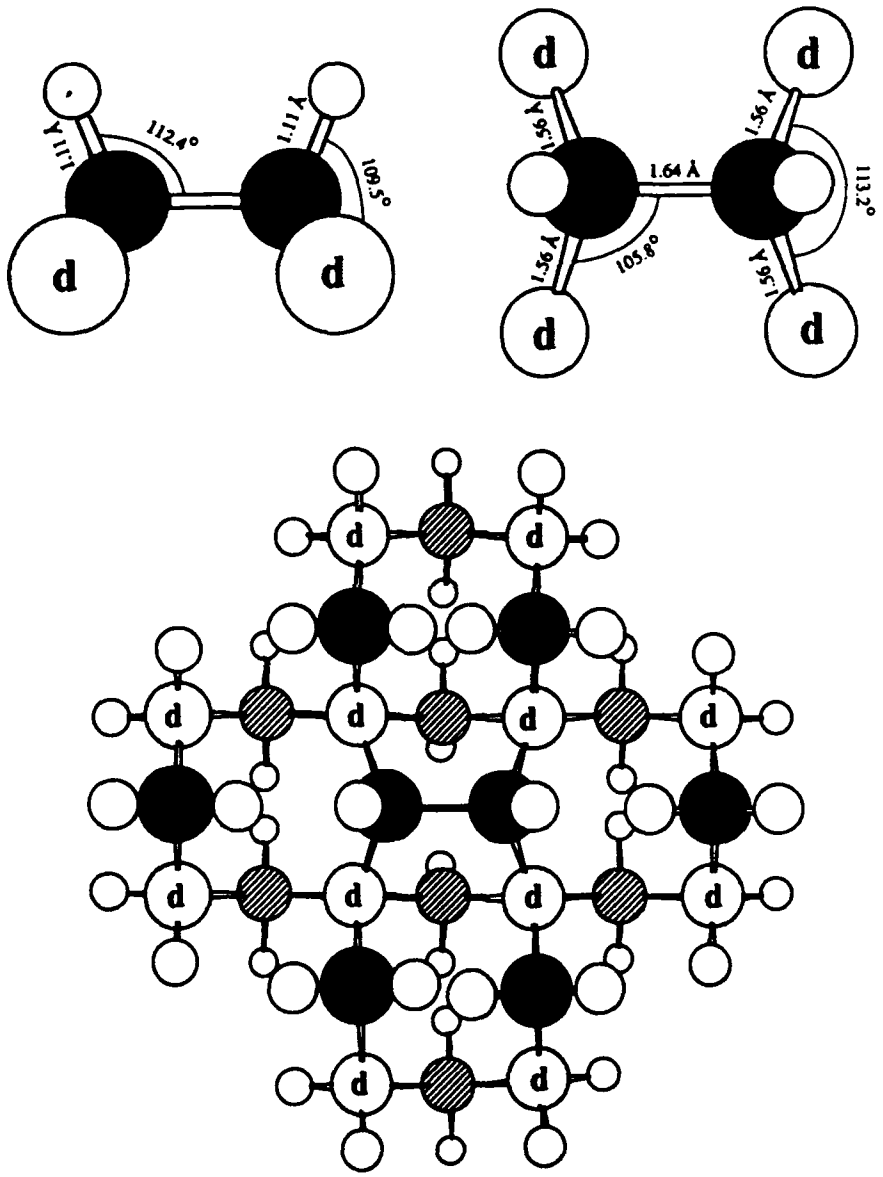

Figure 1. The "background" (100) surface element. The filled circles designate carbon atoms and the open circles—hydrogen atoms. Carbon atoms of different layers are shaded with different patterns. Letters a, b, c, and d identify distinct reaction sites at the top two layers. The bottom of the figure gives top view of the model compound, and the top of the figure—side (left) and top (right) views of the reacting monohydride dimer.

the positions of an ideal diamond lattice (with distance between the dihydride carbons of 2.53 Å), and the positions of the rest of the carbon atoms were obtained by full minimization of the total potential energy.

3. RESULTS

3.1 Experimental Results

Upon annealing, more than 90% of the freshly polished surfaces used in the present study exhibited a transformation from the 1 × 1 configuration to the 2 × 1 configuration. During the initial annealing sequence the samples would typically show indications of the 2 × 1 structure at approximately 800°C, with the transformation completed by 1050°C on successive anneals. No correlations were observed between sample preparation conditions and failure of the surface to reconstruct.

Figures 2 and 3 show LEED patterns from two series of experiments where samples were annealed to convert the surface to the 2 × 1 state and then exposed to atomic hydrogen. First, Figure 2(a) shows a sample as loaded; then before [Figure 2(b)] and after [Figure 2(c)] exposure to H/H_2 at a pressure of 5×10^{-5} Torr for 30 minutes are shown. There was perhaps a slight diminishment in the intensity of the second-order spots, but the 2 × 1 pattern is still quite evident. The dose used represents an exposure of 40,000 L, where 1 L was equivalent to 1×10^{-6} Torr-s. In contrast, a dose of 300 L under identical conditions was sufficient to convert the silicon (100) surface from the 2 × 1 state back to the 1 × 1 state [14]. We note again that doses referred to here are for a total hydrogen dose of molecular plus atomic hydrogen. The dose was calculated from uncorrected ion gauge tube readings. Diamond samples were also exposed to molecular hydrogen at equivalent doses, and no evidence of reversion to the 1 × 1 structure was observed. Figure 3(a) shows LEED results from samples exposed to H/H_2 at much higher pressures, 0.95 Torr [Figure 3(b)] and 6.5 Torr [Figure 3(c)]. These pressures are similar to what is currently used in plasma enhanced CVD diamond growth systems. Again, no evidence of conversion of the 2 × 1 surface to the 1 × 1 configuration can be seen.

3.2 Calculational Results

The geometric results for the dimer of the background surface cluster are shown at the top of Figure 1. The dimer bond length was calculated to be 1.64 Å. For the addition of hydrogen to the surface, two reactions

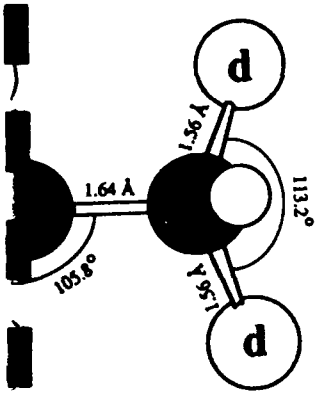

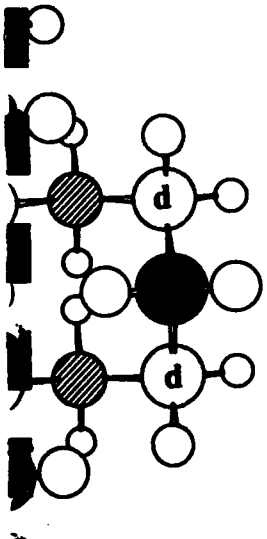

e filled circles designate carbon
toms of different layers are shaded
tinct reaction sites at the top two
del compound, and the top of the
monohydride dimer.

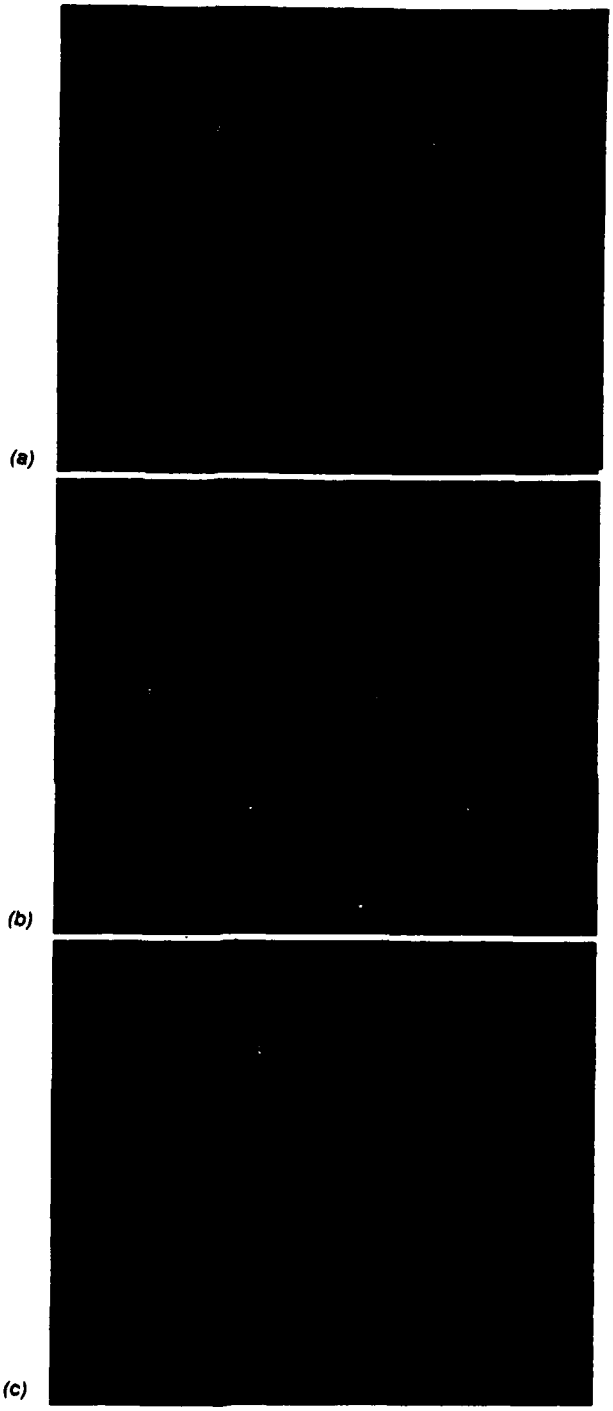

Figure 2. LEED patterns at 157 eV from diamond (100)-(2 × 1) surface as loaded [Figure 2(a)], before [Figure 2(b)], and after [Figure 2(c)] exposure to atomic hydrogen for 30 min at a total hydrogen pressure of 5×10^{-5} Torr. There may be a slight diminishment of the second order spots in Figure 2(c) but the 2 × 1 pattern is clearly evident.

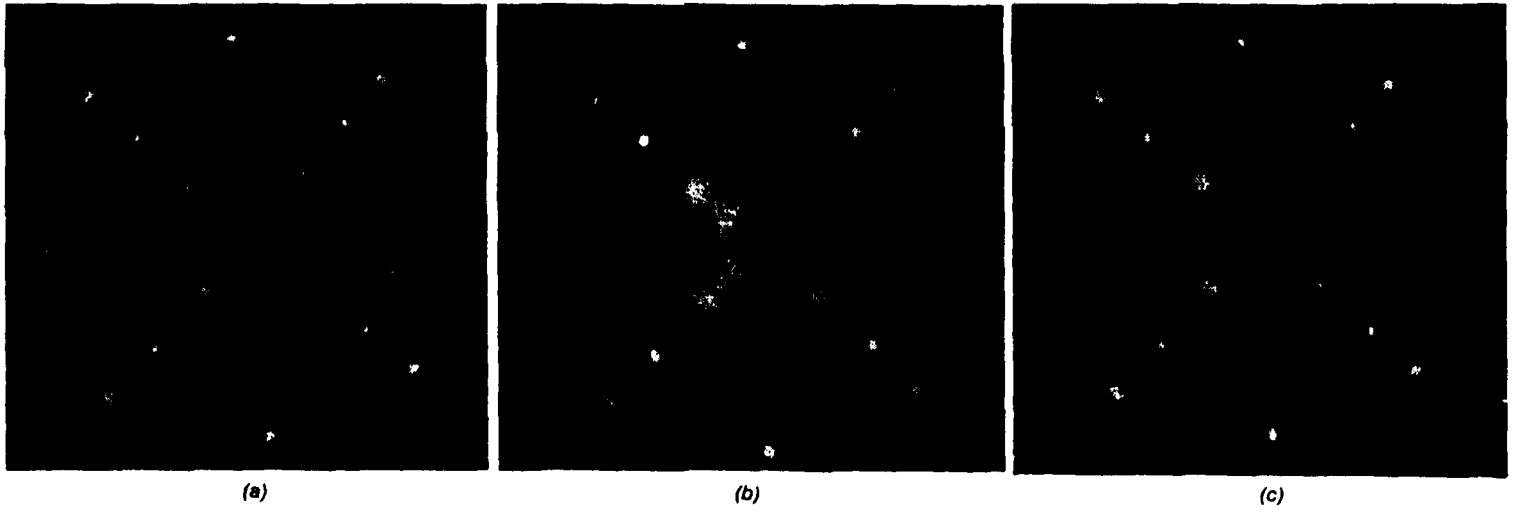

(a) (b) (c)

Figure 3. This figure shows LEED patterns from a sample exposed to H/H_2 at much higher pressures than used for the sample shown in Figure 2. Figure 3(a) shows the sample after thermal cleaning. The 2 × 1 pattern is evident. Figure 3(b) shows the sample after dosing at .95 Torr for 5 min at 25°C. The 2 × 1 surface structure is still visible. Figure 3(c) shows the sample after annealing at 1150 eV and atomic hydrogen dosing at 6.5 Torr. The 2 × 1 pattern is still present.

of the H atom with the dimer were considered: first was the attack on the dimer carbon atom, C_s, and second was the attack on the second-layer carbon atom, C_d. In the former case, the results indicate the breaking of C_s—C_s dimer bond. The variational potential energy surface diagram and the corresponding change of C_s—C_s dimer bond length with the H atom approaching the dimer C_s atom are shown in Figure 4. The potential energy barrier obtained for this reaction is 48.7 kcal/mol. The variational potential energy surface diagram and the corresponding change of C_s—C_d back bond length with the H atom approaching a C_d atom are shown in Figure 5. The results in this case indicate that the C_s—C_s dimer bond does not break but instead the C_s—C_d back bond is cleaved. However, the potential energy barrier obtained for this reaction, 76.1 kcal/mol, is substantially larger than that of the direct dimer attack.

4. DISCUSSION

The dimer bond length of 1.64 Å calculated here is in good agreement with Yang and D'Evelyn's [7] 1.63 Å and Verwoerd's [8] 1.67 Å, but somewhat apart from the result of Mehandru and Anderson [9], 1.73 Å, and the result of Zheng and Smith, 1.56 Å [10]. Although LEED observations have been made of the reconstructed surface [2–4,6], no quantitative experimental data have been published to date on the bond lengths.

Reconstruction of the diamond (100) surface to the 2 × 1 state is an experimentally well-documented phenomena [2–4,6]. The resulting structure appears very similar to the 2 × 1 silicon reconstruction [2,3]. Although the process seems to be quite similar to that seen on silicon, researchers report that a varying percentage of the freshly polished surfaces studied do not reconstruct to the 2 × 1 structure upon annealing [2–4,6]. Hamza et al. [2] have reported an association between residual oxygen on the surface detected by electron stimulated desorption and the ability of the surface to reconstruct [2]. Samples with the most oxygen detected were less likely to reconstruct. Given the surface preparation techniques available both in situ and ex situ for diamond, it seems reasonable to assume that surface contamination may explain the failure of some samples to reconstruct. The effect of impurities on surface reconstruction has been noted in a number of other systems including silicon and platinum [22].

Conversion of the surface back to the 1 × 1 state by exposure to atomic hydrogen has been studied experimentally by only one other group [2]. Results reported by Hamza et al. indicated that the surface

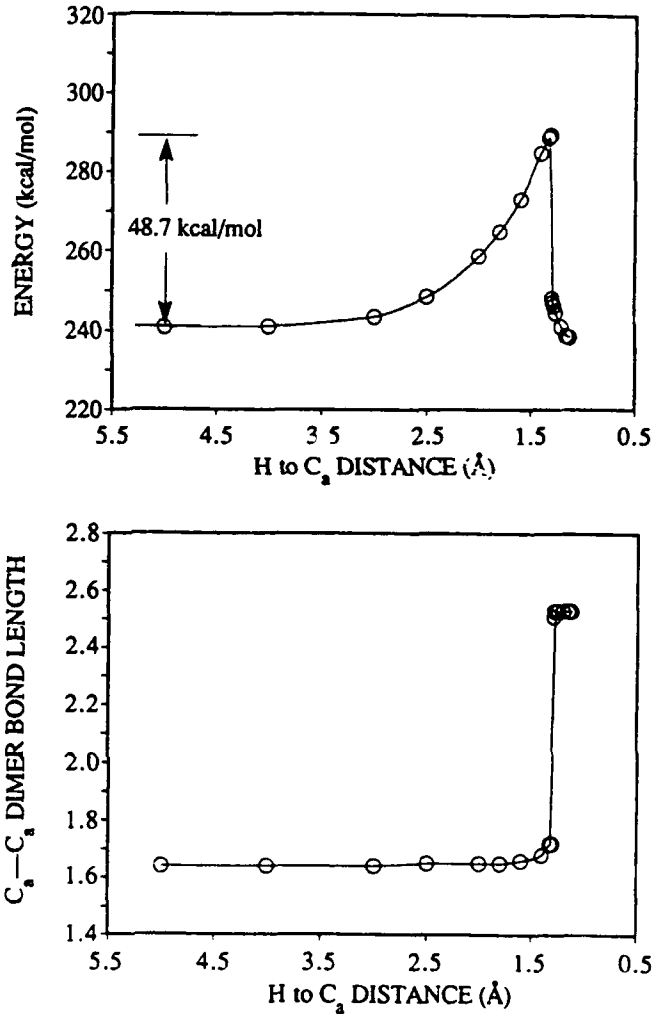

Figure 4. Variational diagram for the addition of a H atom to a C_b atom of the dimer: top—potential energy, and bottom—dimer C—C bond length.

converted to the 1 × 1 configuration upon dosing with atomic hydrogen at 180 K coupled with annealing at 700 K [2]. LEED patterns disappeared following the dosing and the 1 × 1 pattern was then seen after annealing [2]. We see no evidence of either obscuration of the LEED pattern following dosing or of a reversion to the 1 × 1 surface structure. The LEED patterns gradually deteriorated with repeated dosing and desorption cycles until only weak first-order spots remained coupled with a very high background. One expects the dimer bond on the C(100)-(2 × 1) surface to be stronger than what is seen on the

Si(100)-(2 × 1) surface given the greater C—C bond strength, 83 kcal/mol [23] versus 46 kcal/mol [23] for Si—Si, and the ability of carbon to form double bonds. Theoretical calculations in the present study indicate that it is difficult to break the C—C dimer bond with atomic hydrogen. A large potential energy barrier, 48.7 kcal/mol, was found for breaking of the dimer bond by hydrogen atom addition. The calculated energy barrier for hydrogen addition to the dimer bond is in fairly close agreement with the 39 kcal/mol reported by Verwoerd [8], and with the

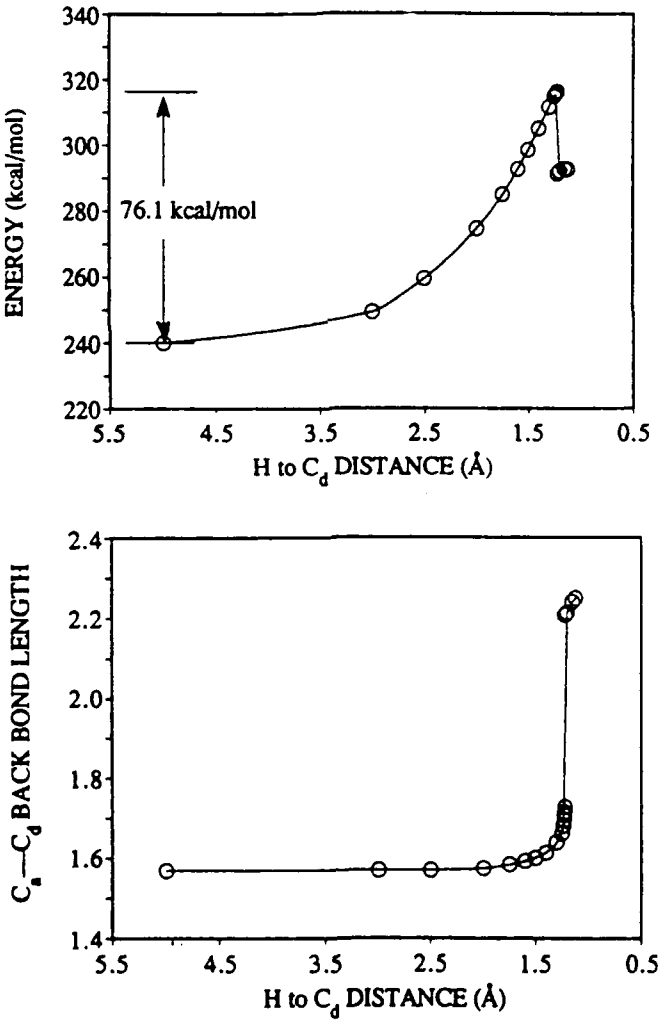

Figure 5. Variational diagram for the addition of a H atom to a C_d atom: top—potential energy, and bottom—C—C back bond length.

bond strength, 83 kcal/
the ability of carbon to
n the present study in-
dimer bond with atomic
kcal/mol, was found for
addition. The calculated
ner bond is in fairly close
rwoerd [8], and with the

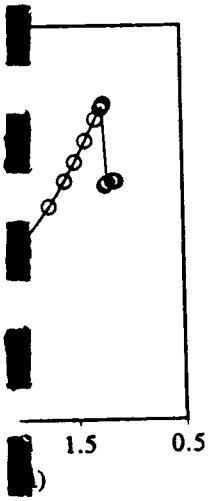

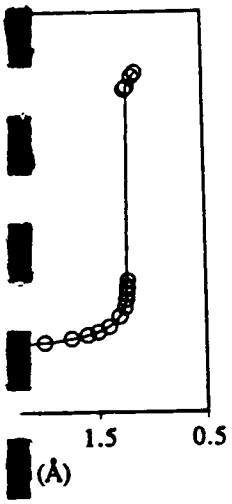

atom to a C_d atom: top—potential

34.1 kcal/mol estimated recently by Zheng and Smith [10]. The theoretical results obtained here support the LEED observations, which indicate the 2 × 1 surface does not convert back to the 1 × 1 configuration even after substantial dosing with atomic hydrogen.

The results obtained for hydrogen attack of the dimer backbond reinforce the observation that the C(100)–(2 × 1) surface is resistant to restructuring by atomic hydrogen. The potential energy barrier obtained for addition to the backbond, 76.1 kcal/mol, is substantially larger than for direct attack of the dimer bond. Although the potential energy barrier for dimer attack is relatively lower than for backbond attack, neither reaction appears likely in light of the substantial absolute value of the potential energy barriers. Furthermore, Yang and D'Evelyn have argued that even if individual dihydride units form, steric constraints severely limit the ability of the surface to saturate in the dihydride phase and at most the surface assumes a disordered dihydride with random dihydride units scattered among monohydride pairs [7].

It should be noted that all of the dosings used in the present study were with an atomic hydrogen flux considerably lower than found in a typical CVD growth environment and with a substrate temperature also much lower. Breaking of the dimer bond by atomic hydrogen was predicted to have a large potential energy barrier at low temperature. In a CVD environment, with much higher fluxes of atomic hydrogen, it may be that significant numbers of dimer bonds could be broken to form the dihydride. At higher substrate temperatures it is also likely that the reaction probability for dimer bond breaking and hydrogen atom insertion will increase. However, at room temperature and with nominal dosing fluxes, the conversion to the 1 × 1 structure appears to be very much slower than what is seen on silicon.

5. CONCLUSIONS

Atomic hydrogen appears relatively inefficient at breaking C—C dimer bonds on the C(100)–(2 × 1) surface compared to the Si(100)–(2 × 1) surface under identical conditions [14]. LEED patterns show only slight changes even after exposure of the surface to 40,000 L of H/H_2. Under similar conditions a silicon–(2 × 1) surface converts to the 1 × 1 phase after an exposure of less than 300 L [14]. MNDO calculations were done for two atomic hydrogen insertion reactions: direct attack of the dimer bond and attack of the backbond. Calculations indicate that there are substantial potential energy barriers to both reactions. The barrier to the dimer addition was calculated as 48.7 kcal/mol; attack of the backbond was calculated at 76.1 kcal/mol. Based

on experimental and theoretical results it does not appear that exposure of the C(100)–(2 × 1) surface to atomic hydrogen at 25°C readily converts the surface to the 1 × 1 state.

ACKNOWLEDGEMENTS

RTI wishes to thank the Innovative Science and Technology Program of the Strategic Defence Initiative Organization for support of the LEED studies under Contract No. N00014-86-C-0460. The computations were performed using the facilities of the Pennsylvania State University Center for Academic Computing. The work at Penn State was supported in part by Innovative Science and Technology Program of the Strategic Defence Initiative Organization (SDIO/IST) via the U.S. Office of Naval Research, under Contract No. N00014-86-K-0443.

REFERENCES

1. Messier, R., J. T. Glass, J. E. Butler and R. Roy, eds. 1991. *Proceedings of the Second International Conference on New Diamond Science and Technology*. Pittsburgh, PA: Materials Research Society, and *Conf. Proc., 179th Meeting of the Electrochemical Society, Washington, DC, May, 1991.*
2. Hamza, A. V., G. D. Kubiak and R. H. Stulen. 1990. *Surf. Sci.*, 237:35.
3. Pate, B. B. 1986. *Surf. Sci.*, 165:83.
4. Thomas, R. E., R. A. Rudder and R. J. Markunas. Conference proceedings to be published. "Thermal Desorption from Hydrogenated Diamond (100) Surfaces," presented at *179th Meeting of the Electrochemical Society, Washington, DC, May, 1991.*
5. Sellschop, J. P. F., C. C. P. Madiba and H. J. Annegarn. 1980. *Nucl. Instrum. Meth.*, 168:529.
6. Lurie, P. G. and J. M. Wilson. 1977. *Surf. Sci.*, 65:453.
7. Yang, Y. L. and M. P. D'Evelyn. Submitted. *J. Am. Chem. Soc.*
8. Verwoerd, W. S. 1981. *Surf. Sci.*, 108:153.
9. Mehandru, S. P. and A. B. Anderson. 1991. *Surf. Sci.*, 248:369.
10. Zheng, X. M. and P. V. Smith. 1991. *Surf. Sci.*, 256:1.
11. Huang, D. and M. Frenklach. In press. *J. Phys. Chem.*
12. Gates, S. M., R. R. Kunz and C. M. Greenlief. 1989. *Surf. Sci.*, 207:364.
13. Boland, J. J. 1992. *Surf. Sci.*, 261:17.
14. Thomas, R. E., R. A. Rudder and R. J. Markunas. 1992. *Mats. Res. Soc. Symp. Proc.*, 204:327.
15. Boland, J. J. 1991. *Surf. Sci.*, 244:1.

16. Pauly, H. 1988. In *Atomic and Molecular Beam Methods*, G. Scoles, ed., NY: Oxford U. Press, p. 108.
17. Huang, D., M. Frenklach and M. Maroncelli. 1988. *J. Phys. Chem.*, 92:6379.
18. Huang, D. and M. Frenklach. 1991. *J. Phys. Chem.*, 95:3692.
19. Dewar, M. J. S. and W. Theil. 1977. *J. Am. Chem. Soc.*, 99:4899.
20. See for example: Sadlej, J. 1985. *Semi-Empirical Methods of Quantum Chemistry*, translated by I. L. Cooper, Chichester: Ellis Horwood.
21. 1985. Quantum Chemistry Program Exchange (Chemistry Department, Indiana University) as QCPE Program #506.
22. Zangwill, A. 1988. *Physics at Surfaces*. Cambridge, England: Cambridge University Press, pp. 96, 258.
23. Jolly, W. L. 1984. *Modern Inorganic Chemistry*. New York: McGraw Hill, p. 60.

Chemical vapor deposition of diamond films from water vapor rf-plasma discharges

R. A. Rudder, G. C. Hudson, J. B. Posthill, R. E. Thomas, R. C. Hendry, D. P. Malta, and R. J. Markunas
Research Triangle Institute, Research Triangle Park, North Carolina 27709-2194

T. P. Humphreys and R. J. Nemanich
North Carolina State University, Raleigh, North Carolina 27695-8202

(Received 3 September 1991; accepted for publication 29 October 1991)

Polycrystalline diamond films have been deposited from water vapor rf-plasma discharges at 1.0 Torr containing various alcohol vapors. No other gases such as H_2, F_2, or Cl_2 were admitted to the growth chamber. Scanning electron microscopy and Raman spectroscopy have been used to characterize the diamond films. In addition, a water-ethanol mixture has been used for homoepitaxial deposition with a full-width-half-maximum narrower than the bulk substrate (2.60 and 2.75 cm^{-1}, respectively). This technique represents a remarkable new approach to the growth of diamond which does not depend on delivery of hydrogen, fluorine, hydrocarbon, or halocarbon gases that have been typically used by other workers. The nucleation density and topography of the polycrystalline diamond films deposited from the water alcohol mixtures are quite sensitive to the choice of alcohol. Water vapor discharges, by producing H atoms and OH radicals, become the functional equivalent to molecular H_2 discharges producing H atoms characteristic of many other diamond chemical vapor deposition techniques.

A variety of techniques have been developed for the deposition of diamond from the gas phase using plasma and thermal activation.[1-10] Early theories of diamond deposition hypothesized that the deposition of diamond was a codeposition process in which both diamond and graphite were being deposited simultaneously.[1,2] Atomic hydrogen produced by dissociation of molecular hydrogen in plasma discharges, arc discharges, or hot filaments dissolves the nondiamond phases from the depositing layer and, thus, promotes the diamond phase. Recently, oxyacetylene torches have been used to grow diamond films.[9,10] The oxyacetylene flame, in addition to forming H_2O, CO, and CO_2 by-products, provides atomic hydrogen to the growth surface. Many gaseous carbon sources have been used for the deposition of diamond. Hydrocarbons, halocarbons, fluorocarbons, and alcohols have all been used in the deposition of diamond films. In a plasma or a thermally activated process, those carbonaceous gases are driven toward their high-temperature, equilibrium product distributions. Not surprisingly, the quality of the diamond films does not depend as critically on the carbon source as it depends on the C/H ratio, or perhaps more appropriately, the C/H/O ratio in the gas phase.[11] If one examines the list of radicals and gases which gasify graphite, H atoms, F atoms, and F_2 molecules are included on the list.[12] Also present on the list are O atoms, OH radicals, and O_2 molecules. Oxygen has certainly been added to diamond producing environments, either by using carbon carriers containing oxygen or through intentional addition of oxygen to the gas stream in microwave discharges. Indeed, Buck *et al.*[13] have deposited diamond in a relatively limited set of conditions using only methanol or methanol/Ar mixtures. Initial microwave plasma results showed an improvement in diamond growth with a small percentage of O_2 addition, but they also showed a degradation in crystalline quality for films deposited with more than 2% O_2 addition.[14] However, more recently, the work of Bachmann, Leers, and Lydtin,[11] and Chen, Hon, and Lin[15] has demonstrated that higher oxygen concentrations can certainly yield diamond deposition with correspondingly higher carbon concentrations.

We report here on a novel, low temperature growth technique for the chemical vapor deposition (CVD) of diamond films from low-pressure, rf-plasma discharges containing principally water vapor. Carbon for diamond deposition was supplied to the plasma gas by admitting alcohol vapor with the water vapor. No other gases were admitted to the growth chamber. Hence, this work is quite different from the work of Saito *et al.*[16,17] wherein 0%–6% concentrations of water in H_2-CH_4 microwave plasmas were investigated for diamond growth. In this letter, predominantly water-based discharges produce OH and H radicals. The water discharge becomes functionally equivalent to hydrogen discharges in other diamond CVD techniques. Emission from a pure water discharge and the water-alcohol discharges described in this letter show strong H_α emission and OH emission. The atomic hydrogen emission from a pure water rf-plasma discharge at 1.0 Torr is so dominant that the plasma has a characteristic red color from the 656 nm emission. The ratio of water to alcohol admitted to the growth chamber was fixed by the partial pressures of water and alcohol above the mixed solutions of 20% alcohol in water. In addition to polycrystalline growth, homoepitaxial diamond growth has been accomplished.

Study of polycrystalline diamond growth in the water vapor system was undertaken using Si(100) substrates. Prior to introduction into the growth chamber, the samples were subjected to polishing with graphite fibers[18] and/or

 0003-6951/92/030329-03$03.00

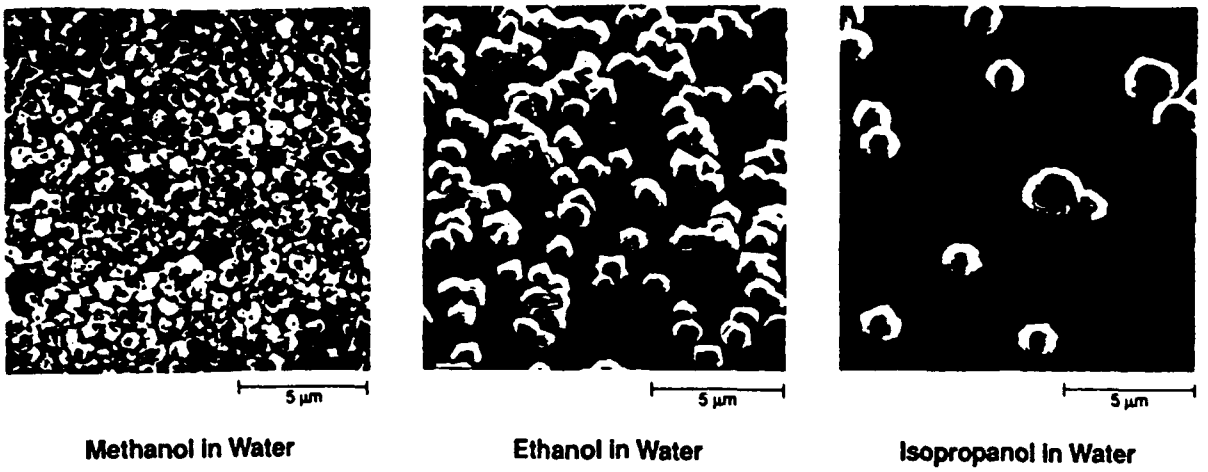

FIG. 1. SEM micrographs of the polycrystalline deposits on Si(100) obtained using water/methanol, water/ethanol, and water/isopropanol.

diamond paste to promote nucleation. Descriptions of the growth system have been reported elsewhere.[19] The samples are located on a graphite susceptor just beneath a three-turn rf induction coil. The rf induction coil maintains the water vapor discharge and heats the graphite susceptor upon which the sample is located. The liquid mixture is stored in a metal flask connected to the vacuum chamber. The water vapor/alcohol gas mixture is metered into the chamber at a rate of ~ 20 sccm. The vapor mixture was admitted into the metal vacuum cross at the base of the plasma tube. The ratio of water to alcohol admitted is determined by the product of the mole fractions of water and alcohol and the respective vapor pressures of the water and the selected alcohol. A process pressure control valve is used to vary the effective pumping speed in order to maintain a pressure in the growth chamber of 1 Torr. To initiate deposition, a 1000 W, 13.56 MHz signal is applied to the rf coil. The power level results in a sample temperature of 625 °C during deposition. Following 2 h of deposition, the samples were removed from the reactor and examined with a scanning electron microscope (SEM) prior to Raman analysis. Figure 1 shows electron micrographs of the samples deposited for 2 h using water vapor mixtures containing either methanol, ethanol, or isopropanol. The micrographs show that the nucleation is highly dependent on the choice of alcohol. The alcohols with the higher vapor pressures nucleate at a higher density. If one uses the average crystallite size as a measure of the growth rate, the growth rate does not vary considerably with the choice of alcohol. However, the morphology of the diamond crystallites does change as the alcohol molecular group becomes larger. Using methanol or ethanol, the crystallites growing from the nucleation sites are composed of individual diamond crystals, some of which appear to be twinned. Using isopropanol, the crystallites growing from the nucleation sites are composed of many diamond crystals clustered about the nucleation site. Raman spectroscopy from all the samples (see Fig. 1) shows a distinct 1332 cm^{-1} diamond longitudinal optical peak on a broad background which is centered around 1500 cm^{-1}. Figure 2 shows the Ramanspectra for the water/methanol, water/ethanol, water/isopropanol growths.

In addition to polycrystalline growth on Si(100) substrates, homoepitaxial growth on a natural Type IA diamond (100) substrate was accomplished using a water/ethanol mixture equivalent to the one used for the polycrystalline growth. The Raman spectrum from the homoepitaxial deposition did not exhibit any scattering from the 1500 cm^{-1} nondiamond material. The full-width-half-maximum (FWHM) of the homoepitaxial layer, as determined using micro-Raman focused on the epitaxial layer, is 2.60 cm^{-1}. Examination of the bulk substrate by performing micro-Raman on the opposite substrate face from the

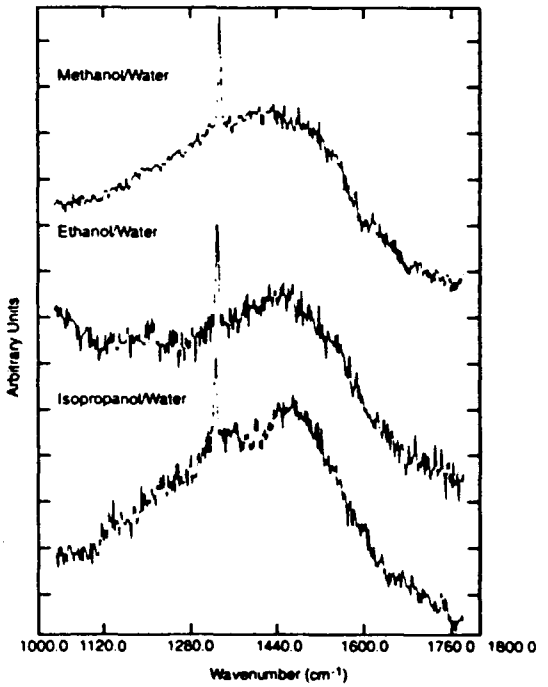

FIG. 2. Raman spectra from the polycrystalline deposits on Si(100) obtained using water/methanol, water/ethanol, and water/isopropanol.

epitaxial layer found the FWHM of the bulk material to be 2.75 cm^{-1}. Hence, the growth using water/ethanol produced a diamond epitaxial layer of apparently higher structural perfection than the starting natural diamond crystal.

This work clearly demonstrates that water vapor discharges can promote diamond growth. Attempts to grow diamond with only methanol vapor admitted to the reactor resulted in poor nucleation and growth. Faceting was not observed on any of the diamond particles grown using only methanol. These results contrast the results of Buck *et al.*,[13] where microwave discharges of pure methanol deposited well-faceted diamond. Conversely, attempts to deposit diamond with only water vapor admitted to the reactor (in the attempt to grow by chemical vapor transport from carbon on the graphite susceptor) resulted in no deposition. The water vapor discharges contribute both OH and H radicals to the growth environment. Obviously, the activation or production of atomic hydrogen from water vapor and from molecular H_2 will be different. We have no way to *in situ* measure the relative production of atomic hydrogen in these processes; however, we can measure the relative dissolution rates of solid graphite for the two processes by measuring dimensional changes on the graphite susceptor. The water process at 1000 W and 1 Torr etches graphite at approximately 25 μm/h as compared to 5 μm/h for the H_2 process at 2000 W and 5 Torr. Hence, it is observed that the water process at lower pressure and lower power produces a much higher graphite etch rate. Despite this higher gasification rate, no chemical vapor transport growth is observed. Alcohol must be added to the water for diamond growth to occur.

The authors cannot dismiss the possibility that the water vapor discharge is merely a hydrogen source and that the role of OH in diamond deposition is minor. However, growth of diamond in the same reactor using H_2-CH_4 rf discharges produces high-quality diamond, but only at much higher pressures and higher power levels. Typically, 5.0 Torr and 2500 W of rf power input are necessary for well-faceted crystallites when 1% CH_4 in H_2 discharges are used. Furthermore, in the H_2-CH_4 rf discharges, the ratio of carbon to hydrogen in the gas phase is small, typically less than 2% for high-quality diamond growth. Using the vapor pressures of water and methanol, the ratio of carbon to hydrogen to oxygen in this process is calculated to be 1:6:2. Emission spectra from water-alcohol discharges are dominated by emissions from the atomic hydrogen Balmer series. In addition, OH emission is observed. Emission from atomic O was not observed.

In conclusion, we have demonstrated the growth of polycrystalline diamond films from rf-plasma discharges fed solely by water and alcohol vapors. Characterization of the films by SEM shows the films to be well faceted with the choice of alcohol effecting the nucleation density and the crystal habit. Characterization of the films by Raman spectroscopy shows the polycrystalline films to be diamond with some nondiamond bonding. Raman spectroscopy shows the single-crystalline homoepitaxial films to have a FWHM of 2.60 cm^{-1} which is narrower than the starting natural crystal whose FWHM was 2.75 cm^{-1}. This technique represents a remarkable method for the manufacture of diamond films through the use of noncorrosive, nonexplosive, and relatively inexpensive sources. Design and implementation of growth systems using water-based processes should be straightforward and should avoid the complexities, the safety hazards, and the expense of H_2 or halogen gas processing.

The authors wish to acknowledge the financial support of the Strategic Defense Initiative/Innovative Science and Technology Office through the Office of Naval Research, Contract No. N-00014-86-C-0460. The authors also wish to thank M. J. Mantini, A. D. Brooks, S. A. Ammons, and R. V. Durkee for technical support of this work.

[1] B. Derjaguin and V. Fedoseev, Russ. Chem. Rev. 39, 783 (1970).
[2] B. V. Spitsyn, L. L. Bouilov, and B. V. Derjaguin, J. Cryst. Growth 52, 219 (1981).
[3] S. Matsumoto, Y. Sato, M. Kamo, and N. Setaka, Jpn. J. Appl. Phys. 21, 183 (1982).
[4] Y. Hirose and Y. Teresawa, Jpn. J. Appl. Phys. 25, L51 (1986).
[5] M. Nakazawa, T. Nakashima, and S. Seikai, Appl. Phys. Lett. 45, 823 (1984).
[6] M. Kamo, Y. Sato, S. Matsumoto, and N. Setaka, J. Cryst. Growth 62, 642 (1983).
[7] S. Matsumoto, M. Hiro, and T. Kobayashi, Appl. Phys. Lett. 51, 737 (1987).
[8] K. Kurihara, K. Sasaki, M. Kawarada, and N. Koshiro, Appl. Phys. Lett. 52, 437 (1988).
[9] L. M. Hanssen, W. A. Carrington, J. E. Butler, and K. A. Snail, Mater. Lett. 7, 289 (1988).
[10] G. Janssen, W. J. P. Van Enckevort, J. J. D. Schaminee, W. Vollenberg, L. J. Giling, and M. Seal, J. Cryst. Growth 104, 752 (1990).
[11] Peter K. Bachmann, Dieter Leers, and Hans Lydtin, Diamond Rel. Mater. 1, 1 (1991).
[12] D. E. Rosner and J. P. Strakey, J. Phys. Chem. 77, 690 (1973).
[13] M. Buck, T. J. Chuang, J. H. Kaufman, and H. Seki, Mater. Res. Soc. Symp. Proc. 162, 97 (1990).
[14] J. A. Mucha, D. L. Flamm, and D. E. Ibbotson, J. Appl. Phys. 65, 3448 (1989).
[15] C. F. Chen, T. M. Hon, and C. L. Lin, presented at 18th Int. Conf. on Metallurgical Coatings and Thin Films (ICMCTF), San Diego, CA, April 23, 1991.
[16] Yukio Saito, Kouji Sato, Hideaki Tanaka, Kazunori Fujita, Shinpei Matuda, J. Mater. Sci. 23, 842 (1988).
[17] Yukio Saito, Kouji Sato, Kenichi Gomi, Hiroshi Miyadera, J. Mater. Sci. 25, 1246 (1990).
[18] R. A. Rudder, G. C. Hudson, R. C. Hendry, R. E. Thomas, J. B. Posthill, and R. J. Markunas, Materials Science Monograph 73, 395 (1991).
[19] R. A. Rudder, G. C. Hudson, D. P. Malta, J. B. Posthill, R. E. Thomas, and R. J. Markunas, Materials Science Monograph 73, 583 (1991).

Chemical Vapor Deposition of Diamond Films Using Water:Alcohol:Organic-Acid Solutions

R.A. Rudder, J.B. Posthill, G.C. Hudson, D.P. Malta, R.E. Thomas, and R.J. Markunas, T.P. Humphreys[†] and R.J. Nemanich[†]

Research Triangle Institute, Research Triangle Park, NC 27709-2194

[†] Dept. of Physics, North Carolina State University, Raleigh, NC 27695-8202

ABSTRACT

A low pressure chemical vapor deposition technique using water-alcohol vapors has been developed for the deposition of polycrystalline diamond films and homoepitaxial diamond films. The technique uses a low pressure (0.50 - 1.00 Torr) rf-induction plasma to effectively dissociate the water vapor into atomic hydrogen and OH. Alcohol vapors admitted into the chamber with the water vapor provide the carbon balance to produce diamond growth. At 1.00 Torr, high quality diamond growth occurs with a gas phase concentration of water approximately equal to 47% for methanol, 66% for ethanol, and 83% for isopropanol. A reduction in the critical power necessary to magnetically couple to the plasma gas is achieved through the addition of acetic acid to the water:alcohol solution. The lower input power allows lower temperature diamond growth. Currently, diamond depositions using water:methanol:acetic-acid are occurring as low as 300 °C with only about 500 W power input to the 50 mm diameter plasma tube.

INTRODUCTION

To date, diamond films produced by chemical vapor deposition techniques have been grown principally using heavy dilution of organic gasses with molecular hydrogen.[1-12] The role of molecular hydrogen to the process is manifold, but the dissociation of molecular hydrogen into a high fraction of atomic hydrogen is critical to diamond stabilization and growth. A plethora of techniques have been applied to create concentrations of atomic hydrogen sufficient for high quality diamond growth. Typically, these techniques involve a high-temperature region (hot-filament, oxy-acetylene torch, microwave plasma, dc arc discharges, etc.) wherein high dissociations of molecular hydrogen is feasible. Some workers have avoided the use of molecular hydrogen by using source gasses rich in oxygen.[8-10] Other workers have augmented the molecular hydrogen with small percentages of water.[11-12] We report here on a low pressure rf-inductive plasma-assisted chemical vapor deposition technique for the growth of diamond which uses water not molecular hydrogen as a process gas stabilizing diamond growth. Atomic hydrogen necessary for diamond growth (in this process) is supplied from plasma-dissociation of water and alcohol vapors. Unlike previous work, addition of water to the alcohol is necessary to produce well-facetted diamond growth in this low pressure rf-plasma technique.[9] Furthermore, it has been observed that addition of acetic acid to this CVD process enables diamond growth to occur at reduced rf power levels and consequently at lower substrate temperatures

EXPERIMENTAL APPARATUS AND APPROACH

A description of the chemical vapor deposition system used in this work has been previously reported.[13-14] The system produces diamond from both traditional H_2 - CH_4 mixtures as well as the water:alcohol:organic-acid solutions. The system consists of a 50 mm id plasma

Mat. Res. Soc. Symp. Proc. Vol. 242. ©1992 Materials Research Society

tube appended to a standard six-way cross. A radio frequency (13.56 MHz) induction coil couples power from the rf power supply into the plasma discharge. Samples are located on a graphite carrier located immediately underneath the induction plasma. The rf excitation induces currents in the graphite susceptor which serve to heat the sample. Samples are introduced into the vacuum system via a vacuum load-lock which isolates the main chamber. The gasses (water, alcohol, acetic-acid) are introduced into the chamber through a leak valve on a storage tank which contains solutions of the water/alcohol or water/acetic-acid/alcohol. Vapors above the liquid are pumped from the storage tank into the growth chamber. The vapor pressure of the constituents above the liquid should be a produce of their molar concentration and their respective vapor pressures. Water and alcohol solutions at room temperature have sufficient vapor pressures to supply a low pressure discharge (< 10 Torr). High pressure operations might require the liquid solutions to maintained at an elevated temperature. For the growths reported here, vapors from various volumetric mixtures have been evaluated for diamond growth. The leak rate into the growth chamber from the solutions results in a loss of ~ 0.2 cc/min from the liquid solutions. While there will be some depletion of the higher vapor pressure component, the practice of mixing allows a convenient method for evaluating different ratios of water-to-alcohol without the necessity of a gas manifold.

Samples are introduced to the growth system through a vacuum load lock. Prior to insertion, samples have been subjected to a diamond abrasive treatment with 1 μm diamond paste to enhance nucleation. Diamond growth proceeds by initiating a rf induction plasma with sufficient power to magnetically couple to the gas. J. Amorrim et al.[15] have shown that rf coils couple to the plasma gas at low power levels through *E*-field coupling. At higher power levels, the rf coil couples power to the plasma gas through *B*-field coupling. The *B*-field coupling is characterized by an intense plasma luminescence from a region of high density electrons, $\sim 10^{12}$ cm^{-3}. The *E*-field coupling at lower powers results only in a low density plasma, $\sim 10^{10}$ cm^{-3} with weak plasma luminescence. Introduction of water vapor alone to a low pressure (1.0 Torr) rf inductive discharge results in intense atomic H emission. The water plasma has a characteristic red color associated with atomic H emission at 656 nm. OH emission lines are clearly visible but not as dominant as the atomic H emission lines. One thus observes that water discharges are capable of generating ample atomic H along with OH from the water dissociation. Atomic O lines, if pesent in the emission spectrum, are minor and have not been identified at this time. Addition of alcohol to the water plasma changes the color of the plasma emission to a bluer spectrum as CH and CO emissions are observed along with the atomic hydrogen Balmer lines

EXPERIMENTAL RESULTS

A. Water:alcohol results

We have previously reported the growth of polycrystalline diamond films using water/methanol, water/ethanol, or water/isopropanol mixtures.[16] In that work, the vapor mixture entered the deposition system and diffused from the main chamber into the plasma tube. The vapors were not admitted into the system through the plasma gas feed. For this work, the storage bottle containing the liquid solutions was located on the plasma gas feed. Various water-alcohol mixtures were used to determine the effect of the C/O ratio on diamond growth. Figure 1 shows SEM micrographs from samples deposited at 1.0 Torr from volumetric water-methanol mixtures ranging from 80% methanol to 33% methanol. The results for 80% methanol produce poorly faceted diamond. These results contrast remarkably from the work

by Buck et al and Bachmann et al. in a microwave discharge at higher pressures using 100% methanol. In that work, high quality diamond was obtained from only methanol. In this work, water addition to the methanol is critical to the formation of well-faceted crystalline diamond. As observed in Figure 1, the quality of diamond growth increases as the methanol volumetric concentration is reduced. At 33% methanol in the water solution, well-faceted diamond growth is observed. From the respective vapor pressures of water and methanol at 20°C, we estimate the vapor pressures of water and methanol to be 11.7 and 31.5 Torr, respectively, above the 33% methanol mixture. Using these vapor pressures, one calculates the C/C+O, the O/O+H, and the H/C+H ratios to be 0.42, 0.22, and 0.83, respectively. According to the deposition phase diagram of Bachmann, the low C/C+O ratio of 0.42 should result in no diamond growth. Nonetheless, this oxygen rich ratio is necessary for diamond growth in this system. As noted in the Bachmann work, actual gas phase concentrations may vary due to interactions of the plasma with the carbonaceous walls of the reactor. In this case, the reactions of the water-vapor plasma with the graphite susceptor undoubtedly increase the carbon concentrations in the gas phase. The graphite susceptor has been observed to be etched by the water-alcohol discharges at a rate of 25/h.

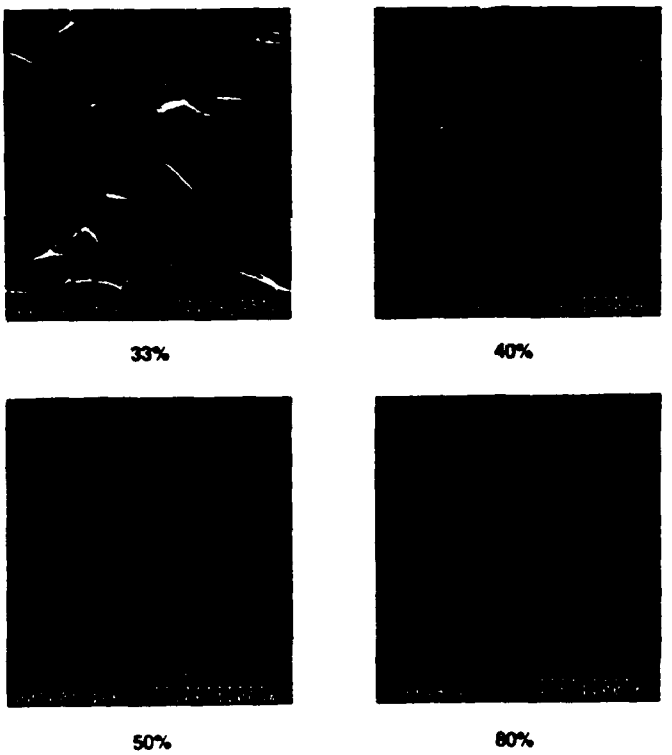

Figure 1. SEM micrographs from diamond films deposited from various volumetric concentrations.

B. Acetic-acid:water:methanol results

It was observed that diamond growth from the water-alcohol solutions required less rf power than diamond growth from more traditional H_2/CH_4. The lower rf power most likely was a consequence of the water-methanol have lower ionization potentials than the H_2 - CH_4 Water, for instance, has an ionization potential of 12.61 eV as compared to an ionization potential of 15.43 eV for H_2. Methanol, for instance, has an ionization potential of 10.84 eV as compared to an ionization potential of 12.64 eV for CH_4. The lower ionization potentials permit lower rf power levels to be applied for sufficient plasma ionization. Correspondingly, we have observed that the addition of organic acids to the water solutions substantially reduces the critical power necessary to magnetically couple to the plasma gas. It is suspected that these organic molecules have even lower ionization potentials than water.

As a consequence, diamond growth in the low-pressure rf-induction plasma can be evaluated at lower substrate temperatures (through reduction in the induced current in the graphite sample carrier). Figure 2 shows SEM micrographs of diamond films deposited at 0.50 Torr using a volumetric mixture of 2:2:1 acetic-acid:water:methanol. The sample temperature

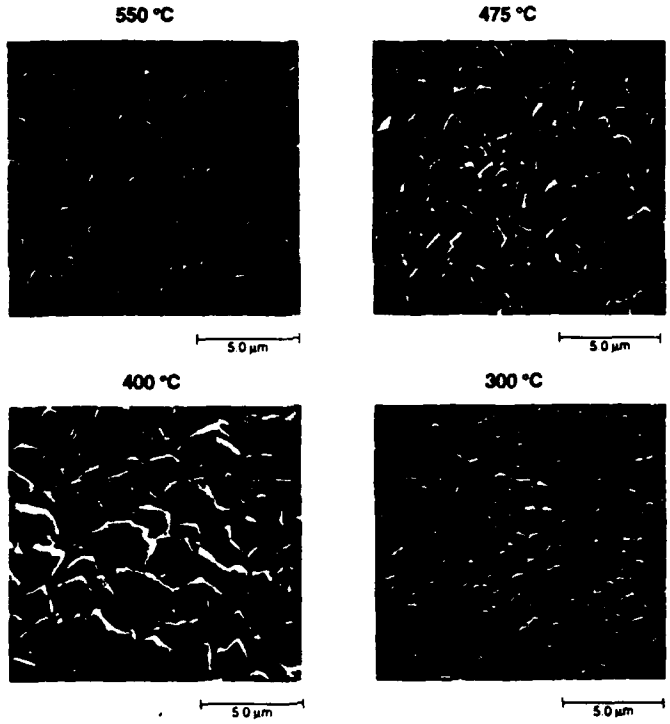

Figure 2. SEM micrographs from diamond films deposited at different temperatures using acetic-acid:water:methanol (2:2:1).

is reduced from one sample to the next by the reduction in rf applied power. The growths at all temperatures show well-faceted diamond polyhedra. There appears to be no severe degradation of the film properties despite the $\sim$ 300 °C reduction in growth temperature. An assessment of the crystalline quality of the films as measured from the full width half maximum of the 1332 cm^{-1} phonon line would tend to indicate that higher quality growth was achieved between 300-400 °C than at higher temperatures. Raman spectra for the films grown at 300 and 400 °C are shown in Figure 3. All these films showed an amorphous carbon component at 1500 cm^{-1}. The reduction in applied power did reduce the deposition rate. The film deposited at 575 °C grew at a linear rate of 6000 Å/hr while the film deposited at 300 °C grew at a linear rate of 2000 Å/hr.

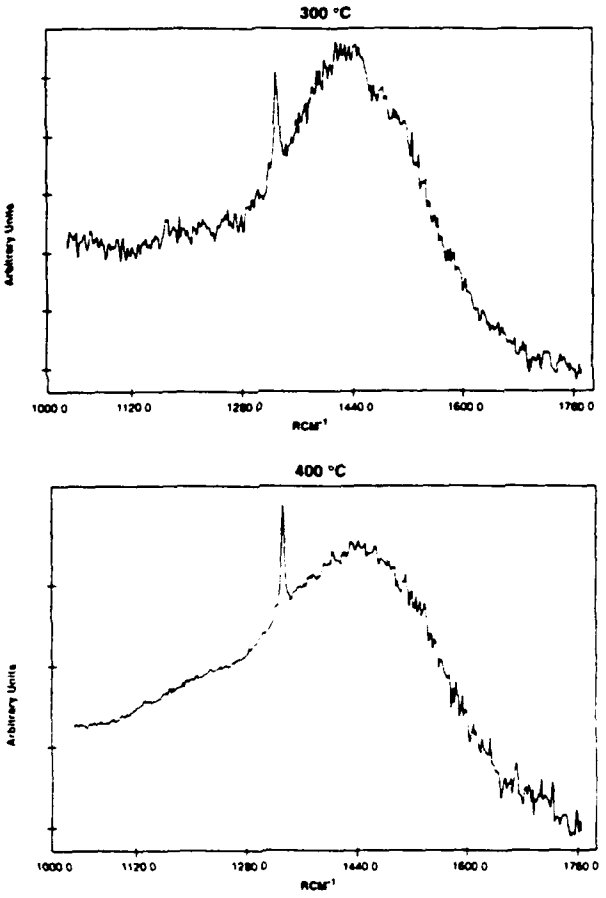

Figure 3. Raman spectra from the films deposited with acetic-acid:water:methanol at 300 and 400 °C.

DISCUSSION

The growth of diamond is undoubtedly facilitated in the low-pressure rf-induction plasma by the high electron density achieved when at a critical power the coupling changes from *E*-field to *B*-field coupling. In this work, we have replaced molecular hydrogen and methane with various mixtures of water, alcohols, and organic acids. The vapor discharges from the water-based solutions are easily ionized in the rf plasma owing to lower ionization potentials for the water, alcohol, and acetic acid molecules. As a consequence, lower power levels are necessary for a *B*-field coupling.

Once the *B*-field coupling occurs, the high electron density and high electron temperature allows atomization of the parent molecules. Atoms and free radicals of both graphite etchant species such as H and OH and carbon-containing radicals are present at the diamond growth surface. Dissociation of those species will depend directly on the bond strengths. If one compares bond-strengths for the various molecules and radical species used in this work, a number of interesting observations are apparent. First, the H-OH bond (5.2 eV) is not significantly weaker than the H-H bond (4.5 eV). Thus, the high generation of atomic hydrogen from water discharges is probably a consequence of the lower ionization potential and a larger cross-section for electron-impact dissociation. Second, the bond strengths for H-liberation for a radical such as CH_2O—H (1.3 eV) from the methanol has a significantly lower dissociation energy than the parent CH_3O—H (4.9 eV) molecule. The CH_2O—H dissociation energy is also significantly lower than any of the energies for methane, methyl, or methylene dissociation. One would expect that electron energies in the plasma sufficient to dissociate hydrogen from the methyl group on methanol would be more than sufficient to dissociate the CH_2O—H bond. And third, the lowest dissociation energies for H- liberation are found for the carboxyl radical COO-H (0.5 eV). These radicals are contained on the organic acid and halogenated organic acid groups. It is the dissociation of this bond that gives the acidity to water solutions containing these organic molecules. One would expect then that, besides the lower ionization potential offered by the addition of the organic acid molecules to the plasma discharge, the organic acids would readily release H atoms to the plasma gas. The organic acid group behaves as graphite solvent in this process. To date, we have not been successful in depositing diamond from solutions of exclusively water and acetic acid. Concentrations of acetic acid in excess of 80% in water solution have not been evaluated. For the concentrations of acetic acid that we are using for the low temperature diamond growth 2:2:1 (acetic-acid:water:methanol), the primary roles of the organic acid group are (1) to promote ionization in the rf induction coil and (2) to contribute H atoms to the growth process.

We have previously been discussing mechanisms by which the water-based processes promote diamond growth in low-pressure rf-induction plasmas. These mechanisms have all been concerned with H- atom generation. At low pressures, diffusion of H atoms to walls and recombination of H atoms on the walls limit the steady-state population of H atoms. The steady state population being the difference of the generation and loss rates. The water-based processed (besides producing higher generation rates per unit power than the molecular-hydrogen based processes) may also significantly reduce the loss rates at low pressure. Water passivation of tube walls in flowing afterglow hydrogen discharges has been used to reduce wall recombination. Water vapor (integral to the diamond growth in this work) would continuously passivate the reactor walls. Indeed, it might be possible to maintain the reactor walls at a temperature low enough to condense multiple layers of water on the plasma tube walls. The water condensate would serve to buffer the wall materials from the extremely aggressive plasma environment. In addition to wall passivation, the water-based process may also reduce loss

rates by permitting H^+ complexing with neutral H_2O water molecules. The hydronium ion H_3O^+ as in acidic-water solutions should remain highly reactive, yet complexed so as to retard rapid diffusion to the plasma walls. It, thus, seems plausible that the water-based processes for diamond growth can enhance diamond growth both by permitting higher generation rates of active species and by reducing loss mechanisms.

CONCLUSION

A low pressure chemical vapor deposition technique using water-alcohol vapors has been developed for the deposition of polycrystalline diamond films and homoepitaxial diamond films. The technique uses a low pressure (0.50 - 1.00 Torr) rf-induction plasma to effectively dissociate the water vapor into atomic hydrogen and OH. Alcohol vapors admitted into the chamber with the water vapor provide the carbon balance to produce diamond growth. Unlike previous results obtained from microwave sources using only methanol or Ar:methanol mixtures, the rf-induction source grows poor quality diamond unless water vapor is admitted. At 1.00 Torr, high quality diamond growth occurs with a gas phase concentration of water approximately equal to 47% for methanol, 66% for ethanol, and 83% for isopropanol. In the operation of the rf induction plasma, there exists a critical power level at which the coupling to the plasma changes from *E*-field coupling to *B*-field coupling. The *B*-field coupling has been shown in Ar plasmas to produce about two orders of magnitude increase in the electron density. We have observed that the critical power to achieve *B*-field coupling is substantially lower for the water-based processes as compared to the traditional molecular hydrogen-based processes. Furthermore, reduction in the critical power necessary to *B*-field couple is achieved through the addition of acetic acid to the water:alcohol solution. The water-alcohol vapors permit diamond growth to occur at lower power levels as compared to the H_2/CH_4 discharges. The lower input power level required in turn reduces substrate-carrier inductive heating and allows lower temperature diamond growth. Currently, diamond depositions using water:methanol:acetic-acid are occurring as low as 300 °C with only about 500 W power input to the 50 mm diameter plasma tube.

ACKNOWLEDGEMENTS

The authors would like to acknowledge the support of this work by SDIO/IST through the ONR Contact No. N0014-86-C0460. The authors would also like to thank R. Durkee, S. Ammons, and D. Brooks for their outstanding technical support of this work.

REFERENCES

1. B. Derjaguin and V. Fedoseev, Russ. Chem. Rev. 39, 783 (1970).
2. B.V. Spitsyn, L.L. Bouilov, and B.V. Derjaguin, J. Cryst. Growth 52, 219 (1981).
3. S. Matsumoto, Y. Sato, M. Kamo, and N. Setaka, Jpn. J. Appl. Phys. 21, 183 (1982).
4. Y. Hirose and Y. Teresawa, Jpn. J. Appl. Phys. 25, L51 (1986).
5. M. Kamo, Y. Sato, S. Matsumoto, and N. Setaka, J. Cryst. Growth 62, 642 (1983).
6. L.M. Hanssen, W.A. Carrington, J.E. Butler, and K.A. Snail, Mater. Letters 7, 289 (1988).
7. G. Janssen, W.J.P. Van Enckevort, J.J.D. Schaminee, W. Vollenberg, L.J. Giling, M. Seal, J. Cryst. Growth 104, 752 (1990).
8. Peter K. Bachmann, Dieter Leers, and Hans Lydtin, Diamond and Related Materials 1, 1 (1991).

9. M. Buck, T.J. Chuang, J.H. Kaufman, and H. Seki, Mat. Res. Soc. Symp. Proc. 162, 97 (1990).

10. C.F. Chen, T. M. Hon and C.L. Lin, presented at 18th Int. Conf. on Metallurgical Coatings and Thin Films (ICMCTF), San Diego, CA, April 23, 1991.

11. Yukio Saito, Kouji Sato, Hideaki Tanaka, Kazunori Fujita, Shinpei Matuda, J. Mater. Sci. 23, 842 (1988).

12. Yukio Saito, Kouji Sato, Kenichi Gomi, Hiroshi Miyadera, J. Mater. Sci. 25, 1246 (1990).

13. R.A. Rudder, G.C. Hudson, R.C. Hendry, R.E. Thomas, J.B. Posthill, and R.J. Markunas, "Applications of Diamond Films and Related Materials", Materials Science Monograph 73, 395 (1991).

14. R.A. Rudder, G.C. Hudson, J.B. Posthill, R.E. Thomas, and R.J. Markunas, Appl. Phys. Lett 59, 791 (1991).

15. J. Amorim, H.S. Maciel, and J.P. Sudano, J. Vac. Sci. Technol. B9, 362 (1991).

16. R.A. Rudder, G.C. Hudson, J.B. Posthill, R.E. Thomas, R.C. Hendry, D.P. Malta, R.J. Markunas, T.P. Humphreys, and R.J. Nemanich, to appear Jan 20, 1992 in Appl. Phys. Lett.

presented at the ICHMS, Breckenridge, CO, March 1992

Chemical Vapor Deposition of Diamond Films From Water-Vapor rf-Plasma Discharges

R.A. Rudder
Research Triangle Institute
P.O. Box 12194
Research Triangle Park, NC 27709-2194
(919) 541-6765
(919) 541-6515 FAX

Abstract:

Both polycrystalline and homoepitaxial diamond films have been deposited from low pressure ($\leq$ 1.0 Torr) rf plasma discharges using vapors from water:alcohol and water:alcohol:acetic-acid solutions. The low pressure rf discharges operate at sufficient power and circulating current so as to inductively couple power from the rf coil to the plasma gas. This inductive coupling results in a high plasma density and high gas dissociation of the water:alcohol vapors. Optical emission spectroscopy and mass quadruple spectroscopy have been used to study the differences between rf capacitively coupled and rf inductively coupled discharges. The inductive discharges appear to be far more dissociative, creating H_2, H_2O, CO, C_2H_2 from the H_2O:CH_4O vapors. The inductive water-based discharges readily produce ample atomic H as evidenced by intense atomic H emission. Besides producing H_2, CO, and C_2H_2 (traditional growth species), the water-based processed contribute OH species to the growth process. These OH species like halogens are highly electronegative and may contribute to the diamond growth process either by stabilization (termination) of the diamond surface with OH or by gasification of surface graphitic components via CO formation.

The water-based processes require far less power input for diamond growth than molecular-hydrogen-based rf discharges. As a consequence, less induction heating occurs in the substrate, and diamond growth proceeds at lower substrate temperatures. Currently, diamond growth near 300°C is possible. The lower power input, the low temperature, the low pressure operation, the availability of rf power, the elimination of explosive gasses from the growth process, all make the new technology an exciting technology for large area diamond manufacture.

Thermal desorption from hydrogenated and oxygenated diamond (100) surfaces

R. E. Thomas, R. A. Rudder, and R. J. Markunas
Research Triangle Institute, Research Triangle Park, North Carolina 27709

(Received 17 December 1991; accepted 3 February 1992)

Low energy electron diffraction (LEED) has been used to study the effects of atomic and molecular species of hydrogen and oxygen on the reconstructed C(100)-(2×1) surface. Thermal desorption spectroscopy was also used to study desorption products and kinetics from hydrogenated and oxygenated surfaces. Atomic hydrogen appears relatively inefficient at breaking C–C dimer bonds on the (100)-(2×1) surface. Atomic oxygen, in contrast, readily converts the surface from the 2×1 state to the 1×1 state. This process is reversible for a limited number of cycles before degradation of the surface obscures the 2×1 LEED pattern. Oxygen is thought to adsorb in one of two configurations, bridging carbon atoms on the surface, or double bonded to a single carbon atom on the surface. Thermal desorption of molecular hydrogen from hydrogenated C(100)-(2×1):H surfaces occurs at approximately 900 °C for a heating rate of 20 °C/s. Molecular hydrogen is the major desorption product and the desorption temperature appears to be coverage independent. Thus the desorption kinetics are most likely first order. Thermal desorption of carbon monoxide from oxygenated C(100)-(1×1):O surfaces occurs at approximately 600 °C for a heating rate of 20 °C/s. Carbon monoxide is the major product seen, with small quantities of carbon dioxide also observed. For increasing oxygen coverages, the desorption peak is observed to shift to lower temperatures. A peak shift to lower temperatures can be interpreted as either first order kinetics with a coverage dependent activation energy or second order kinetics. The reaction order is not known in this case, but from analysis of the peak shapes and from the fact that CO can desorb without prepairing, the data suggest that the reaction is first order.

I. INTRODUCTION

Hydrogen plays an integral role in many of the chemical vapor deposition (CVD) diamond growth processes developed to date.[1] Hydrogen is thought to function in the growth process in a number of ways, including maintenance of sp^3 hybridization of carbon atoms at the growth surface. Oxygen has been used in concentrations of approximately 1%–2% in H_2/CH_4 plasmas to extend the diamond growth regime with respect to gas composition and substrate temperature.[2,3] The role oxygen plays is perhaps more complicated. It has been suggested that oxygen increases the atomic hydrogen concentration through gas phase reactions and also etchs nondiamond carbon.[2] Recently, however, oxygen has been introduced to the growth process in much larger concentrations in the form of water and alcohols.[4] Bachmann *et al.* have assembled data from a variety of growth techniques to produce an empirical H–C–O diamond growth phase diagram.[5] The diagram indicates that diamond can be successfully grown with carbon and oxygen alone. In spite of numerous growth studies, the details of the roles of hydrogen and oxygen in the CVD growth environment are still unclear, as are fundamental questions concerning interactions of these two gasses with the diamond surface. In order to greatly simplify the systems under consideration, we have used a combination of low pressure gas dosing, temperature programmed desorption, and low energy electron diffraction (LEED) to study interactions of relatively simple gasses such as atomic hydrogen and atomic oxygen with a clean diamond surface.

Although similar in structure to the silicon (100) surface, the diamond (100) surface has not been studied nearly as intensively, with only a handful of experimental studies published to date.[6–10] Important questions remain concerning the details of the reconstruction and the effect of adsorbates on surface structure. As with silicon (100) the diamond (100) surface reconstructs to a rotated 2×1 dimer configuration upon heating.[6,8,10] Due to the higher bond strengths in the carbon system the reconstruction does not occur until the diamond is annealed to approximately 1000 °C, as opposed to 450 °C for silicon. There is also evidence that the reconstruction is not necessarily coupled with the thermal desorption of hydrogen from the surface as in the case of silicon. Hamza *et al.* report that both thermal desorption signals and "fast" protons generated by electron stimulated desorption are eliminated below 925 °C.[6] However, they report that the LEED half-order spot intensity does not begin to appear until the sample is annealed at 965 °C.[6]

Adsorption of atomic hydrogen has been reported to convert the surface back to the 1×1 configuration.[6] However, subsequent annealing to 1200 °C did not convert the surface back to the 2×1 configuration.[6] Theoretical calculations indicate a substantial barrier for the insertion of hydrogen into the C–C dimer bond.[11–13] From these calculations it appears difficult to form the dihydride from the

 0734-2101/92/042451-07$01.00

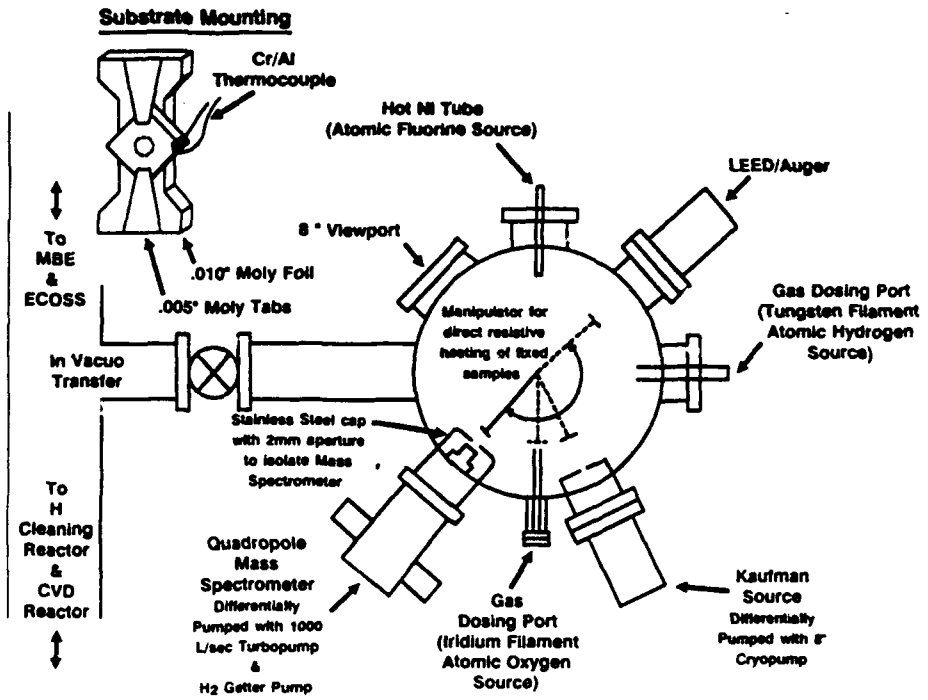

FIG. 1. Schematic view of system. Inset is a drawing showing details of the sample mounting and heater geometry.

monohydride by the exposure of the 2×1 surface to atomic hydrogen at 25 °C.

Oxygen interactions with the (100) surface are less well studied than those of hydrogen. Lurie and Wilson report no observable effect on LEED patterns upon exposure of the (100) surface to molecular oxygen.[10] Matsumoto exposed diamond powder to molecular oxygen at atmospheric pressure and room temperature and at 1 Pa at 500 °C.[14] In the case of the powder desorption, CO desorption peaks were seen at approximately 600 °C. Smaller desorption peaks were seen for CO_2 at approximately 500 °C.

In the present article we have used LEED to study the effects of atomic and molecular species of hydrogen and oxygen on the reconstructed 2×1 surface. Thermal desorption spectroscopy was also used to study desorption products and kinetics from hydrogenated and oxygenated surfaces.

II. EXPERIMENTAL PROCEDURES

Thermal desorption spectroscopy and LEED observations were performed in a stainless steel UHV system shown in Fig. 1. Turbomolecular pumps were used both on the main chamber and to differentially pump the chamber housing the quadrupole mass spectrometer. Additional hydrogen pumping capacity for the quadrupole chamber was provided by a bulk getter pump. Base pressure was 5×10^{-10} Torr for the sample chamber and 1×10^{-10} Torr for the quadrupole chamber. The sample chamber was separated from the quadrupole chamber by a 2 mm diam stainless steel aperture.

Sample heating was accomplished by clipping the crystals to a 0.25 mm thick molybdenum resistive strip heater. (inset Fig. 1) All parts associated with the heater stage, including the clamps and current leads were manufactured from molybdenum. The sample temperature was measured by a 0.125 mm diam chromel/alumel thermocouple threaded through a laser drilled hole in the diamond and held in tension against the crystal. (inset Fig. 1) Sample heating was controlled by feedback from the thermocouple to a silicon controlled rectifier power supply. After an initial warm-up phase, temperature ramps are linear from approximately 150 °C to over 1100 °C.

A series of control experiments were performed to ensure that thermal desorption signals observed actually originated from the sample surface. For both atomic hydrogen and atomic oxygen, samples were dosed in the standard manner and thermal desorptions run with the sample either adjacent to, but not in front of, the aperture, or with the aperture centered on a portion of the sample mounting assembly. No thermal desorption peaks were observed in any of the control experiments.

Two type IIa (100), $5\times5\times0.25$ mm, diamond crystals were used in the course of the present study. Other than thermal cleaning, no technique is available *in situ* for removing surface contamination from the diamond crystals. Particular attention was therefore paid to preparing the diamond surface before mounting in the vacuum system. The samples are initially hand polished for 5 min with 0.25 μm diamond grit and deionized (DI) water on a nylon polishing pad. The samples are then ultrasonically degreased in a series of solvents, trichloroethylene, acetone, methanol, and deionized water. Following the deionized water rinse, the samples are swabbed under DI water to remove particles. The samples are rinsed again in the solvent series and then placed in CrO_3/H_2SO_4 (125 °C) solution for 20 min to remove nondiamond carbon. The sam-

ples are rinsed in DI water and then boiled in a 3:1 solution of HCl/HNO_3 for 20 min to remove any metals contamination. Finally the samples are rinsed in DI water and blow-dried with compressed nitrogen. Samples subjected to this cleaning process typically show a good quality 1×1 LEED pattern at beam voltages as low as 50 V with no annealing. For the initial thermal cleaning the samples were ramped up in temperature at approximately 10 °C/s until the pressure in the main chamber rose to 5×10^{-8} Torr at which point the power was shut off and the samples cooled. This cleaning cycle continued until a maximum temperature of 1150 °C was reached.

In all cases atomic hydrogen was generated via a tungsten filament operating at a temperature of approximately 1500 °C. Filament temperatures were measured with a hand held optical pyrometer. The sample was positioned approximately 2 cm from the filament during dosing. The sample was not actively cooled and at the lowest dosing pressures remained at room temperature. Atomic oxygen was generated via an iridium filament at 1100 °C. Very large scale integrated (VLSI) grade hydrogen and oxygen gasses were used with no further purification. No attempt was made to quantify the percentage of atomic species generated by the filaments. From earlier experiments on silicon (100) substrates, under conditions identical to those used in the present study, we can estimate the degree of molecular hydrogen dissociation. It was found that for unterminated silicon 2×1 surfaces an exposure for 300 s at a chamber pressure of 1×10^{-6} Torr was sufficient to convert the surface to the 1×1 configuration. Therefore, the surface has been exposed to at least one monolayer of atomic hydrogen. The effective pressure at the surface from the doser is probably higher than 1×10^{-6} Torr so the maximum degree of dissociation is approximately 1%. We have not performed similar experiments for oxygen dissociation but given the higher bond strength for the oxygen molecule, 119 kcal/mol, and the lower filament temperature used, we expect the degree of dissociation to be much less than that of molecular hydrogen. All doses quoted in the text are given for the total H_2 and O_2 exposure from uncorrected ion gauge tube readings. X-ray photoelectron spectroscopy was done *ex situ* after extensive dosing with both the tungsten and the iridium filaments and no evidence of metals contamination was seen.

III. EXPERIMENTAL RESULTS

A. Hydrogen dosing studies

Upon annealing more than 90% of the freshly polished surfaces used in the present study exhibited a transformation from the 1×1 configuration to the 2×1 configuration. During the initial annealing sequence the samples would typically show indications of the 2×1 structure at approximately 800 °C, with the transformation completed by 1050 °C on successive anneals. No correlations were observed between sample preparation conditions and failure of the surface to reconstruct.

Initial studies were concerned with exposure of the reconstructed diamond surface to atomic hydrogen. We find that even after extensive dosing with atomic hydrogen the surface remains in a 2×1 configuration. The maximum dose the samples received was approximately 40 000 $L(H/H_2)$. In contrast, a dose of 600 L under identical conditions is sufficient to convert the silicon (100) surface from the 2×1 state back to the 1×1 state. Given that we were unable to convert the surface back to the 1×1 configuration with atomic hydrogen, the subsequent adsorption and desorption experiments were all performed on the 2×1 surface.

In the next series of experiments clean 2×1 surfaces were dosed with varying quantities of atomic hydrogen and thermal desorption spectra were recorded. The primary desorption product observed was molecular hydrogen at approximately 900 °C. Figure 2 shows a series of desorption spectra taken after increasing atomic hydrogen exposures. There is no evidence of a shift in desorption peak temperature as a function of coverage, indicating the desorption process is first order. Exposure of the clean surface to equivalent doses of molecular hydrogen with no heated filament gave no thermal desorption features. Figure 3 shows a plot of integrated H_2 desorption peak area versus hydrogen dose. We can see that uptake for the surface is not linear with dose and that the surface appears to approach saturation while still in the 2×1 configuration. In addition to monitoring hydrogen, masses 12–18, 26–32, and 44 were scanned in the course of the experiments. Small quantities of masses 15, and 26 were observed to desorb from the surface but contamination from the source gas cannot be ruled out at this time.

B. Oxygen dosing results

Exposure of a reconstructed 2×1 surface to a mixture of atomic and molecular oxygen at 1×10^{-6} Torr for 300 s results in conversion of the surface to the 1×1 state. Exposure of an identical surface to a molecular oxygen dose an order of magnitude larger has no apparent affect on the surface structure; the LEED remains in a 2×1 pattern. Annealing of the 1×1:O surfaces to 1000 °C results in the restoration of the 2×1 surface. The cycle can be repeated approximately 10–15 times before the LEED pattern is left with weak first order spots only and a very high background. It should be emphasized that the surface is etched during each CO desorption cycle which may lead to roughening of the surface and deterioration of the LEED pattern.

Figure 4 shows a series of thermal desorption spectra for mass 28 (CO) from a diamond surface. The desorption traces show very broad peaks with a maximum in the desorption rate at approximately 600 °C. We also see a shift to lower desorption temperatures as coverage increases. Figure 5 shows the integrated area under the desorption peaks plotted as a function of total oxygen exposure. The sample shows a steep initial uptake followed by a much slower uptake at the higher exposures. The sample does not completely saturate after a dose of 4500 L although the uptake does decrease markedly.

In addition to mass 28, masses 2,16,17,18,32, and 44 were monitored. Small amounts of mass 44 were observed

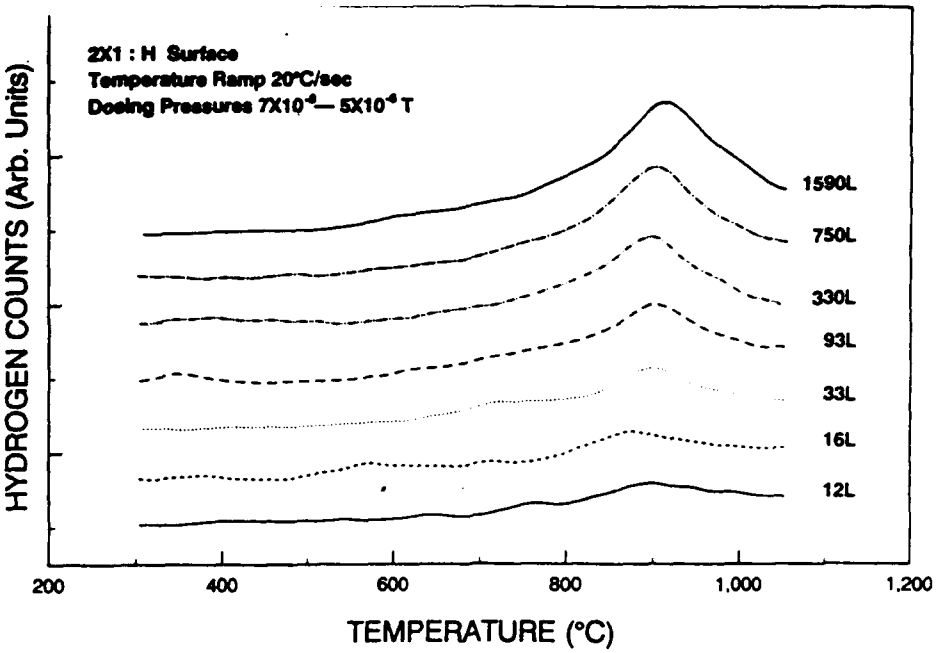

FIG. 2. Thermal desorption spectra from hydrogenated diamond-(2×1) surfaces. Molecular hydrogen was the major desorption product observed from all surfaces dosed with atomic hydrogen. All dosing was performed at 25 °C. Samples were exposed to a mixture of H and H_2 produced by the tungsten filament.

and were presumed to arise from CO_2. Figure 6 shows a comparison of the mass 44 thermal desorption and the mass 28 from the same desorption experiment. Note that the vertical scale for mass 44 has been expanded by a factor of 4. The maximum desorption rate occurs at approximately 550 °C for both masses but the CO_2 peak is much more asymmetric than the CO peak.

IV. DISCUSSION

Reconstruction of the diamond (100) surface to the 2×1 state is a well documented phenomena.[6–8,10] However, most researchers report that a percentage of the freshly polished surfaces studied do not reconstruct to the 2×1 structure upon annealing. Hamza *et al.* have reported an association between residual oxygen on the surface detected by electron stimulated desorption and the ability of the surface to reconstruct.[6] Samples with the most oxygen detected were less likely to reconstruct. Given the surface preparation techniques available (both *in situ* and *ex situ*) for diamond, it seems reasonable to assume that surface contamination may explain the failure of some samples to reconstruct. The effect of impurities on surface reconstruction has been noted in a number of other systems including silicon and platinum.[15]

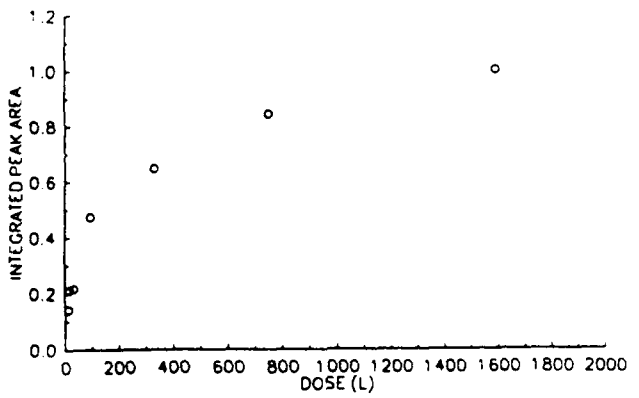

FIG. 3. Plot of H_2 integrated peak area vs total dose H/H_2. The peak areas were normalized to the largest H_2 area measured.

Conversion of the surface back to the 1×1 state by exposure to atomic hydrogen has been studied in detail by only one other group.[6] Results reported by Hamza *et al.* indicated that the surface converted to the 1×1 configuration upon dosing with atomic hydrogen at 180 K coupled with annealing at 700 K.[6] LEED patterns disappeared following the dosing and the 1×1 pattern was then seen after annealing.[6] We see no evidence of either obscuration of the LEED pattern following dosing or of a reversion to the 1×1 surface structure. The LEED patterns gradually deteriorated with repeated dosing and desorption cycles until only weak first order spots remained coupled with a very high background. One expects the dimer bond on the C(100)-(2×1) surface to be stronger than what is seen on the Si(100)-(2×1) surface given the greater C–C bond strength, 83 kcal/mol versus 46 kcal/mol for Si–Si, and the ability of carbon to form double bonds. Calculations of hydrogen addition to the 2×1 surface by several groups indicates that there is an energy barrier to the breaking of the dimer bond by the addition of atomic hydrogen.[11–13] Verwoerd[10] calculates an energy barrier of approximately 39 kcal/mol, an energy barrier of 34.1 kcal/mol was estimated by Zheng, and Smith,[12] and 48.7 kcal/mol by Tho-

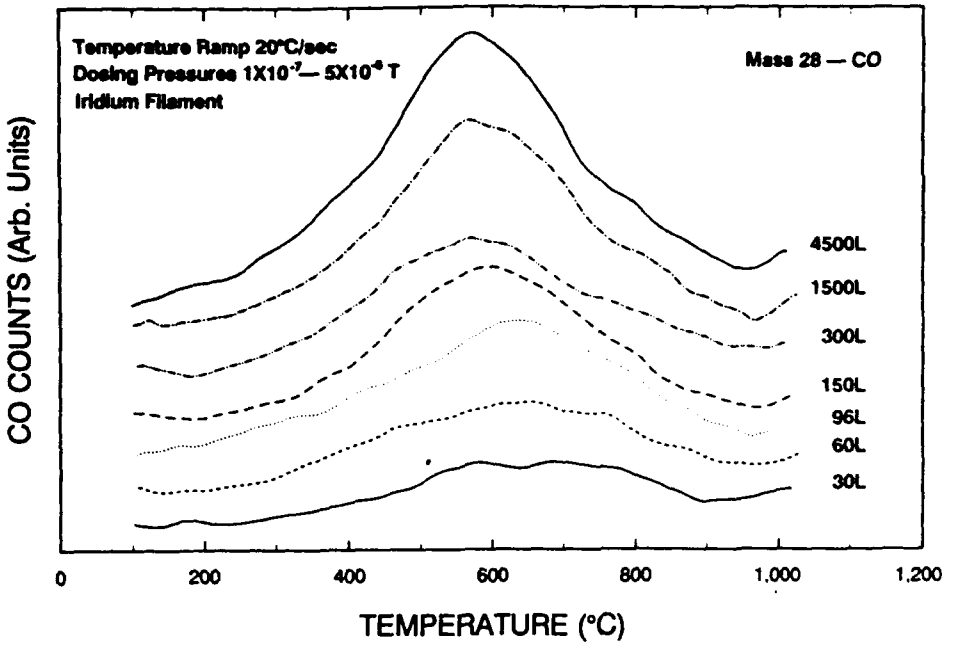

FIG. 4. Thermal desorption spectra showing CO desorption from oxygen dosed diamond surfaces. Samples were exposed to a mixture of O and O_2 after molecular oxygen was passed over an iridium filament.

mas *et al.*[13] Yang and D'Evelyn have argued that steric constraints severely limit the ability of the surface to saturate in the dihydride phase, and at most the surface assumes a disordered dihydride with random dihydride units scattered among monohydride pairs.[16] Based on these results it appears unlikely that adsorption of atomic hydrogen at room temperature will result in a conversion to the dihydride state.

As noted above, since we were unable to obtain a 1×1 structure by hydrogen adsorption, all desorption results discussed here are from a 2×1 surface. Saturation coverage for the 2×1 surface corresponds to one hydrogen atom per carbon atom. We see no evidence of a peak shift with respect to surface coverage to within the resolution of the measurement, (10 °C). The lack of a peak shift argues for first order desorption kinetics. Application of the rate equation with an assumed frequency factor of 10^{13}/s gives 72.7 kcal/mol for the activation energy of desorption. Although we have only observed a single desorption peak, Hamza *et al.* have measured hydrogen evolution by electron stimulated desorption from diamond (100) surfaces at temperatures above the thermal desorption peak.[6] We have no means of directly measuring hydrogen on the diamond surface and it may be that there are higher energy bonding sites available to the hydrogen. The maximum desorption temperature used in the present study was 1150 °C. No evidence of additional desorption features were observed up to the maximum temperature. If in fact there are additional sites available, then with the temperatures used in the present study we are probing only a portion of the bonding sites. In control experiments several samples were dosed with atomic hydrogen and then had thermal desorption spectra collected. After cooling, the samples were ramped in temperature again with no intentional dosing. No thermal desorption features were observed for these samples. If there are multiple sites it is apparently not easy for hydrogen to diffuse between the sites.

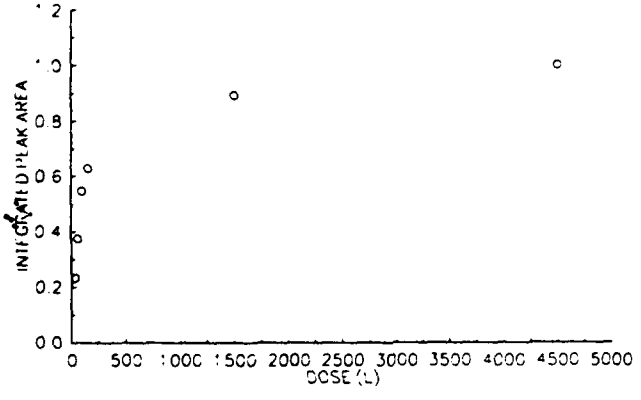

FIG. 5. Plot of CO integrated peak area vs total dose of O/O_2. As in Fig. 3, the peak areas were normalized to the largest CO peak area measured.

Oxygen behaves in a very different fashion than hydrogen on the diamond surface. The most dramatic difference is the apparent ability of atomic oxygen to break the C–C dimer bonds on the surface. We have no effective method of monitoring products formed during dosing as a result of atomic oxygen interactions with the diamond surface. As such, the oxygen may be etching the C–C dimers from the surface and then attaching oxygen atoms to the bulk crystal structure. The other case of course is for oxygen to attack the dimers directly and break the dimer bond.

Once the oxygen has attached to the surface there are several possible bonding configurations. The oxygen could bridge two adjacent carbon atoms with a single bond to

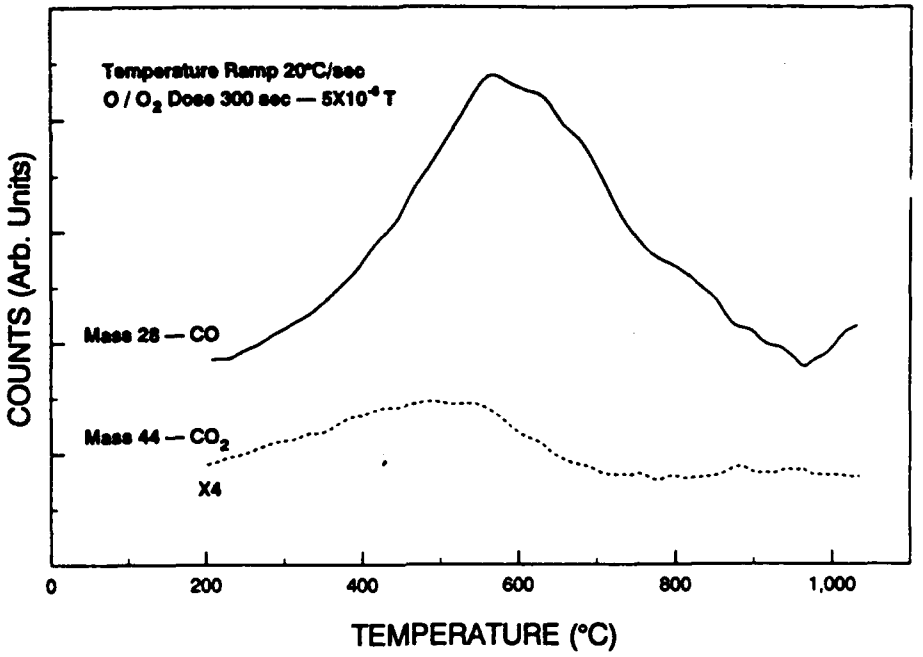

FIG. 6. This desorption spectrum shows both mass 28 (CO) and mass 44 (CO_2) as taken simultaneously from an O/O_2 dosed sample. The mass 44 vertical scale has been expanded by a factor of 4 for clarity.

each, as shown in Figure 7. Table I shows the bond angle oxygen would have to assume in the bridging configuration. At 125°, the angle is well within the range of bond angles that oxygen assumes in various molecules. In order to calculate the bond angle the C–O bond length was taken as 1.43 Å and the separation distance between the two carbon atoms that the oxygen bridges was taken as 2.52 Å.

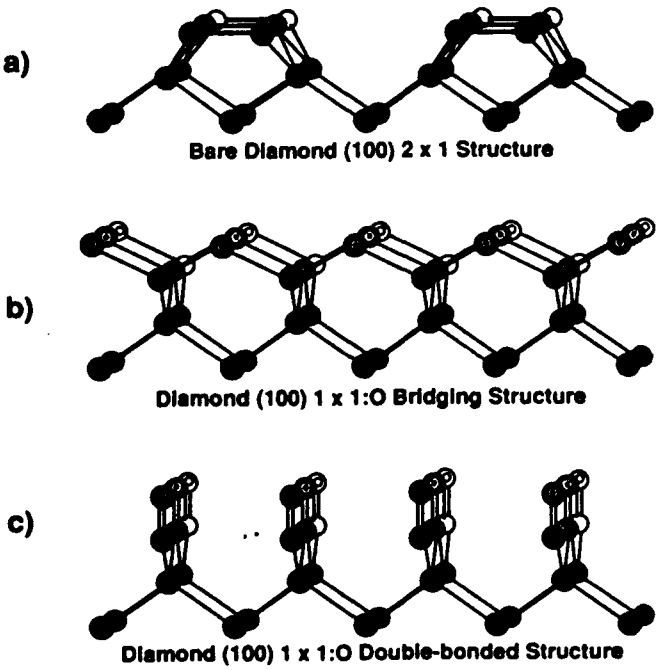

FIG. 7. (a) shows a clean diamond (100) surface in the 2×1 configuration. (b) and (c) show 2 possible oxygen bonding configurations which would give a 1×1 LEED pattern.

Another possibility is for each oxygen to double bond to a single carbon as shown in Fig. 7. One would expect 1×1 LEED patterns from both of these bonding configurations so it may be difficult to distinguish between the two cases on the basis of qualitative electron diffraction. Based on the models described above, oxygen should exhibit very different behavior on the diamond (111) surface. On the unreconstructed diamond (111) surface there is only one dangling bond available. In order to satisfy both oxygen bonds the adsorbed oxygen will either have to break a C–C bond or try and bridge two dangling bonds.

Results from thermal desorption experiments indicated that as the coverage increased the temperature for the maximum CO desorption rate decreased. This can be interpreted as either a first order desorption with a coverage dependent activation energy or a second order desorption process. One might expect desorption of CO from the surface to be first order rather than second order as there is no requirement for pairing of atoms prior to desorption. For a first order process we would expect to see an asymmetric peak with the high temperature side of the peak more steeply sloped. In fact the asymmetry appears to be in the opposite direction with the high temperature side of the

TABLE I. Bonding angles of oxygen.

Molecule	Bond angle (deg)		Bond length (Å)
Water	104	O–H	0.96
α-quartz	144	O–Si	1.6
Methyl ether	110	O–C	1.43
Diamond	125	O–C	1.43(assumed)

peak less steeply sloped than the low temperature side. One explanation for the asymmetry may be additional peaks on the high temperature side of the main peak. A slower heating rate, perhaps 1 °C/s may resolve any additional peaks which may be present. Figure 7 shows two possible bonding configurations for oxygen on the diamond surface. Although it does not appear that LEED can distinguish the two cases the desorption process may be radically different for the two. For the bridging structure, two C–C bonds and two C–O bonds need to be broken to desorb a CO pair, while for the double-bonded structure only two C–C bonds need be broken. It is not clear if both structures coexist on the surface after atomic oxygen dosing but if that is the case one may expect desorption from the bridging structure to be a higher energy process and thus occur at a higher temperature than from the double-bonded structure. Supporting evidence for additional CO peaks above 600 °C comes from powder desorption work done by Matsumoto.[14] Matsumoto has measured oxygen desorption from diamond powders exposed to molecular oxygen at temperatures between 420 and 554 °C.[14] Adsorption was done at a pressure of 1 Pa. CO peaks are seen at 600 and 800 °C for heating rates of 20 °C/min. A smaller CO_2 peak is seen at approximately 500 °C. The heating rate used by Matsumoto *et al.* is a factor of 60 slower than the rate used in the study reported here. One might expect the peak to shift down in temperature as a result of the slower heating rate.

The peaks seen for CO desorption are very broad, with a full width at half-maximum (FWHM) of approximately 350 °C for the highest coverages. Hydrogen desorption peaks in contrast had a FWHM of about 100 °C. Part of the peak width may be explained if in fact there are additional peaks in the CO desorption curves. Relatively broad CO desorption peaks, FWHM approximately 300 °C, are also observed from from oxygen dosed single crystal graphite surfaces.[17] It is interesting that two peaks, 800 and 1000 °C, were recorded from these surfaces.

V. CONCLUSIONS

Thermal mass desorption and LEED have been used to study and contrast atomic hydrogen and atomic oxygen interactions with the diamond (100)-(2×1) surface. Atomic hydrogen appears relatively inefficient at breaking C–C dimer bonds on the (100)-(2×1) surface. Atomic oxygen, in contrast, readily converts the surface from the 2×1 state to the 1×1 state. This process is reversible for a limited number of cycles before degradation of the surface obscures the 2×1 LEED pattern. Oxygen is thought to adsorb in one of two configurations, bridging carbon atoms on the surface, or double bonded to each carbon atom on the surface.

Thermal desorption from hydrogenated C(100)-(2×1):H surfaces occurs at approximately 900 °C for a heating rate of 20 °C/s. Molecular hydrogen is the major desorption product and the desorption temperature appears to be coverage independent. Thus the desorption kinetics are most likely first order. Thermal desorption from oxygenated C(100)-(1×1):O surfaces occurs at approximately 600 °C for a heating rate of 20 °C/s. Carbon monoxide is the major desorption product seen, but small quantities of carbon dioxide were also observed. For increasing oxygen coverages, the desorption peak is observed to shift to lower temperatures. The reaction order is not known in this case, but from analysis of the peak shapes and from the fact that CO can desorb without prepairing, the data suggest that the reaction is first order. Clear differences exist between the behavior of hydrogen and oxygen on the diamond (100) surface. Oxygen is able to convert the 2×1 surface back to the 1×1 configuration whereas hydrogen appears relatively inefficient at this process. Although the dosing studies were performed at room temperature the results may help to explain the role of oxygen in H_2/CH_4 growth environments. If surface dimers form during the growth process it appears that atomic hydrogen is relatively inefficient at breaking the dimer bonds. Atomic oxygen appears to restore the surface much more efficiently than atomic hydrogen.

ACKNOWLEDGMENTS

The authors wish to thank R. Alley, R. Hendry, C. Jones, and D. Brooks for technical support on this research. The financial support of the Strategic Defense Initiative Organization/Innovative Science and Technology Office through the Office of Naval Research (N-00014-86-C-0460) is gratefully acknowledged.

[1] See references in *Proceedings of the Second International Conference on New Diamond Science and Technology*, edited by R. Messier, J. T. Glass, J. E. Butler, and R. Roy (Materials Research Society, Pittsburgh, PA, 1991).
[2] J. A. Mucha, D. L. Flamm, and D. E. Ibbotson, J. Appl. Phys. **65**, 3448 (1989).
[3] S. J. Harris, and A. M. Weiner, Appl. Phys. Letts. **55**, 2179 (1989).
[4] R. A. Rudder, G. C. Hudson, J. B. Posthill, R. E. Thomas, R. C. Hendry, D. P. Malta, R. J. Markunas, T. P. Humphreys, and R. J. Nemanich, Appl. Phys. Lett. **60**, 329 (1992).
[5] P. K. Bachmann, D. Leers, and H. Lydin, Diamond Rel. Mater. **1**, 1 (1991).
[6] A. V. Hamza, G. D. Kubiak, and R. H. Stulen, Surf. Sci. **237**, 35 (1990).
[7] B. B. Pate, Surf. Sci. **165**, 83 (1986).
[8] R. E. Thomas, R. A. Rudder, and R. J. Markunas, *Proceedings of the Second International Symposium on Diamond Materials*, edited by A. J. Purdes, J. C. Angus, B. M. Meyerson, K. E. Spear, R. F. Davis, and M. Yoder (The Electrochemical Society, Pennington, NJ, 1991), p. 186.
[9] J. P. F. Sellschop, C. C. P. Madiba, and H. J. Annegarn, Nucl. Instrum. Methods **168**, 529 (1980).
[10] P. G. Lurie, and J. M. Wilson, Surf. Sci. **65**, 453 (1977).
[11] W. S. Verwoerd, Surf. Sci. **108**, 153 (1981).
[12] X. M. Zheng, and P. V. Smith, Surf. Sci. **256**, 1 (1991).
[13] R. E. Thomas, R. A. Rudder, R. J. Markunas, D. Huang, and M. Frenklach, J. Chem. Vapor Deposition **1**, 1 (1992).
[14] S. Matsumoto, and N. Setaka, Carbon **17**, 485, (1979); S. Matsumoto, Y. Sato, and N. Setaka, *ibid.* **19**, 232, (1981).
[15] A. Zangwill, *Physics at Surfaces* (Cambridge University, Cambridge, England, 1988), pp. 96, 258.
[16] Y. L. Yang, and M. P. D'Evelyn, J. Am. Chem. Soc. (in press).
[17] B. Marchon, J. Carrazza, H. Heinemann, and G. A. Somorjai, Carbon **26**, 507 (1988).

Carbon and oxygen removal from silicon (100) surfaces by remote plasma cleaning techniques

R. E. Thomas, M. J. Mantini, R. A. Rudder, D. P. Malta, S. V. Hattangady, and R. J. Markunas
Research Triangle Institute, Research Triangle Park, North Carolina 27709-2194

(Received 5 December 1991; accepted 3 February 1992)

A hydrogen plasma-based technique for carbon removal has been combined with a modest anneal for oxide desorption at 720 °C to produce atomically clean Si(100)2×1 surfaces. Carbon and oxygen contamination can be removed from silicon surfaces by a 30 s hydrogen plasma exposure at 480 °C (for carbon removal) followed by a 5 min anneal in molecular hydrogen at 720 °C (for oxygen removal). Surface hydrocarbon removal is thought to occur by volatilization through hydrogenation. The mechanism for oxygen removal is believed to be more straightforward and consist of thermal desorption of SiO at approximately 700 °C. Hydrogen plasma exposures on the order of 5 min are seen to induce microscopic surface roughness without complete oxygen elimination. Samples which are devoid of oxygen following the 720 °C anneal are found to reoxidize upon re-exposure to the hydrogen plasma. The origin of the oxygenating species is unclear, but likely sources include, SiO or OH from tube wall erosion, or contamination produced by interactions of atomic hydrogen with the chamber walls. A subsequent anneal at 720 °C effectively removes any surface reoxidation. Anneals at 720 °C with carbon present on the surface results in a surface reaction which complexes the carbon and oxygen on the surface, rendering the surface contamination resistant, under nominal conditions, to subsequent plasma processing or annealing.

I. INTRODUCTION

Plasma based cleaning techniques are currently being pursued by a number of researchers as part of a general effort to develop single-wafer processing technologies and more extensive *in situ* processing capabilities. *In situ* cleaning techniques must also be adapted to meet the growing demand for low-temperature processes which leave surfaces with a minimum of process induced damage. Demands for low temperature processes and minimal surface damage are driven in turn by the constraints of subhalf-micron device scaling and the requirements for defect-free surfaces essential for active interface formation. In designing a hydrogen based plasma cleaning process, there are several competing reactions in progress which have to be balanced. Silicon surfaces are etched upon exposure to the atomic hydrogen. Small quantities of process generated oxygen containing species can chemisorb on the surface upon exposure to the hydrogen plasma. Finally, carbon and oxygen are removed from the surface, although the oxygen removal rate appears much slower than the carbon removal rate. All of the above reactions are temperature dependent of course; the silicon etch rate tends to decrease as the sample temperature increases, and the other reaction rates increase with temperature. A further consideration in designing a cleaning process is the identity of the molecule carrying the oxygen and carbon contamination to the surface. One expects oxygen contained in methanol to be easier to remove from the surface than oxygen bonded directly to the silicon. In many cases, however, the nature of the contamination on the surface is not well characterized and, furthermore, can be altered by the cleaning process itself.

The use of hydrogen plasmas to clean semiconductors has been reported by a number of groups and includes atomic hydrogen generation by radio frequency (rf) remote plasma sources,[1,2] rf plasma sources,[3] and microwave electron cyclotron resonance (ECR) sources.[4,5] In general, removal of carbon contamination from the surface has proved easier than oxygen removal; primarily due to the relatively slow etch rate of silicon oxides by atomic hydrogen. Tasch *et al.* have reported using a remote plasma rf source, operating at 9 W of power, to reduce carbon to levels below the detectability limit as measured by Auger electron spectroscopy (AES).[6] Yamada has reported on ECR techniques to remove carbon from the silicon surface by atomic hydrogen exposure at 650 °C.[7] Contamination levels were measured by secondary ion mass spectroscopy (SIMS).

Removal of oxygen in the form of suboxides appears to be a more difficult task. In one case, samples were exposed to a rf remote hydrogen plasma for 45 min at 305 °C to remove the oxygen from the surface.[6] Furthermore, wafers exposed to ambient for 120 min could not be deoxygenated, while samples exposed to ambient for 15 min were cleaned to below the Auger detection limit.[6] It appears that the structure of the oxide, which is related to the thickness, is the major factor in determining ease of removal. In the second case, Nakashima *et al.* have also reported a reduction to background levels in the Si^{+4} $2p$ peak associated with the Si $2p$ x-ray photoelectron spectroscopy (XPS) peak following cleaning with a hydrogen ECR source.[4]

Silicon has also been very effectively cleaned by simple thermal annealing. Although oxygen is removed after an anneal at 830 °C, temperatures over 1100 °C are required to remove carbon from the surface.[8] Ishizaka *et al.* have demonstrated a thermal process for cleaning silicon at consid-

 0734-2101/92/040817-06$01.00

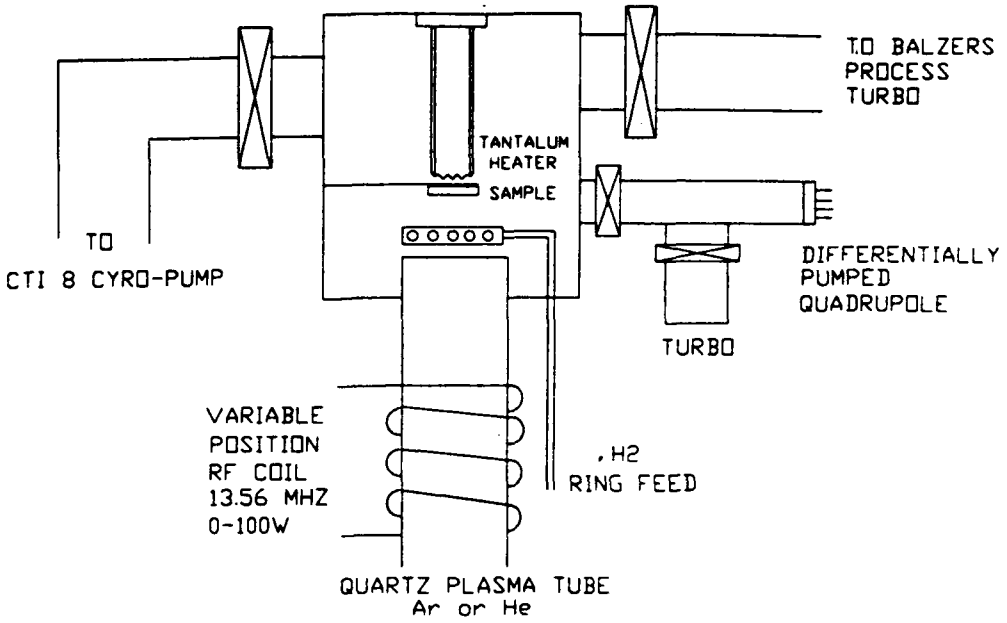

FIG. 1. Schematic of rf remote plasma cleaning system.

erably lower temperatures through careful wet chemistry to remove carbon from the surface and an anneal at 800 °C to remove the remaining oxide from the surface.[8] They found that if the oxide layers were thin enough following the wet chemistry the desorption temperature was lowered from 1000 °C for a full oxide to less than 800 °C. The correlation between oxide thickness and desorption temperature is supported in a recent study by Engstrom *et al.* of thermal desorption from oxygen dosed silicon surfaces.[9] At submonolayer coverages SiO desorbs from the surface at approximately 700 °C. The desorption temperature rises as the oxide thickness increases to a maximum of 1000 °C for the fully developed dioxide.

In the present work, we have applied sequential processing steps to reduce both the carbon and oxygen on the silicon surface. We found that a combination of steps tailored to the removal of carbon and oxygen, respectively, gave the best results. A brief exposure to the remote hydrogen plasma to reduce the residual surface carbon, followed by a brief thermal anneal to remove the remaining oxygen left the surface with carbon and oxygen levels below the limit of detectability by XPS.

II. EXPERIMENTAL PROCEDURES

The cleaning chamber that was used in the present work is shown in Fig. 1. The chamber is pumped by a cryogenic pump while in standby mode and a 500 ℓ/s turbomolecular pump while process gas is flowing. After baking, the chamber typically achieves an ultimate pressure of 5×10^{-10} Torr. The plasma is generated by rf excitation of a five-turn coil located approximately 45 cm from the sample position. rf power is supplied to the excitation coil at 13.56 MHz with an available power range of up to 100 W. Tube conditioning is performed prior to sample introduction by running a hydrogen plasma discharge. Hydrogen is injected into the system via a ring feed located approximately 5 cm below the sample, and all cleans are performed with hydrogen as the sole feed gas. The sample is radiantly heated by a tantalum filament located approximately 1 cm behind the sample. A sheathed reference thermocouple is positioned in close proximity to the coils of the filament heater and is used for routine determination of the sample temperature. The temperature offset of the reference thermocouple relative to the sample temperature was calibrated by introducing a silicon wafer with a thermocouple attached to the front face by a high-temperature ceramic adhesive. Calibration of the reference thermocouple was performed while flowing hydrogen through the chamber. We estimate an accuracy of 20 °C for the sample temperature with this measuring arrangement. Very large scale integrated (VLSI) grade hydrogen, further purified with a Nanochem filter, was used for all cleans. A differentially pumped quadrupole mass spectrometer (QMS) is located beside the main chamber to sample gasses during processing.

Silicon samples used in the study consisted of 2.5 cm diam, (100), *p*-type, 10 Ω cm wafers. All samples receive a modified RCA clean prior to introduction to the cleaning system with final buffered HF dip immediately before loading into the transfer system.

Low-energy electron diffraction (LEED), XPS, and AES are available via ultrahigh vacuum (UHV) transfer from the cleaning chamber to the respective analytical facilities. Transfers can be accomplished in approximately 5 min with a background pressure of about 1×10^{-9} Torr. All samples are mounted on molybdenum carriers.

III. EXPERIMENTAL RESULTS

Figures 2 and 3 show XPS results from two silicon samples which were given hydrogen plasma cleans at 480 °C for 5 min followed by 5 min anneals at 720 °C in flowing molecular hydrogen. The samples were treated identically except that one of the samples, Fig. 2, was loaded into the vacuum system immediately after HF cleaning (approximately 7 min exposure to air), and the second sample, Fig.

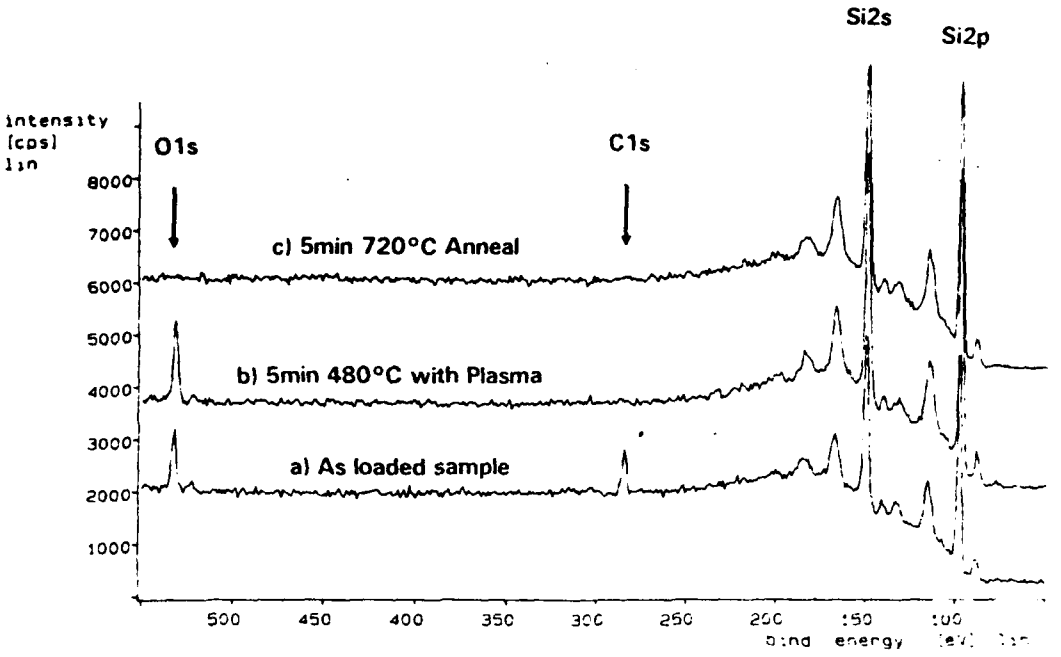

FIG. 2. XPS spectra taken from a silicon sample at selected stages of the cleaning process. This sample was exposed to laboratory ambient for approximately 7 min between a HF clean and introduction to the vacuum system.

3, was exposed to laboratory ambient for 120 min prior to insertion into the vacuum system. Figures 2(a) and 3(a) give XPS spectra of the samples as introduced to the chamber. Both carbon and oxygen are evident on the surface of the samples. The first step of the cleaning process consisted of exposing the samples to a hydrogen plasma for 5 min at 480 °C to remove carbon. Figures 2(b) and 3(b) show the samples after exposure to the hydrogen plasma. No evidence of carbon is seen on the surface for either sample, even with an expanded scale. However the oxygen peak is still present, and in some cases is slightly higher. Figures 2(c) and 3(c) show XPS spectra of the samples after the second step in the cleaning process, a 5 min anneal at 720 °C in flowing molecular hydrogen at 5 mTorr. After annealing the samples were cooled in flowing hydrogen. No plasma was used during the anneal or during the cooldown phase. Although the second sample, due to a longer ambient exposure time, had slightly higher levels of carbon and oxygen on the surface as loaded, the same cleaning sequence removed all traces of both contaminants.

Additional experiments were performed to investigate the minimum operating parameters required to remove carbon and oxygen from a sample surface. Figures 4(a)–4(c) show XPS spectra for a cleaning process where the plasma-processing time was reduced from 5 min to 30 s and where the desorption anneal was reduced from 720 to

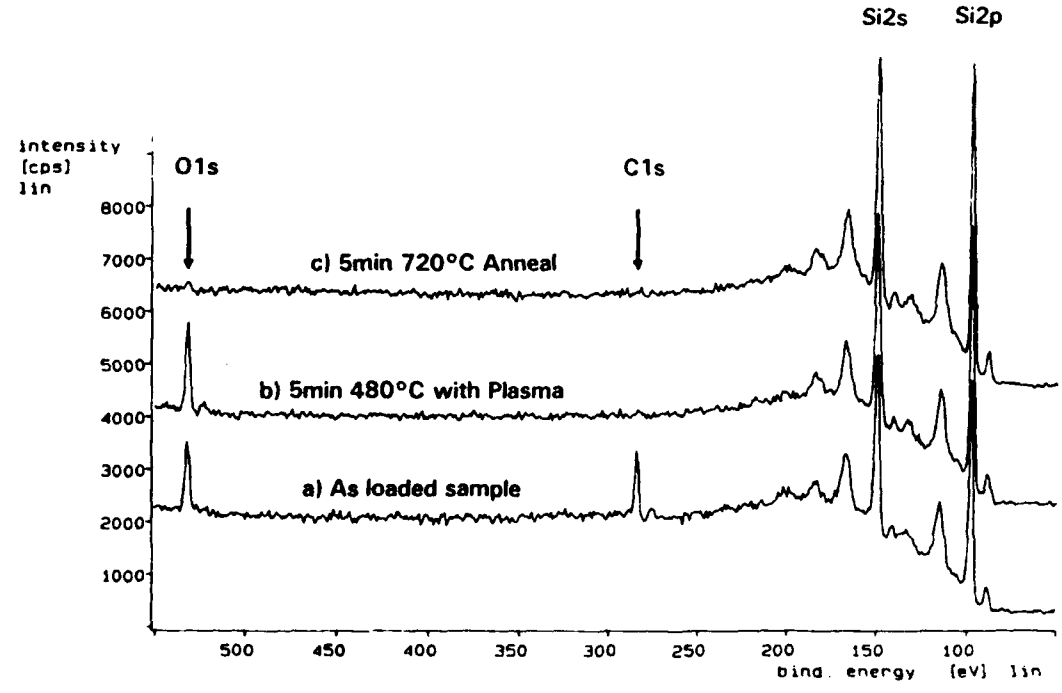

FIG. 3. XPS spectra taken from a silicon sample undergoing a cleaning process identical to that of the sample from Fig. 2. The only difference was that the sample shown in this figure was exposed to ambient for 120 min between the HF clean and introduction to the vacuum system. As a result of the longer ambient exposure slightly higher levels of oxygen and carbon can be seen in (a).

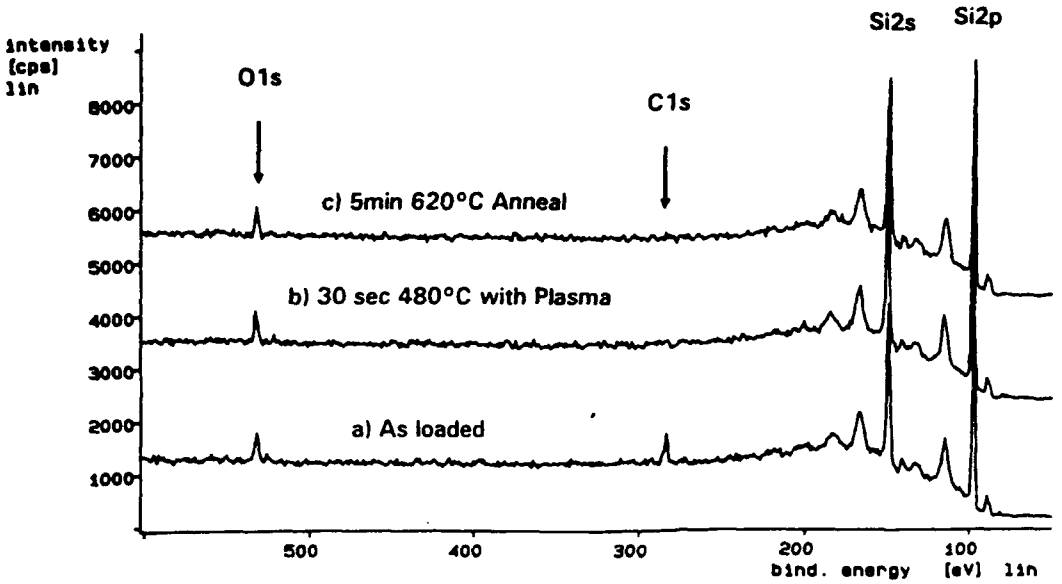

FIG. 4. XPS spectra taken from a silicon sample undergoing a cleaning process where the plasma exposure time and the final annealing temperature have both been reduced from parameters used to clean samples seen in Figs. 2 and 3. The shorter plasma exposure time still removes all evidence of carbon from the surface. However, the lower annealing temperature was not sufficient to desorb the oxide.

600 °C. Figure 4(a) shows an XPS spectra from the sample as loaded. Results in Fig. 4(b) show that a 30 s exposure to the hydrogen plasma was sufficient to reduce the carbon to levels below detectability. However, annealing at 600 °C did not prove effective at removing oxygen from the surface, as shown in Fig. 4(c).

LEED was performed on the samples at intervals during the cleaning process. Samples cooled from 720 °C to room temperature in molecular hydrogen exhibited a 2×1, 1×2 LEED pattern. Samples in the 2×1, 1×2 state were easily converted to the 1×1 state by a 2 s exposure at room temperature to the hydrogen plasma. These results are consistent with previous studies on hydrogen adsorption and desorption from the silicon(100) surface. A hydrogen terminated silicon 1×1 surface will reconstruct to the 2×1 configuration upon heating to approximately 450 °C. Annealing to this temperature results in a surface where each silicon atom is terminated by one hydrogen atom. Annealing to approximately 550 °C results in the desorption of the remaining hydrogen from the surface as molecular hydrogen. Reexposure of the clean 2×1 surface to atomic hydrogen at a temperature below the first desorption temperature of 425 °C results in a 1×1 hydrogen terminated surface again.

Atomic hydrogen is known to etch silicon relatively easily,[10] and comparisons were therefore made of the surface morphology as a function of processing parameters. Figure 5 shows scanning electron micrographs of three surfaces: before *in situ* cleaning, after *in situ* cleaning with a 5 min plasma exposure, and after *in situ* cleaning with a 30 s plasma exposure. The first sample which was exposed for 5 min has been severely etched. The second sample exposed for 30 s shows no evidence of surface damage, and has a surface morphology comparable to the sample before cleaning.

Although carbon was removed by exposure to the hydrogen plasma at 480 °C, many of the samples showed slight increases in the O 1*s* XPS peaks. Examination of the Si 2*p* peak intensities revealed a similar increase after carbon removal. It is likely that a substantial percentage of the differences in oxygen and silicon peak intensities seen can be attributed to carbon attenuation of both the oxygen and silicon signals. However, in order to determine the role of the plasma in producing oxygen contamination of the surface, samples were cleaned and then reexposed to the plasma under the conditions used to remove carbon. Figure 6 shows XPS spectra for a sample after cleaning and then after exposure to the plasma at 400 °C for 5 min. At the power levels and pressures used here, we find that subsequent exposure to the plasma adsorbs oxygen onto what had previously been an oxygen-free silicon surface. Annealing the sample to 720 °C, once again, easily removes the oxygen.

Tests were also made to ascertain the importance of carbon removal prior to desorbing oxides from the surface. Samples were heated to 720 °C without first exposing the surfaces to a hydrogen plasma for carbon removal. XPS spectra taken after plasma treatment showed that oxygen was not removed from the surface. Samples were then exposed to the hydrogen plasma for 5 min at 480 °C. XPS spectra in this case revealed that little if any carbon was removed from the surface by the plasma. It appears that if samples are annealed at 720 °C with both carbon and oxygen on the surface, the oxygen will not desorb. Subsequent hydrogen plasma processing is rendered ineffective at carbon removal.

IV. DISCUSSION

Although carbon removal from the silicon surface has been reported by a number of research groups, the exact mechanism is still unclear. It is thought to be by hydrogenation to form volatile hydrocarbons. Removal of oxygen from the surface by hydrogen plasma cleaning has proved to be more difficult.[4–7,11] It is not clear if oxygen removal occurs by etching back the silicon or by direct attack of the Si–O bonds by the atomic hydrogen. Certainly the Si–Si

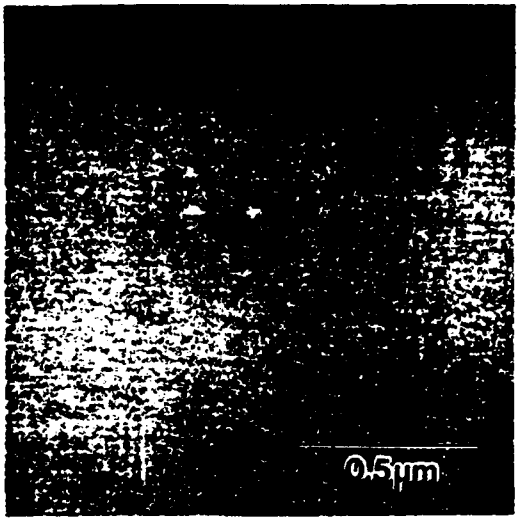

(a)

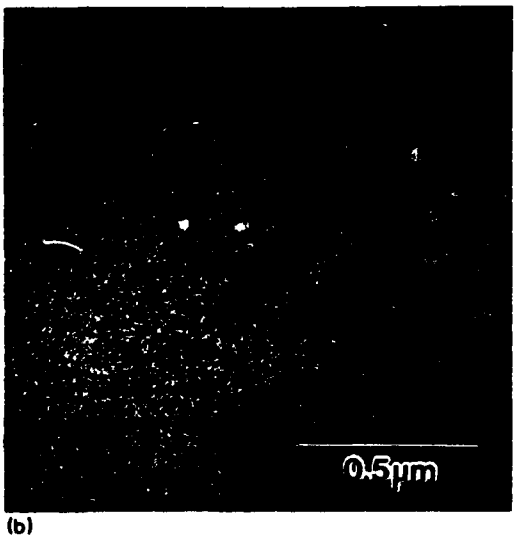

(b)

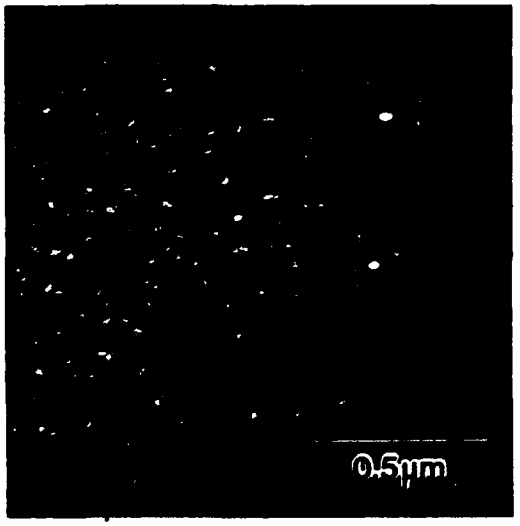

(c)

FIG. 5. Scanning electron micrographs showing surface morphology as a function of plasma exposure time. (a) Shows a sample after wet chemistry cleaning and before plasma exposure. (b) Shows a sample after a 30 s plasma exposure. No evidence of surface damage is discernible. (c) Shows a silicon sample after a 5 min plasma exposure. Surface degradation is clearly evident.

bonds are much weaker, and perhaps are easier for the atomic hydrogen to break than the Si–O bonds.

The mechanism for oxygen removal in the cleaning process reported here is relatively easy to understand. For submonolayer coverages of oxygen on silicon, the desorption temperature of the oxide, as SiO, has been reported as approximately 700 °C.[9] This was found for a heating rate of 6 °C/s; presumably a longer time at a lower temperature would achieve the same effect. As the oxygen coverage is increased the desorption temperature increases to a maximum beyond 1000 °C for a fully developed oxide.[9] One key to minimizing the oxide desorption temperature is to start the *in situ* cleaning process with as little adsorbed oxygen as possible.

Reoxidation of clean surfaces upon exposure to the plasma is observed to occur at a slow rate. No evidence of oxygen adsorption is seen when clean samples are simply exposed to flowing molecular hydrogen, so we can assume the plasma is activating some species or process. Possibilities include residual gasses in the cleaning chamber, and etching of the quartz plasma tube. No evidence is seen for contamination of the hydrogen with the quadrupole mass spectrometer while the plasma is off. Base pressure for the system is 5×10^{-10} Torr, of which a significant component is mass 18, or water. The plasma could easily transform a portion of the residual water vapor into OH radicals which could then chemisorb on the silicon surface. A concurrent process may be etching of the quartz plasma tube to form SiO, which again would adsorb on the surface.

Of particular interest in this work is the observation that if carbon and oxygen are left on the surface prior the the 720 °C anneal, neither species are removed during the high-temperature anneal, and, furthermore, subsequent processing by either plasma treatment or thermal desorption has no effect. The presence of carbon on the surface appears to prevent the desorption of suboxides of silicon from the surface at 720 °C, and, in turr, the carbon species on the surface seem to be altered by the anneal. It is unlikely that the carbon on the surface initially exists as pure carbon bonded to silicon. A more likely form is a hydrocarbon physisorbed or partially chemisorbed on the silicon. Bozack *et al.* have studied the relationship between hydrocarbon species and desorption products from the silicon surface.[12] In general, higher molecular weight hydrocarbons adsorb more easily on the silicon surface and will tend to decompose as the temperature is increased, eventually forming silicon carbide.[12] Correlations were also found between number of C–C bonds and reactivity with the silicon surface. For example, ethylene was found to desorb in greater quantities without decomposition than acetylene. However, hydrocarbons and perhaps halocarbons on the surface are apparently susceptible to attack by atomic hydrogen before they are thermally decomposed. Once the hydrocarbons have thermally decomposed on the surface, the desorption temperature is raised to well over 1000 °C.[13]

Any oxygen remaining on the surface with the carbon can potentially be bound to the silicon, to the carbon or bridge the two atoms. One expects carbon to be bound to the silicon with two of four available bonds. The remaining

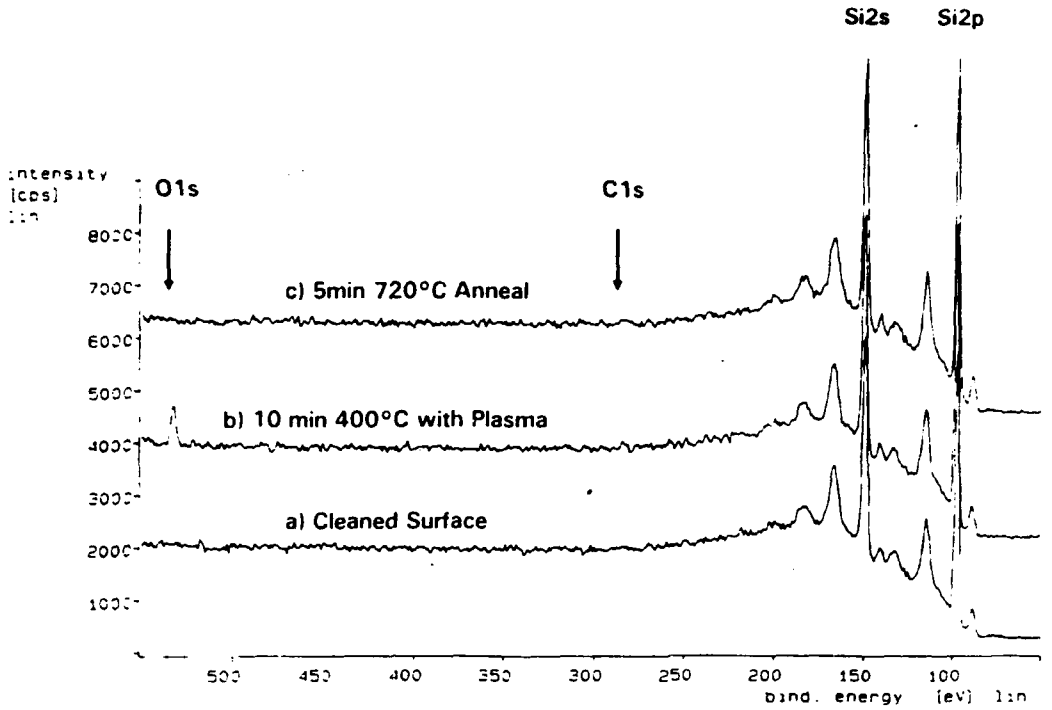

FIG. 6. XPS spectra taken from a silicon which was first cleaned with the same process parameters used on the sample in Fig 2 and then reexposed to the hydrogen plasma for 10 min at 400 °C. (a) Shows the sample after the plasma clean and thermal anneal. (b) Shows an XPS spectrum from the sample after exposure to the hydrogen plasma for 10 min. (c) Shows an XPS spectrum after the sample was annealed at 720 °C for 5 min.

two bonds offer sites for carbon–oxygen bonds. Oxygen desorption from graphite has been measured to be approximately 800 °C.[14] This was for a heating rate of 50 °C/s so it is not clear what the desorption rate would be for an isothermal anneal at a lower temperature. If the oxygen is thus bound preferentially to the carbon, the oxygen/graphite desorption results may account for the inability to desorb oxygen at 700 °C from silicon surfaces which are contaminated with carbon.

V. CONCLUSIONS

A hydrogen plasma-based technique for carbon removal has been combined with a modest anneal for oxide desorption at 720 °C to produce atomically clean Si(100)2×1 surfaces. Carbon and oxygen contamination can be removed from silicon surfaces by a 30 s hydrogen plasma exposure at 480 °C (for carbon removal) followed by a 5 min anneal in molecular hydrogen at 720 °C (for oxygen removal). Carbon removal is thought to occur by volatilization through hydrogenation. The mechanism for oxygen removal is believed to be more straightforward and consist of thermal desorption of SiO at approximately 700 °C. Longer duration exposures to the hydrogen plasma, under the reported conditions, are seen to induce microscopic surface roughness without oxygen elimination. Samples which are devoid of oxygen following the 720 °C anneal are found to reoxidize upon reexposure to the hydrogen plasma. It is not known at this time whether the oxidizing species originates as an impurity in the hydrogen gas, is present as a residual background impurity, or is generated from interactions between the hydrogen plasma and the quartz plasma tube. The effect of the oxidizing species, however, is clear. It compromises the plasma cleaning at 480 °C. Hence, the hydrogen plasma cleaning process is seen to be a competition between silicon etching, hydrogenation of surface contaminants, and reoxidation of the silicon surface.

The approach taken here to obtain clean Si(100):2×1 surfaces was to first remove the surface carbon with a short plasma exposure to minimize surface damage and, second to thermally desorb the remaining oxygen from the surface in flowing hydrogen gas. Anneals at 720 °C with carbon present on the surface results in a surface reaction which complexes the carbon and oxygen on the surface, rendering the surface contamination resistant to subsequent plasma processing or annealing.

[1] R. A. Rudder, G. G. Fountain, and R. J. Markunas, J. Appl. Phys. **60**, 3519 (1986).
[2] B. Anthony, T. Hsu, L. Breaux, R. Qutan, S. Banerjee, and A. Tasch, J. Electron. Mater. **19**, 1027 (1990).
[3] T.-R. Yew, and R. Reif, J. Appl. Phys. **68**, 4681 (1990).
[4] K. Nakashima, M. Ishii, I. Tajima, and M. Yamamoto, Appl. Phys. Lett. **58**, 2664 (1991).
[5] A. Kishimoto, I. Suemune, K. Hamaoka, T. Koui, Y. Honda, and M. Yamanishi, Jpn. J. Appl. Phys. **29**, 2273 (1990).
[6] T. Hsu, L. Breaux, B. Anthony, S. Banerjee, and A. Tasch, J. Electron. Mater. **19**, 375 (1990).
[7] H. Yamada, J. Appl. Phys. **65**, 775 (1989).
[8] A. Ishizaka and Y. Shiraki, J. Electrochem. Soc. **133**, 666 (1986).
[9] J. R. Engstrom, D. J. Bonser, M. M. Nelson, and T. Engel, Surf. Sci **256**, 317, (1991).
[10] J. Abrefah and D. R. Olander, Surf. Sci. **209**, 291 (1989).
[11] T. Shibata, Y. Nanishi, and M. Fujimoto, Jpn. J. Appl. Phys. **29**, L1181 (1990).
[12] M. J. Bozack, P. A. Taylor, W. J. Choyke, and J. T. Yates, Jr., Surf. Sci. **177**, L933 (1986).
[13] G. E. Becker and J. C. Bean, J. Appl. Phys. **48**, 3395 (1977).
[14] B. Marchon, J. Carrazza, H. Heinemann, and G. A. Somorjai, Carbon **26**, 507 (1988).

Effect of Thin Interfacial SiO_2 Films on Metal Contacts to B Doped Diamond Films

V. Venkatesan, K. Das
Kobe Steel Research Laboratories, USA, Electronic Materials Center, P. O. Box 13608, Research Triangle Park, NC 27709
G. G. Fountain, R. A. Rudder, J. B. Posthill and R. J. Markunas
Research Triangle Institute, Research Triangle Park, NC 27709-2194

ABSTRACT

The effect of thin interfacial films of SiO_2 (~20 Å) on the electrical characteristics of metal contacts fabricated on polycrystalline and homoepitaxial diamond films has been studied. The diamond films were grown using plasma-enhanced chemical vapor deposition techniques. In order to minimize the effect of defects and/or hydrogen on the metal contact characteristics, these films were annealed at 950°C for 30 min. Metal-semiconductor contacts were formed by electron-beam evaporation of Al on both as-received and annealed polycrystalline films, whereas, Au metallization was used for the homoepitaxial film. Active diode areas were defined by a standard photolithographic process. It has been demonstrated in this investigation that, in certain cases, the introduction of a thin SiO_2 film at the interface between the metal and the diamond semiconductor film allows the fabrication of a rectifying contact that is not obtainable without the interfacial film.

Introduction

Semiconducting diamond, as a potential material for high temperature, high speed and high power device applications, has been the subject of some excellent reviews (1-7). A number of these devices will rely on a rectifying metal / semiconductor contact for their operation. A metal / semiconductor contact also provides a suitable vehicle for electrical characterization of the device material. However, it has been observed that the formation of good rectifying contacts is not always easily accomplished on diamond films grown by chemical vapor deposition (CVD) (8). Contacts established with Al or Au on CVD films exhibit highly resistive ohmic or nominally asymmetric behavior, whereas these metals can be used almost routinely to form rectifying contacts on synthetic (9) and natural semiconducting diamond crystals (10). However, Grot *et al.* (11) have been successful in

fabricating Au rectifying contacts, through a chemical treatment in a heated $CrO_3 + H_2SO_4$ solution, on CVD grown homoepitaxial films. Similar results have also been reported by Mori *et al.* (12), in their investigation of CVD diamond films. According to Mori *et al.*, surface treatment of diamond films in a hot solution of CrO_3 in H_2SO_4 or in an oxygen plasma results in a submonolayer oxygen coverage of these films. They concluded that, contact characteristics on CVD diamond films without oxygen on the surface depend on the electronegativity of the metal, while those on films with oxygen on the surface do not exhibit such a dependence. Characteristics of rectifying contacts on CVD grown films of both homoepitaxial (13) and polycrystalline diamond (14) have been improved by growing an insulating undoped diamond film on a previously deposited B doped semiconducting film.

In the present investigation, the effect of thin interfacial SiO_2 films on the electrical characteristics of metal contacts fabricated on B doped polycrystalline and homoepitaxial films has been studied. Rectifying metal contacts were obtained in certain cases on semiconducting diamond thin films with the introduction of a ~ 20 Å thick SiO_2 film at the interface between the metal and the diamond film.

Experimental

Both the polycrystalline and homoepitaxial B doped diamond films used for the study were grown using plasma-enhanced chemical vapor deposition (PECVD) techniques. The diamond films were characterized by scanning electron microscopy (SEM) and by Raman Spectroscopy. In addition, secondary ion mass spectroscopy (SIMS) analysis of selected samples were performed in order to determine the atomic concentration of B in the films.

As-deposited diamond films

A microwave plasma CVD reactor described in reference (15) was employed, in this study, for the deposition of the polycrystalline diamond films. These films were grown on low resistivity (<1 Ω-cm), B doped Si ((111) oriented) substrates, mechanically polished using 0.25 μm diamond paste. A gas composition of H_2 (99.5 %) and CH_4 (0.5 %) at a pressure of 35 torr was employed, and the substrates were maintained at 800°C during deposition. Moreover, these films were doped with B using B_2H_6. The ratio of B_2H_6 to the total gas flow was adjusted to obtain B to C (B/C) ratios of 0.8, 2.0, 3.2, 4.0, 20.0, 200.0, and 400.0 ppm in the gas phase. In some cases O_2 (0.1 %) was also

included in the gas mixture (for (B/C) ratios of 0.8, 2.0, 3.2, 4.0 ppm). These films were grown for 14 hr. For the higher (B/C) ratios (20.0, 200.0 and 400.0 ppm) O_2 was not used and films were grown for 7 hr. Details of the rf plasma CVD reactor utilized for the homoepitaxial film growth are given in reference (16). The homoepitaxial film was grown on a type I A insulating natural diamond crystal using 0.4 % CH_4 and 1 % CO in H_2 rf plasma. The film was also doped with B_2H_6 during growth.

A flow chart of the fabrication steps involved in the processing of metal contacts on the diamond films is shown in Fig. 1. The polycrystalline diamond films were cleaned using the RCA cleaning procedure (17), dehydrated at 120°C for 20 minutes and subsequently a ~2000 Å thick Al film was deposited by electron beam evaporation. For the homoepitaxial diamond sample, prior to RCA cleaning, a chemical treatment in a hot CrO_3 + H_2SO_4 solution (to remove any non-sp^3 component in the diamond film) was also included and an Au metallization employed. An important point to note in the Au metallization procedure is that the electron-beam evaporation was a two step process. The deposition rate was 1Å/s for the first 100 Å of gold and then 5 Å/s for the rest of the ~ 2000Å film. This procedure markedly improved the adhesion of Au on the diamond film. Active diode areas, 100 μm in diameter separated from the field region by a 100 μm annular ring, were delineated by photolithography followed by Al or Au etching, as the case may be. A mask pattern proposed by Ioannou et al.(18) was used for this process. The 'infinitely' large area of the field-region ensured an adequate quasi-ohmic contact with the required current handling capability, particularly in the case of the homoepitaxial film, which was deposited on an insulating natural diamond crystal. Electrical characterization of these metal contacts was performed using a HP 4145 B semiconductor parameter analyzer, equipped with a hot stage for elevated temperature measurements.

The next step in this investigation was to study the effect of an interfacial SiO_2 film on metal contacts fabricated on a selected as-deposited polycrystalline (B/C ratio of 0.8 ppm) film and the homoepitaxial diamond film. Approximately 20 Å thick film of SiO_2 had been deposited on these samples by a remote plasma-enhanced CVD technique (19) prior to metallization. For the homoepitaxial film, following electrical measurements on the Au contacts fabricated directly on the sample (i.e. without the SiO_2 interfacial film), the metal was etched in aqua regia (3HCl + 1HNO_3). The sample was then cleaned employing the RCA cleaning procedure and a ~ 20 Å thick film of SiO_2 was deposited and finally Au contacts fabricated. Schematic diagrams of the cross-section of the contact structure on the diamond films, (a) without, and (b) with the the SiO_2 film are shown in Fig. 2. A

comparative study of the I-V characteristics were conducted for the samples (a) without, and (b) with the the SiO_2 film.

Heat treated diamond films

The polycrystalline films were annealed at a temperature of 950°C for 30 min, in order to minimize the effect of defects and / or hydrogen on the electrical characteristics of metal contacts on these films. Aluminum metal contacts were then fabricated on the annealed films both with and without an SiO_2 interfacial layer, following the procedure described in the previous section. Current-voltage (I-V) measurements were then performed on these metal-semiconductor contacts. For the contacts fabricated on annealed 20.0 ppm ((B/C) ratio) samples with an SiO_2 interfacial layer, I-V measurements were conducted from room-temperature up to ~ 250 °C, at increments of ~ 50 °C.

Results and Discussion

As-deposited diamond films

Scanning electron microscopy of the B-doped diamond films investigated here showed clear (111) facets and multiply twinned particles. Scanning electron microscopy also indicated that the polycrystalline diamond films grown with O_2 (lower (B/C) ratio) had a quality superior to those grown without O_2 (higher (B/C) ratio). Similar improvements in the quality of films grown in the presence of O_2 have been reported by Hirose *et al.* (20). The crystal quality was investigated using laser Raman spectroscopy. The Raman peak position characteristic of diamond was located near 1333 cm^{-1}. A relatively small sp^2 peak at 1500 cm^{-1} was also observed in the Raman spectrum of the diamond films. A SIMS analysis of the as-deposited 20.0 ppm ((B/C) ratio) diamond film showed an atomic B concentration of ~ 1.0×10^{18} cm^{-3}.

Current-voltage characteristics of Al contacts on the lower B/C ratio (0.8, 2.0, 3.2 and 4.0 ppm) polycrystalline diamond samples, in the as-deposited state, showed an apparent improvement in rectifying characteristics with increasing B concentration in the films. A summary of the results obtained from these initial experiments on as-deposited B doped polycrystalline diamond films is shown in Table I. While the diamond film with B/C ratio of 0.8 ppm showed nearly ohmic Al contact characteristics, the 4.0 ppm (B/C ratio) diamond film yielded excellent Al contact rectification characteristics with low reverse leakage current (<1 nA) and high breakdown voltage (~30 V).

As mentioned in the experimental details section, the as-deposited polycrystalline sample with a B/C ratio of 0.8 ppm and the homoepitaxial diamond sample were selected for the study of the effect of interfacial SiO_2 on metal contacts. Current-voltage characteristics of Al contacts on this polycrystalline film, both, (a) with, and (b) without the interfacial SiO_2 film, are shown in Fig. 3. Aluminum contacts deposited directly (curve (a)) on this sample without the interfacial SiO_2 film showed near-ohmic I-V characteristics. The subsequent introduction of the SiO_2 film provided rectifying characteristics, as shown in curve (b). Gold contacts deposited directly on the as-deposited homoepitaxial film also exhibited near-ohmic I-V characteristics, as shown in Fig. 4, curve (a). With the introduction of the thin SiO_2 film good rectification was obtained as shown in Fig. 4, curve (b). In the presence of the SiO_2 film, low leakage currents (< 1 nA at 5 V) in the reverse direction were observed in both the polycrystalline and the homoepitaxial film. A breakdown voltage of ~7 V was observed for both as-deposited polycrystalline and the homoepitaxial films. Several factors could be responsible for the observed rectifying behavior of the contacts upon introduction of a thin dielectric interfacial layer. These factors include: a reduction in leakage current, a reduction in tunneling current, surface passivation and a change in electric field distribution across the metal-semiconductor junction. Further work is in progress to fully understand the mechanisms that result in the observed characteristics.

Heat treated diamond films

Current-voltage characteristics of Al contacts fabricated on annealed films with the lower (B/C) ratios, showed a drastic reduction in current in both the forward and reverse directions. Since the magnitude of the current was approximately the same in all the films (for (B/C) ratios of 0.8, 2.0, 3.2, 4.0 ppm), a representative plot from the 4.0 ppm sample is shown in Fig. 5. This reduction in current conduction on annealing is in conformity with observations reported by Landstrass and Ravi (21, 22), Albin and Watkins (23) and Muto et al. (24). Landstrass and Ravi (21) postulated the low resistivity of the as-grown films to be due to hydrogen passivation of traps present in the films. Annealing of these films results in dehydrogenation with a consequent increase in the resistivity. Defect annihilation during anneal may also be a mechanism that could account for the increased resistivity in these annealed diamond films (25). The apparent improvement in rectification, which was observed in the as-deposited films with increasing B concentration was not observed after the anneal treatment. It is speculated that, carriers contributed by defect states or states

associated with hydrogen are probably responsible for the rectification behavior observed in the as-deposited films.

Current-voltage characteristics of Al contacts deposited directly on annealed polycrystalline diamond films with B/C ratios of 20.0, 200.0 and 400.0 ppm were nearly ohmic. The I-V characteristics for 20.0 ppm (B/C) sample without the interfacial SiO_2 film are shown in Fig. 6, curve (a). The 200.0 and 400.0 ppm (B/C) samples showed a current conduction in the mA range for the same voltage range shown in Fig. 6. For the 20.0 ppm (B/C) sample, subsequent introduction of the SiO_2 film provided rectifying characteristics as shown in Fig. 6, curve (b). A breakdown voltage of ~ 6 V and a reverse leakage current of ~334 nA at 5 V were observed for this film. The higher B concentration films (200.0 and 400.0 ppm) did not yield rectifying Al contact characteristics with the introduction of a ~ 20 Å interfacial SiO_2 film. In these latter films, it is speculated that, the high B concentration produced a large concentration of carriers, which tunnelled through the thin SiO_2 interfacial film resulting in an excess leakage current and a loss of rectification behavior.

The I-V characteristics of the annealed diamond film (20.0 ppm (B/C) ratio) with interfacial SiO_2 measured at temperatures ranging from room temperature (RT) to 248 °C in ~ 50 °C increments, are shown in Fig. 7. It is seen that as the temperature is increased the reverse leakage current increases and the reverse breakdown voltage decreases. Nevertheless, a fairly good rectification behavior can be observed up to ~ 100 °C. The results obtained from the study of the effect of thin interfacial SiO_2 films on metal contacts on both polycrystalline and homoepitaxial diamond films are summarized in Table II.

A background doping concentration of ~ 5.3×10^{18} cm^{-3} in the 20.0 ppm (B/C) film was obtained using an approximate 'universal' expression for the avalanche breakdown voltage given by (26):

$$V_B = 60(E_g/1.1)^{3/2}(N_B/10^{16})^{-3/4}$$

where, V_B is the breakdown voltage for a plane-parallel junction, E_g, the band-gap of the material, and N_B, the doping concentration. A band gap of 5.45 eV for diamond and the experimentally observed breakdown voltage of 6 V was used in the above calculation. Assuming that the electrically active B concentration in this film is the same as the atomic B concentration of ~1.0×10^{18} cm^{-3}, as determined from SIMS analysis, the calculated value of the background doping concentration agrees to within an order of magnitude with the

SIMS results. The calculated value for carrier concentration should only be used as an indicator, and a more direct measurement such as van der Pauw Hall technique should be used to confirm this result. However, for diamond samples deposited on Si substrates, parasitic effects due to the higher mobility of Si may be difficult to eliminate. It should be noted that for high concentrations of B of the order of 10^{19} - 10^{20} cm^{-3} in diamond, a complete activation of the impurity has been reported (27 - 30). However, it has not been established whether a similar effect can be expected at a B concentration of $1.0 \times 10^{18} cm^{-3}$. It should also be pointed out that a plane-parallel junction approximation will provide an underestimation of the breakdown voltage as edge effects are expected to produce a significant lowering of the breakdown voltage for a given doping concentration (26). An estimation of doping concentration from the observed breakdown voltage of the structure used here, therefore, will provide an overestimation of the doping concentration. Moreover, since the dielectric strength of SiO_2 is 10^7 V/cm (Appendix I of reference (26)) the breakdown voltage of ~ 20 Å SiO_2 film is ~ 2 V. Disregarding any effect arising from the oxide and its interface, the experimentally observed breakdown voltage of this film (~ 6 V) is likely to bear some relationship to the avalanche breakdown voltage of the diamond film and not that of the dielectric.

Conclusions

It has been demonstrated that the introduction of a thin SiO_2 film at the interface between the metal and the diamond semiconductor film (polycrystalline diamond: as-deposited 0.8 ppm (B/C) and annealed 20.0 ppm (B/C); as-deposited homoepitaxial film on natural diamond substrate) allows the fabrication of a rectifying contact, that is not otherwise possible for these films. This improvement in characteristics is probably due to (1) a reduction in leakage current, (2) a reduction in tunneling current, (3) passivation of the surface and (4) a change electric field distribution across the metal-semiconductor junction. Annealing of polycrystalline diamond films (B/C ratios of 0.8, 2.0, 3.2 and 4.0 ppm) at 950 °C for 30 min resulted in high-resistivity nearly ohmic behavior for metal deposited directly onto the semiconductor surface. Fairly good rectification up to ~100 °C has been observed on the devices fabricated on annealed polycrystalline diamond film (B/C ratio of 20.0 ppm) with an interfacial SiO_2 film. Moreover, the experimentally observed breakdown voltage of ~ 6 V on these rectifying devices is likely to bear some relationship to the avalanche breakdown voltage of the diamond film and not that of the dielectric interfacial film.

Acknowledgments

The authors are grateful to Dr. K. Kobashi, ERL, Kobe Steel, Ltd. Kobe, Japan, for providing the polycrystalline diamond films used in this investigation. C. P. Tully, KSRL, EMC, is acknowledged for assistance in preparation of the manuscript. Acknowledgements are due to K. Miyata, KSRL, EMC, Dr. D. L. Dreifus, KSRL, EMC, and Professor J. T. Glass, North Carolina State University, for several useful discussions. GGF, RAR, JBP and RJM gratefully acknowledge support from SDIO/IST through ONR (Contract No. N00014-86-C-0460).

REFERENCES

1. A. T. Collins and E. C. Lightowlers, in 'The Properties of Diamond', ed. J. E. Field, Academic Press, San Diego (1979).
2. V. K. Bazhenov, I. M. Vikulin and A. G. Gontar, *Sov. Phys. Semicond.*, **19**, 829 (1985).
3. A. T. Collins, *Semicond. Sci. Technol.*, **4**, 605 (1989).
4. K. Shenai, R. S. Scott, and B. J. Baliga, *IEEE Trans. E. D.*, **36**, 1811 (1989).
5. G. Sh. Gildenblat, S. A. Grot, A. Badzian, *Proc.IEEE.* **79**, 647 (1991).
6. M. W. Geis, *Proc. IEEE*, **79**, 669 (1991).
7. R. J. Trew, J-B. Yan, and P. M. Mock, *Proc. IEEE*, **79**, 598 (1991).
8. V. Venkatesan and K. Das, unpublished work, (1990).
9. G.H. Glover, *Solid St. Elect.*, **16**, 973 (1973).
10. E.C. Lightowlers and A.T. Collins, *J. Phys. D : Appl. Phys.*, **9**, 73 (1976).
11. S.A. Grot, G.Sh. Gildenblat, C.W. Hatfield, C.R. Wronski, A.R. Badzian, T. Badzian and R. Messier, *IEEE Electron Dev. Lett.*, **11**, 100 (1990).
12. Y. Mori, H. Kawarada and A. Hiraki, *This Journal*, **137**, 1598 (1990).
13. H. Shiomi, Y. Nishibayashi and N. Fujimuro, *Proc. 2nd Intl. Conf. New Diamond Sc. Tech.*, eds., R. Messier, J.T. Glass, J.E. Butler and R. Roy, Washington, D.C., Sept 23-27 (1990).
14. K. Miyata, D.L. Dreifus, K. Das, J.T. Glass and K. Kobashi, presented at the Electrochem. Soc. Meeting, Washington, D.C., May 6-10 (1991).
15. K. Kobashi, K. Nishimura, Y. Kawate, and T. Horiuchi, *Phys. Rev. B*, **38**, 4067 (1988).
16. R.A. Rudder, G.C. Hudson, Y.M. LeGrice, M.J. Mantini, J.B. Posthill, R.J. Nemanich, and R.J. Markunas, Mat Res. Soc. EA-19, 89 (1989).
17. W. Kern, and D. A. Puotinen, *RCA Rev.*, **31**, 187 (1970).
18. D. E. Ioannou, N. A. Papanicolaou, and P. E. Nordquist, Jr., *IEEE Trans Electron Devices*, ED-**34**, 1694 (1987).
19. G.G. Fountain, R.A. Rudder, S.V. Hattangady, R.J. Markunas, and P.S. Lindorme, *J. Appl. Phys.*, **63**, 4744 (1988).
20. Y. Hirose and T. Terasawa, *Jpn. J. Appl. Phys.* **25**, 519 (1986).
21. M.I. Landstrass and K.V. Ravi, *Appl. Phys. Lett.*, **55**, 975 (1989).
22. M.I. Landstrass and K.V. Ravi, *Appl. Phys. Lett.*, **55**, 1391 (1989).

23. S. Albin and L. Watkins, *IEEE Electron Dev. Lett.*, **11**, 159 (1990).
24. Y. Muto, T.Sugino, J. Shirafuji and K. Kobashi, *Appl. Phys. Lett.*, **59**, 843 (1991).
25. H. D. Hunn, N. R. Parikh, and K. Das, unpublished work, (1991).
26. S.M. Sze, 'Physics of Semiconduction Devices', Wiley-Interescience publication, New York (1981).
27. G. Braunstein, and R. Kalish, *J. Appl. Phys.* **54**, 2106 (1983).
28. N. Fujimori, T. Imai, and A. Doi, *Vacuum*, **36**, 99 (1986).
29. M. W. Geis, in 'Diamond, Silicon Carbide and Related Wide Bandgap Semiconductors', eds. J. T. Glass, R. Messier, and N. Fujimori, *Mat. Res. Soc. Symp. Proc.* **162**, 15 (1990).
30. K. Nishimura, K. Das, and J. T. Glass, *J. Appl. Phys.*, **69**, 3142 (1991).

Figure Captions

Fig. 1. A flow chart of the processing steps involved in the fabrication of metal contacts on polycrystalline and homoepitaxial diamond films.

Fig. 2. Cross-sectional diagram of contact structure on diamond film, (a) without dielectric layer and (b) with dielectric layer.

Fig. 3. Current-voltage characteristics of Al contacts on polycrystalline diamond film (0.8 ppm), (a) direct metallization and (b) with interfacial SiO_2.

Fig. 4. Current -voltage characteristics of Au contacts on homoepitaxial diamond film, (a) direct metallization and (b) with interfacial SiO_2.

Fig. 5. Current-voltage characteristic of Al contacts on annealed diamond film (4.0 ppm).

Fig. 6. Current-voltage characteristic of Al contacts on annealed diamond film (20.0 ppm), (a) direct metallization and (b) with interfacial SiO_2.

Fig. 7. Current-voltage characteristic of Al contacts on annealed diamond film (20.0 ppm) with interfacial SiO_2 at (a) RT, (b) 50°C, (c) 99°C, (d) 149°C, (e) 198°C and (f) 248°C.

FIG. 1

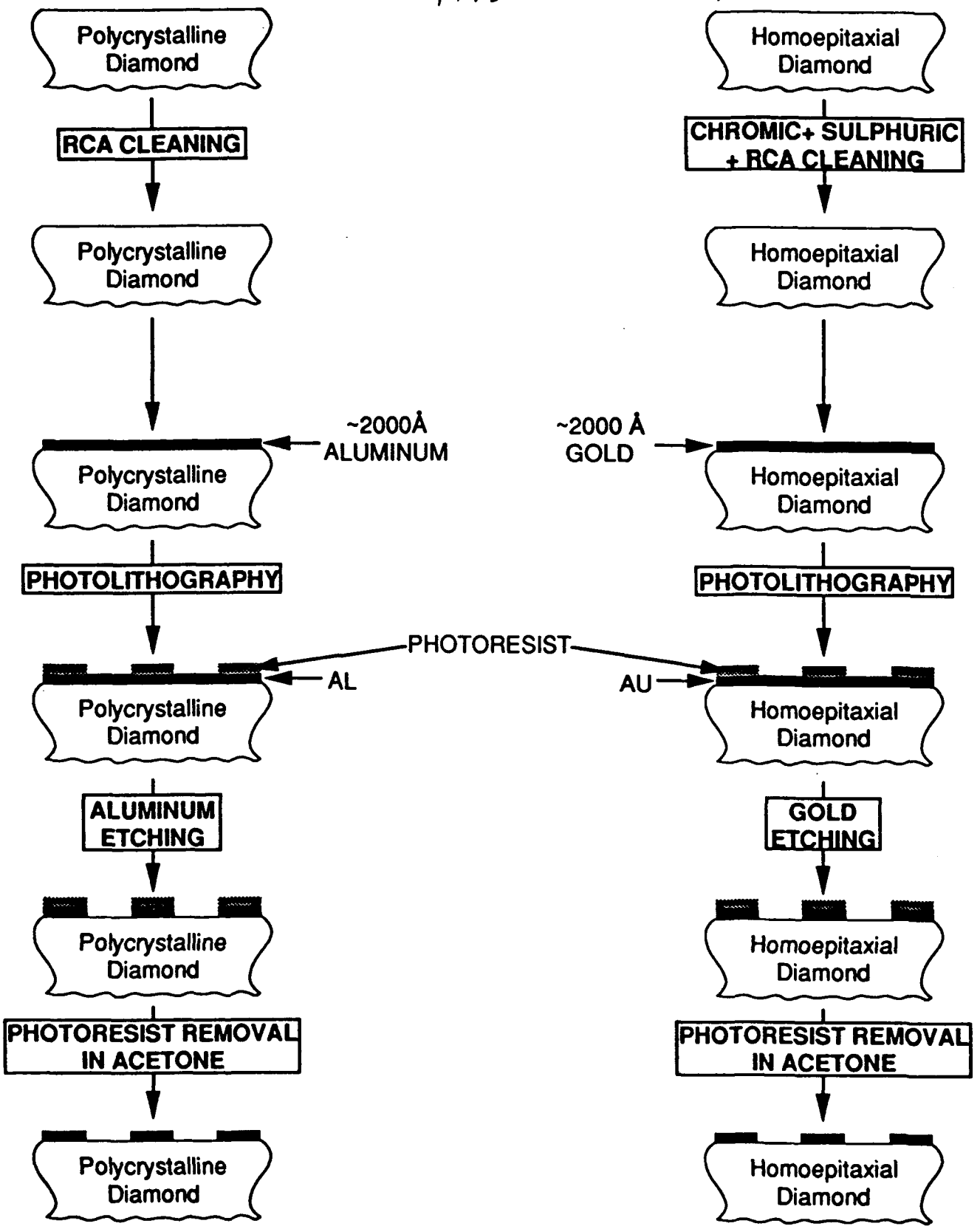
Polycrystalline Diamond
RCA CLEANING
Polycrystalline Diamond
~2000Å ALUMINUM
Polycrystalline Diamond
PHOTOLITHOGRAPHY
PHOTORESIST
AL
Polycrystalline Diamond
ALUMINUM ETCHING
Polycrystalline Diamond
PHOTORESIST REMOVAL IN ACETONE
Polycrystalline Diamond
Homoepitaxial Diamond
CHROMIC+ SULPHURIC + RCA CLEANING
Homoepitaxial Diamond
~2000 Å GOLD
Homoepitaxial Diamond
PHOTOLITHOGRAPHY
AU
Homoepitaxial Diamond
GOLD ETCHING
Homoepitaxial Diamond
PHOTORESIST REMOVAL IN ACETONE
Homoepitaxial Diamond

Table I. Summary of results obtained from initial experiments on polycrystalline diamond films

Sample no.	B/C ratio in gas phase (ppm)	Contact metal	I-V characteristic
2-124 (As-deposited)	0.8	Al	Nearly ohmic
2-130 (As-deposited)	2.0	Al	Poor rectification
2-137 (As-deposited)	3.2	Al	Improved rectification
2-128 (As-deposited)	4.0	Al	Good rectification (<1nA reverse leakage at 5V, ~30V breakdown voltage)
2-124, 2-130, 2-137, 2-128 (Annealed)	0.8, 2.0, 3.2, 4.0	Al	High-resistivity nearly ohmic

FIG. 2

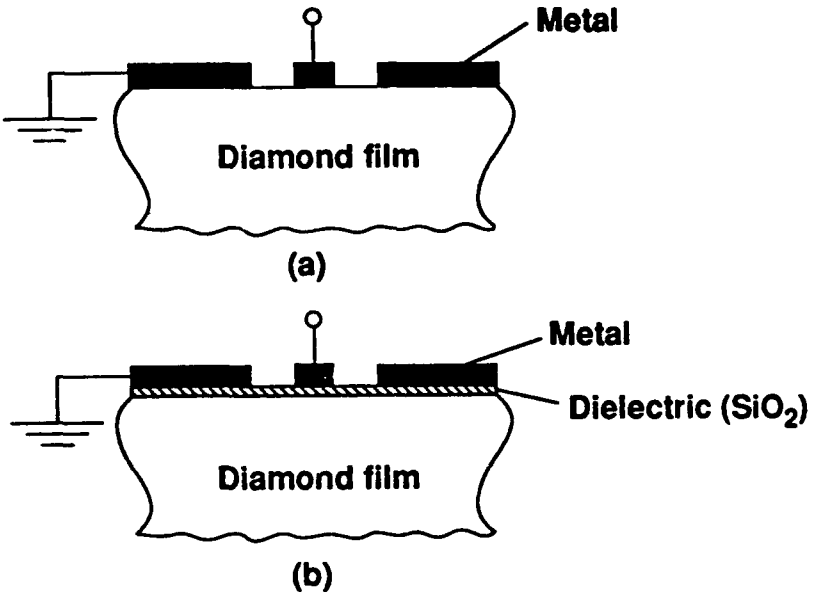

FIG. 3

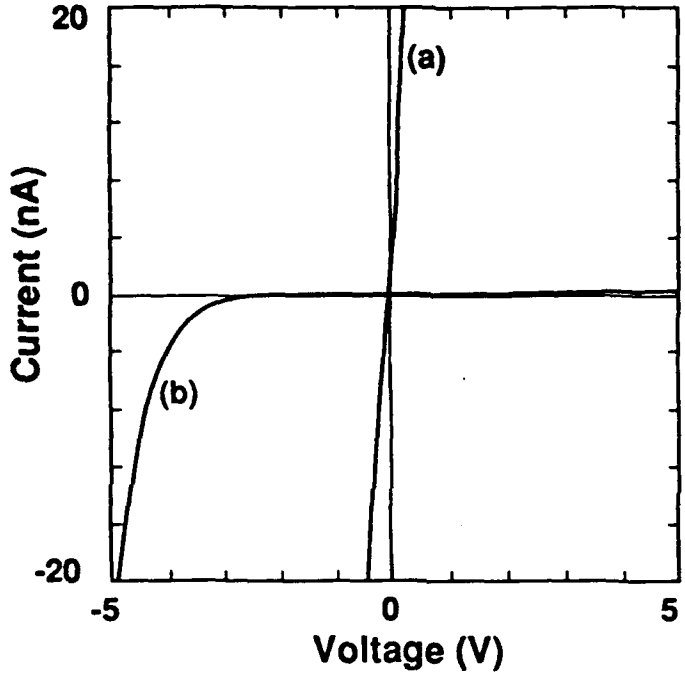

FIG. 4

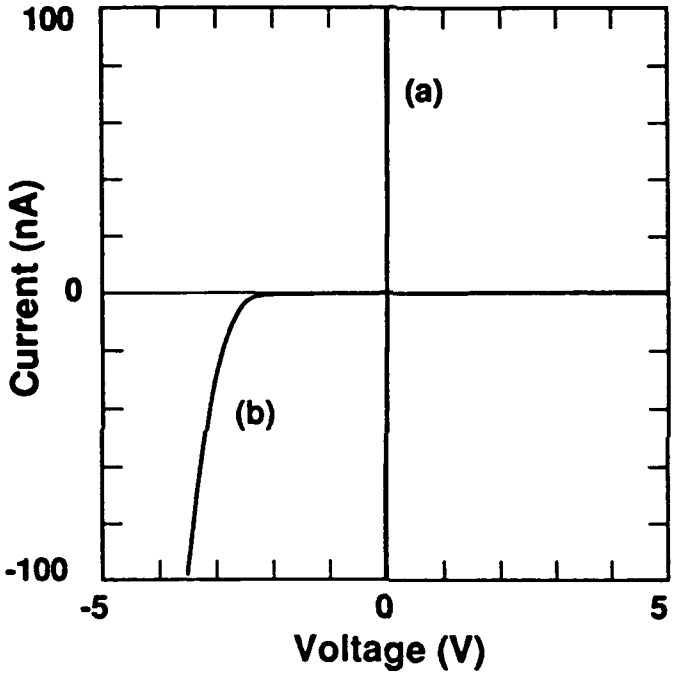

FIG. 5

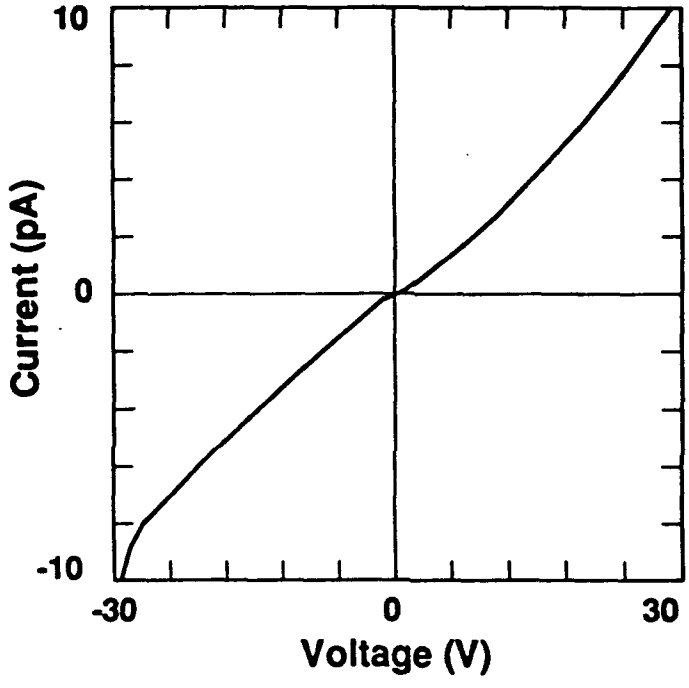

FIG. 6

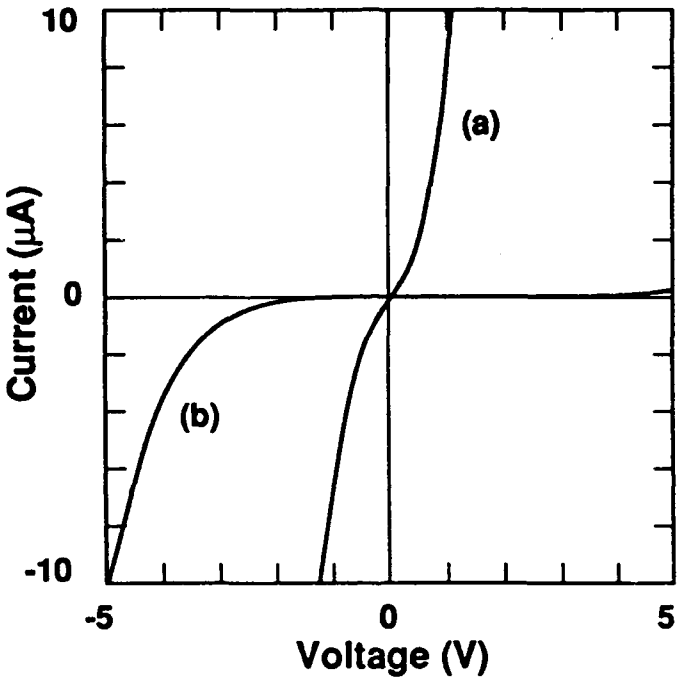

FIG. 7

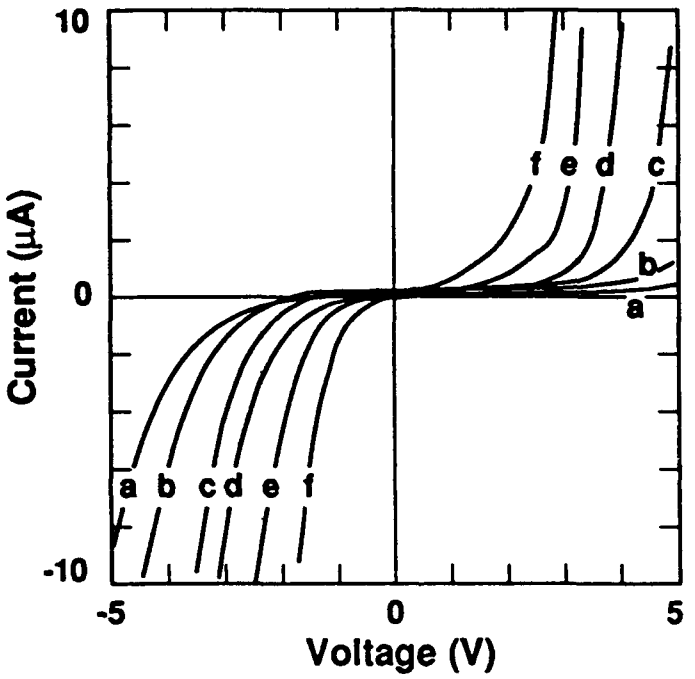

Table II. Summary of results obtained from the study of the effect of thin interfacial SiO_2 film on metal contacts to boron doped diamond films

Sample no.	B/C ratio in gas phase (ppm)	~20Å SiO_2 interfacial layer	Contact metal	I-V characteristic
As-deposited films				
2-124 (control)	0.8	No	Al	Nearly ohmic
RTI C* (control)	-	No	Au	Nearly ohmic
2-124 (test)	0.8	Yes	Al	Good rectification (<1nA reverse leakage at 5 V, ~ 7 V breakdown)
RTI C* (test)	-	Yes	Au	Good rectification (<1nA reverse leakage at 5 V, ~ 7 V breakdown)
Heat treated films				
2-158 (control)	20	No	Al	Nearly ohmic
2-158 (test)	20	Yes	Al	Good rectification (~334 nA reverse leakage at 5V, ~6 V breakdown)

* Homoepitaxial diamond film grown on natural diamond substrate. The other sample numbers correspond to polycrystalline diamond films grown on silicon substrate.

Materials Research Society Symposium Proceedings, Volume 202 (1990).

GROWTH AND CHARACTERIZATION OF HETEROEPITAXIAL NICKEL FILMS ON DIAMOND SUBSTRATES

T.P. HUMPHREYS *, HYEONGTAG JEON *, R.J. NEMANICH*, J.B. POSTHILL**, R.A. RUDDER**, D.P. MALTA**, G.C. HUDSON**, R.J. MARKUNAS**, J.D. HUNN*** and N.R. PARIKH***

* Department of Physics, North Carolina State University, Raleigh, North Carolina 27695-8202.

** Research Triangle Institute, Research Triangle Park, North Carolina 27709-2194.

*** Department of Physics and Astronomy, University of North Carolina, Chapel Hill, North Carolina 27599-3255.

ABSTRACT

In the present study epitaxial Ni(001) films have been grown on natural C(001) substrates (type Ia and IIa) and homoepitaxial C(001) films. Two deposition techniques including electron-beam evaporation of Ni in a molecular beam epitaxy (MBE) system and evaporation of Ni from a resistively heated tungsten filament have been employed. As evidenced by scanning electron microscopy (SEM), the Ni films deposited by electron-beam evaporation were found to replicate the very fine, unidirectional scratches present on the as polished C(001) substrates. Indeed, the coverage and uniformity of the deposited films would imply a two-dimensional (2-D) growth mode. In comparison, the thermal evaporation of Ni on C(001) substrates results in a highly textured and faceted surface morphology indicative of three-dimensional (3-D) nucleation and growth. Moreover, Rutherford backscattering/channeling measurements have demonstrated that the Ni(001) films deposited by electron-beam evaporation are of superior crystalline quality. Differences in the observed microstructure and apparent growth modes of the epitaxial Ni(001) films have been attributed to the presence of oxygen incorporation in those layers deposited by thermal evaporation.

INTRODUCTION

There is at present a significant scientific and technological interest in the growth and use of diamond thin films for high temperature-resistant and radiation-hard electronic device applications [1]. Indeed, it is evident that the fabrication of metal contacts to diamond will play an important role in the development of diamond-based device technologies. Moreover, it is envisaged that an epitaxial metal contact to diamond could find utility in specific device structures and applications. For instance, an epitaxial metal layer could potentially be used in the fabrication of a metal base and/or permeable base bipolar transistor. At present Ni is considered as a suitable choice since both diamond and Ni are face-centered cubic and Ni has a near-lattice match to diamond(a_o(dia) = 3.5668 Å, a_o(Ni) = 3.5238 Å, lattice mismatch ~ -1.2%). For this reason Ni has also been investigated as a potential substrate for the nucleation of heteroepitaxial diamond growth by chemical vapor deposition (CVD) processes [2]. However, this approach has to date proved unsuccessful, although epitaxial (0001) graphite has been grown on Ni(111) [3]. The difficulty experienced to date in nucleating diamond on nickel may find utility by patterning an epitaxial Ni overlayer on diamond single crystal for subsequent selective-area diamond deposition and possible epitaxial lateral overgrowth (ELO) [4].

In this paper we present a comparative study pertaining to the growth of epitaxial Ni(001) films on C(001) substrates using electron-beam and thermal evaporation growth techniques.

EXPERIMENTAL PROCEDURE

Several commercially supplied (D. Drukker & ZN.N.V.) type Ia and type IIa, natural C(001) substrates were chemically cleaned using various concentrated acids and standard RCA cleaning procedures [5]. Homoepitaxial C(001) films of typically ~750 nm thickness were grown

on the chemically clean type IIa C(001) substrates using low pressure rf-plasma-enhanced chemical vapor deposition (PECVD). Prior to Ni deposition, the substrates were annealed by heating to 1200°C for 10 minutes in UHV (<8 x 10^{-9} Torr) to thermally desorb possible physi-adsorbed gas contaminates. For those Ni films deposited by tungsten filament evaporation, *in-situ* low energy electron diffraction (LEED) and Auger electron spectroscopy (AES) techniques were used to examine the corresponding surface structure and interface chemistry of the Ni layers after each evaporation step. Ni films were deposited on type IIa, natural C(001) substrates and homoepitaxial C(001) films at a temperature of 500°C with an evaporation rate of ~0.2 - 0.4 nm/min as determined by a quartz crystal monitor. The pressure during deposition was typically better than 1 x 10^{-8} Torr. The final thickness of the Ni films were ~14 - 24 nm as determined by profilometer measurements. In comparison, the Ni films deposited by electron-beam evaporation in a molecular beam epitaxy (MBE) system were grown at 500°C with an enhanced deposited rate of ~18 nm/min. The pressure in the MBE chamber was typically <10^{-9} Torr during growth. The thickness of the corresponding Ni films were typically ~50 nm.

The grown layers were examined by scanning electron microscopy (SEM), Rutherford backscattering (RBS)/channeling of 1.6 and 2.0 MeV He^+ ions.

RESULTS AND DISCUSSION

Shown in Fig. 1 is an unreconstructed (1x1) LEED pattern obtained from the chemically clean type IIa, natural C(001) substrates. A similar surface structure was observed on subsequent annealing of the substrates to 1200°C in UHV and cooling to room temperature for LEED analysis. In contrast, a (2x1) surface reconstructed pattern was observed from the homoepitaxial C(001) films following high temperature annealing. As reported in the literature, the occurrence of a (2x1) surface reconstruction may be related to the microstructural quality and surface topography of the C(001) surfaces [6]. In particular, SEM inspection of the polished C(001) substrates has revealed the presence of scratches which were visibly absence from the surface of the homoepitaxial C(001) films. Therefore, it is reasonable to conclude that the presence of these microscopic surface imperfections on the natural C(001) substrates may inhibit the surface reconstruction process.

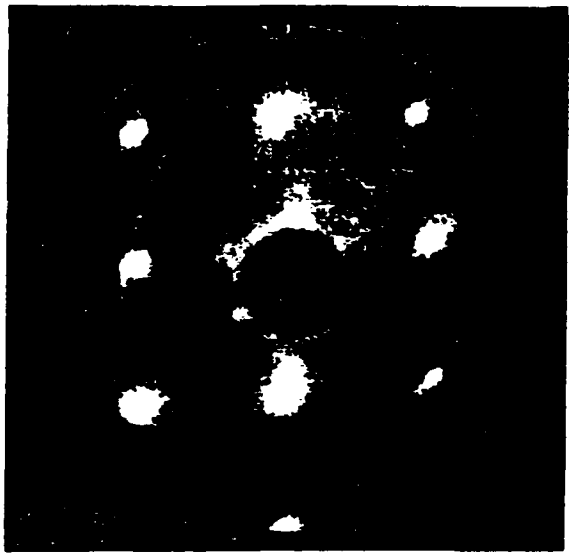

Fig. 1 Unreconstructed (1x1) LEED pattern obtained from the chemically clean C(001) surface, E_p = 135 eV.

The crystalline quality of the C(001) homoepitaxial films grown on type IIa, natural C(001) substrates have been examined using Micro-Raman spectroscopy. In particular, the measured full-width-half-maximum (FWHM) of the 1332 cm^{-1} diamond line for the homoepitaxial films is 2.2 cm^{-1} compared to 2.3 cm^{-1} obtained from the natural C(001) substrates. Corresponding LEED patterns of the Ni films deposited by evaporation from a tungsten filament on the homoepitaxial and natural C(001) substrates are shown in Fig. 2(a) and (b), respectively. The superposition of a p(2x1) and p(1x2) nickel structure is clearly evident for those films deposited on both (1x1) unreconstructed and (2x1) reconstructed homoepitaxial C(001) surfaces. Also observed were extra beams in the diffraction pattern which moved between the integral-order beams in both the <100> and <110> directions as the primary beam energy was changed. These features can be clearly seen in the bottom left hand corner of Fig. 2(a). In contrast, the formation of a p(2x2) nickel structure has been observed on type IIa, natural C(001) substrates which exhibit a clean (1x1) unreconstructed surface structure prior to deposition. Extra features in the LEED pattern which change with beam energy have also been observed in these layers. The presence of the extra diffraction beams have been attributed to the formation of a faceted surface morphology characteristic of the early nucleation of epitaxial Ni(001) islands of preferred orientation on the

C(001) surface. Indeed, AES measurements of the deposited Ni films have established the presence of Ni islands for films of <7 nm thickness. However, with increased Ni coverage there is an apparent coalescence of the individual islands to form a continuous layer.

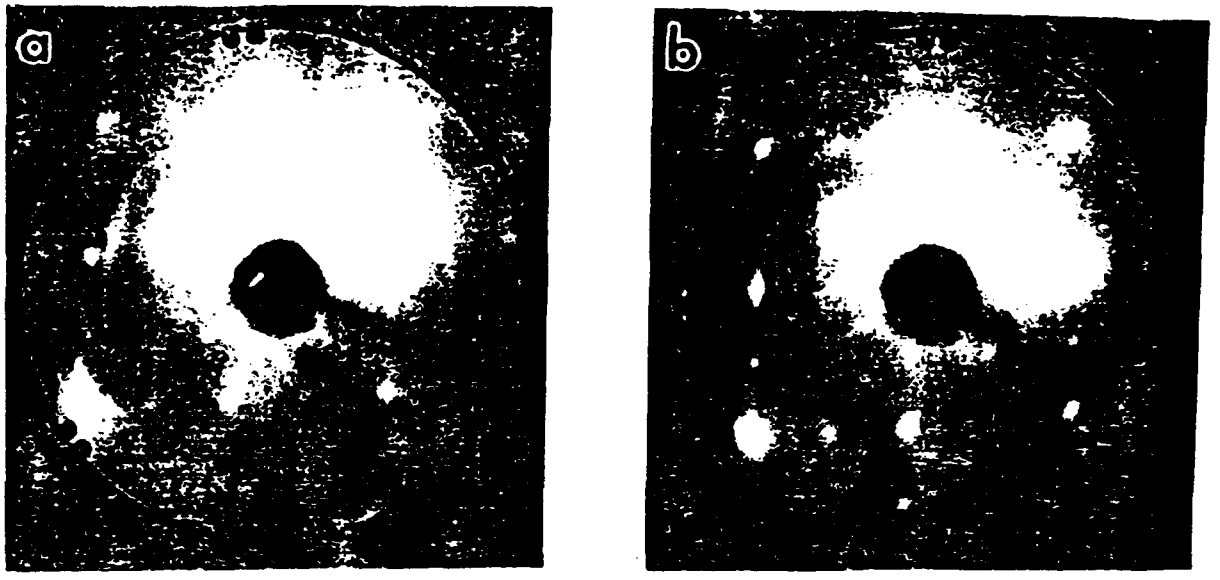

Fig. 2 LEED patterns showing (a) superposition of a p(2x1) and p(1x2) nickel structure and (b) p(2x2) nickel structure for Ni films deposited on homoepitaxial and type IIa, natural C(001) substrates, respectively, E_p = 135 eV.

The SEM micrographs pertaining to the surface morphology of the epitaxial Ni films deposited by tungsten filament evaporation on homoepitaxial C(001) and type IIa, natural C(001) substrates are shown in Fig. 3(a) and (b), respectively. The thickness of the Ni films were typically ~24 nm and ~14 nm, respectively. Clearly, both films exhibit a textured and faceted surface morphology indicative of initial island nucleation and partial coalescence during growth.

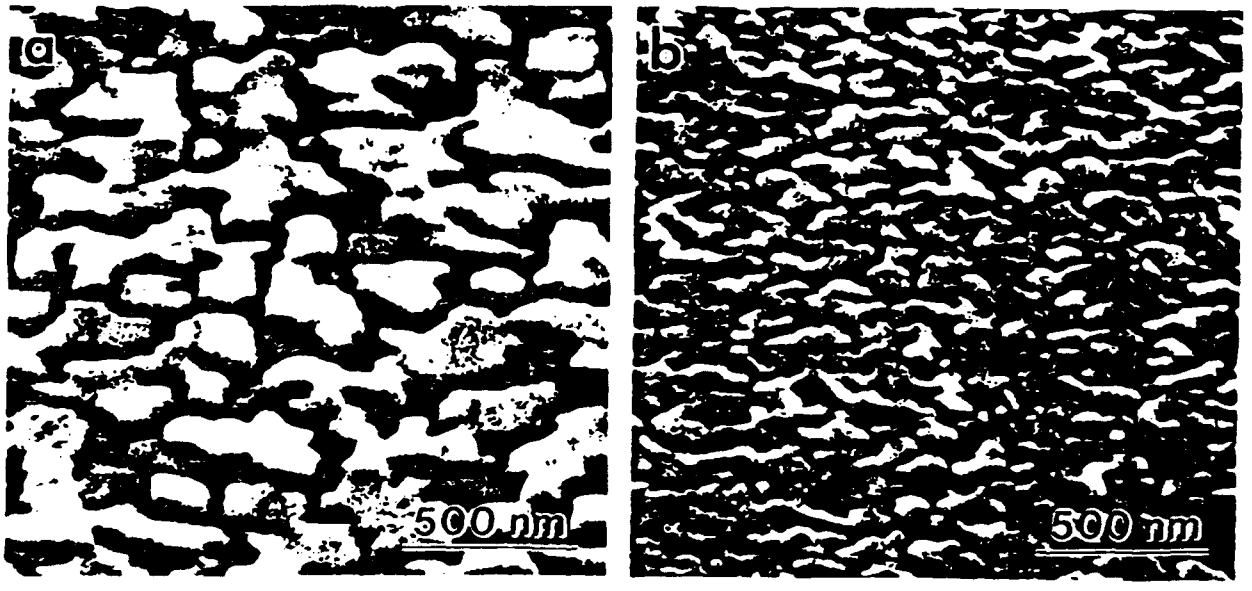

Fig. 3 SEM micrographs of the surface morphology of Ni(001) epitaxial films grown on (a) homoepitaxial C(001) films and (b) type IIa, natural C(001).

The epitaxial quality of the deposited Ni films has been analyzed by RBS/channeling using 1.6 MeV He^+ ions (Fig. 4). The presence of a <001> axial channeling direction clearly indicates that Ni(001) epitaxy has been achieved on C(001). Moreover, the degree of surface roughness and non-uniformity of the Ni films is clearly evidenced by the presence of steps in the backscattering yields of the aligned <001> spectrum for both samples. For instance, the presence of a step at 525 keV in the aligned spectrum of Fig. 4(a) is a consequence of non-uniform Ni coverage indicative of three-dimensional (3-D) film growth. A quantitative measure of the crystalline quality of the Ni

epitaxial layers is given by χ_{Ni}, which is the ratio of the aligned and nonaligned integrated, backscattering ion yields for the Ni layers. The determined values of χ_{Ni} are 33% and 26% for the corresponding epitaxial Ni films deposited on type IIa, natural and homoepitaxial C(001) substrates, respectively. However, it is apparent from RBS analysis that the microstructural quality of the Ni(001) films is degraded by the present of oxygen impurities. Indeed, the presence of oxygen at 730 keV in the Ni films is clearly evident in both RBS spectra. The incorporation of oxygen in the Ni films is a consequence of the relatively slow growth rate and the subsequent degradation of the chamber vacuum as a result of tungsten filament outgasing and/or desorption of oxygen from the chamber walls during Ni deposition. Furthermore, it is believed that the observed 3-D nucleation of the Ni (001) epitaxial films on C(001) is determined by these impurity considerations.

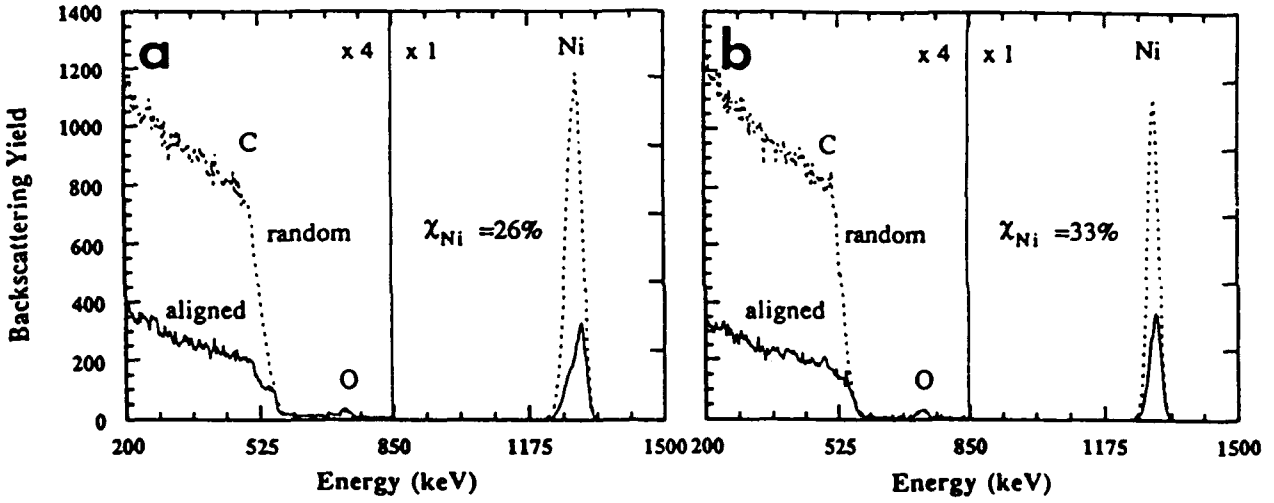

Fig. 4 RBS random (dashed line) and aligned (solid line) spectra for Ni (001) films deposited by tungsten filament evaporation on (a) homoepitaxial C(001) films and (b) type IIa, natural C(001) substrates.

In a comparative study of Ni films deposited by electron-beam evaporation on type Ia, natural C(001) substrates, SEM examination has shown that the Ni films replicate the very fine, unidirectional scratches which are present on the as-polished C(001) substrates (Fig. 5).

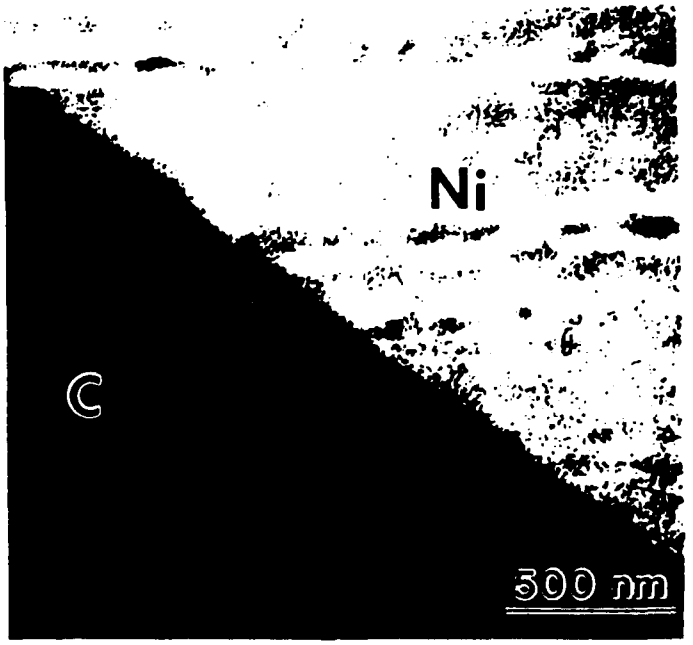

Fig. 5 SEM micrograph of the surface morphology of electron-beam deposited Ni(001) films on type Ia, C(001) substrates.

Corresponding patterned regions pertaining to the Ni epilayer (bright) and the exposed diamond substrate (dark) are clearly shown. Since the Ni layers have been patterned for subsequent selective-area epitaxial studies of diamond, corresponding regions pertaining to the Ni epilayer and the exposed diamond substrate are clearly visible. Evidently, the scratches on the surface of the single crystal diamond are the result of damage incurred by mechanical polishing of the C(001) substrates [7,8]. Moreover, under the deposition conditions employed, the coverage and uniformity of the deposited Ni films would imply a two-dimensional (2-D) growth mode for the nucleation of Ni on C(001). Fig. 6 shows RBS/channeling results obtained using 2.0 MeV He^+ ions which indicate that epitaxial Ni(001) films have been achieved. The determined value of χ_{Ni}~18% is indicative of the superior microstructural quality of the epitaxial Ni(001) layers. Moreover, it is apparent that RBS analysis did not reveal the presence of oxygen incorporation in the Ni films deposited by electron-beam evaporation.

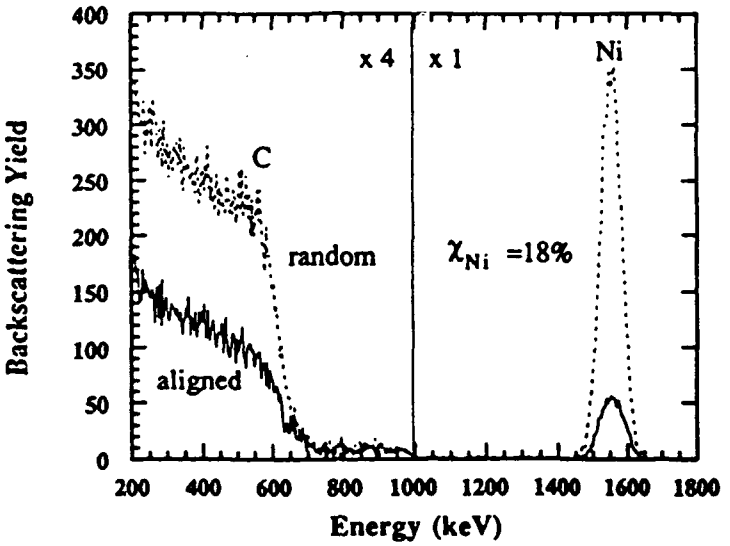

Fig. 6 RBS/channeling spectra for Ni(001) film growth on type Ia, natural C(001) by electron-beam evaporation.

It is also interesting to note that the crystalline quality of the commercially-supplied natural diamond substrates is not consistent as indicated by variations in RBS/channeling backscattered yields [9]. It would therefore appear that utilizing diamond epitaxial films grown by plasma-enhanced chemical vapor deposition (PECVD), which are smoother and may be less defective, represents another potential means to obtain topographically smooth and microstructural upgraded epitaxial metal films on diamond.

CONCLUSIONS

In summary, epitaxial Ni(001) films have been grown on C(001) substrates using thermal and electron-beam evaporation techniques. It has been demonstrated that the thermal evaporation of Ni from a tungsten wire filament on C(001) substrates results in a highly textured and faceted surface morphology indicative of three-dimensional nucleation and growth. In contrast, the Ni epitaxial films deposited by electron-beam evaporation on C(001) substrates has a surface morphology that mimics the topography of the initial, as-polished single crystal C(001) substrate. Differences in the observed microstructure and apparent growth modes of the epitaxial Ni(001) films have been attributed to the presence of oxygen incorporation in those layers deposited by thermal evaporation. Suggestions for future studies to optimize the epitaxial growth of metal films on diamond have been proposed.

ACKNOWLEDGEMENTS

TPH, HJ and RJN gratefully acknowledge partial support from the National Science Foundation (Contract No. DMR-8717816) and also the Office of Naval Research (Contract No.

N00014-90-J-1707). JBP, RAR, DPM, GCH and RJM gratefully acknowledge support from the Strategic Defence Initiative Organization / Innovative Science and Technology through the Office of Naval Research (Contract No. N00014-86-C-0460). JDH and NRP acknowledge the Office of Naval Research (Contract No. N00014-89-K-0243) for support. We also thank Dr. R.E. Thomas (RTI) for many helpful discussions.

REFERENCES

1. M.W. Geis, N.N. Efreman and G.D. Pathman, J. Vac. Sci. Tecnnol. A 6, 1953 (1988).

2. D.N. Belton and S.J. Schmieg, J. Appl. Phys. 66, 4223 (1989).

3. R.A. Rudder, J.B. Posthill,G.C. Hudson, M.J. Mantini and R.J. Markunas, SPIE, 969, 72 (1988).

4. R.A. Rudder, J.B. Posthill, G.C. Hudson, D. Malta, R.E. Thomas, R.J. Markunas, T.P. Humphreys and R.J. Nemanich. presented at the 2nd New Diamond Science and Technology Conference ICNDST-2, Washington, DC (1990).

5. Chemical cleaning of diamond using concentrated acids includes the following processing steps: (1) boiling CrO_3:H_2SO_4 for 15 mins, (2) boiling HCl:HNO_3 for 15 mins, (3) HF:$10H_2O$ for 15 mins, (5) DI rinse and N_2 dry.

6. P.G. Lurie and J. M. Wilson, Surface Science 65, 453 (1977).

7. M.J. Paisley and R.F. Davis, 1990, private communication of unpublished results, North Carolina State University, Raleigh.

8. R.A. Rudder, G.C. Hudson, D.P. Malta, J.B. Posthill and R.J. Markunas, (1989), unpublished results.

9. G.S. Sandu, N.R. Parikh and M.L. Swanson, 1989, private communication of unpublished results, University of North Carolina, Chapel Hill.

Cathodoluminescence from diamond films grown by plasma-enhanced chemical vapor deposition in dilute CO/H_2, CF_4/H_2, and CH_4/H_2 mixtures

R. J. Graham
Center for Solid State Science, Arizona State University, Tempe, Arizona 85287-1704

J. B. Posthill, R. A. Rudder, and R. J. Markunas
Research Triangle Institute, Research Triangle Park, North Carolina 27709-2194

(Received 19 June 1991; accepted for publication 30 August 1991)

Diamond films grown by rf plasma-enhanced chemical vapor deposition in dilute CO, CF_4, and CH_4 (diluent H_2) mixtures have been examined by cathodoluminescence (CL) in a transmission electron microscope to assess the incorporation of optically active impurities and defects. The details of the CL spectra are found to be dependent on the different gas mixtures and are correlated with the different film microstructures. Dislocation-related band *A* CL due to closely spaced donor-acceptor (*D-A*) pairs was observed from both the CO and CH_4-grown films, but was absent in the CF_4-grown material. Band *A* CL due to widely separated (*D-A*) pairs was seen in all samples but was especially dominant in the CF_4-grown film. Emission due to a di-Si interstitial impurity was observed in CO- and CF_4-grown films but was absent in the CH_4-grown material.

The chemical vapor deposition (CVD) of diamond films is currently receiving much attention.[1] At present, attempts at heteroepitaxial growth, usually on Si substrates, have resulted in heterogeneous polycrystalline films containing many defects and impurities. One of the goals of such growth methods must be the control of the formation of these inhomogeneities, especially if potential optical and electronic applications are to be realized. The aim of this study was to investigate how the use of dilute CO and CF_4, rather than the usual CH_4, in the CVD process might affect the incorporation of impurities or defects and the electronic states associated with them. The analytical technique used was spectrally resolved cathodoluminescence (CL) performed in a transmission electron microscope (TEM) which allows a simultaneous correlation of CL emission with specimen microstructure.

Three polycrystalline diamond films, 1–2 μm thick, were grown on Si(100) substrates by rf plasma-enhanced CVD (PECVD) using the following gas compositions and growth conditions: (1) 1% CH_4, 99% H_2, pressure = 5.0 Torr, temperature ~650 °C; (2) 2% CO, 98% H_2, pressure = 3.0 Torr, temperature ~630 °C; (3) 8% CF_4, 92% H_2, pressure = 5.0 Torr, temperature ~820 °C. Details of the growth of this last film are described in another publication.[2] An additional film was grown using 2% CO/98% H_2 at a temperature of ~725 °C on *R*-plane ($10\bar{1}2$) sapphire to examine the effect of the substrate on the presence of impurities and defects. The substrates for the CO- and CH_4-grown films were scratched with diamond paste prior to deposition whereas the CF_4-grown film was grown on an unscratched and untreated Si substrate. Specimens were prepared for TEM by dimple polishing and milling with Ar^+ ions. Detection of CL was performed in TEM,[3] which also allowed the microstructure to be observed, using a 120 keV electron beam and liquid-nitrogen-cooled specimen stage.

Figure 1 shows CL spectra in the 300–900 nm range acquired from 15μm-diam regions from all four films. The CH_4-grown film gave a spectrum which consists of a broad peak at 428±1 nm (2.90±0.01 eV) superimposed on an even broader band with a maximum around 470±1 nm (2.637±0.005 eV). The CF_4-grown film gave a broad band centered at 540±1 nm (2.295±0.004 eV), and a small peak at 737.8±0.5 nm (1.680±0.001 eV). Spectra from both CO-grown films exhibit a number of similar spectral features as summarized in Table I.

The CH_4-grown material consists of a perforated film containing 1–2 μm-sized grains, many with well-developed growth habits and microtwins. The grains often contain a high density of other small defects, possibly stacking faults or inclusions of nondiamond carbon, and associated static

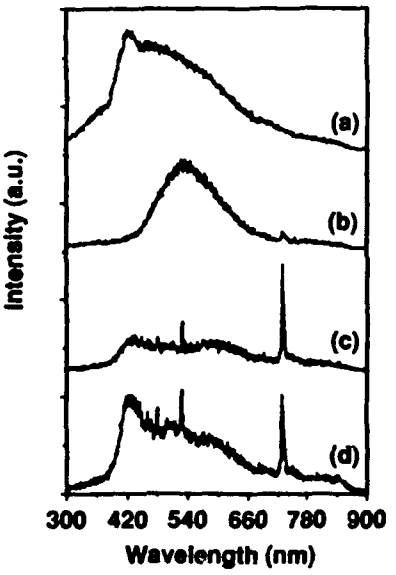

FIG. 1. CL spectra from polycrystalline diamond films: (a) 1% CH_4, 99% H_2, pressure = 5.0 Torr, temperature ~650 °C on Si(100); (b) 8% CF_4, 92% H_2, pressure = 5.0 Torr, temperature ~820 °C on Si(100); (c) 2% CO, 98% H_2, pressure = 3.0 Torr, temperature ~630 °C on Si(100); (d) 2% CO, 98% H_2, pressure = 3.0 Torr, temperature ~725 °C on *R*-plane ($10\bar{1}2$) sapphire.

 0003-6951/91/442463-03$02.00

TABLE I. CL spectral features observed in dilute CO CVD-grown diamond on sapphire and Si substrates.

2% CO/98% H_2 sapphire substrate	2% CO/98% H_2 Si substrate
431 ± 1 nm (2.88 ± 0.01 eV) band	436 ± nm (2.84 ± 0.01 eV) band
464 ± 1 nm (2.671 ± 0.006 eV) peak	not obs.
484 ± 1 nm (2.561 ± 0.005 eV) peak	484 ± 1 nm (2.561 ± 0.005 eV) peak
503 ± 1 nm (2.464 ± 0.005 eV) peak	not obs.
534 ± 1 nm (2.321 ± 0.004 eV) peak	534 ± 1 nm (2.321 ± 0.004 eV) peak
586 ± 1 nm (2.115 ± 0.004 eV) shoulder	607 ± 1 nm (2.042 ± 0.003 eV) band
737.8 ± 0.5 nm (1.680 ± 0.001 eV) peak	737.8 ± 0.5 nm (1.680 ± 0.001 eV) peak

disorder, as also evidenced by significant diffuse scatter in convergent beam electron diffraction (CBED) patterns observed from individual crystals. The CF_4-grown film is continuous with a smaller grain size (0.1–0.3 μm). Although many grains are heavily microtwinned, inclusions are generally absent. Some grains are defect-free and CBED indicates a low degree of static disorder. The microstructure of the CO-grown films is very substrate dependent. On Si the film is continuous consisting of very defective 0.1–0.5 μm-sized grains whereas on sapphire highly defective connected nodules (1 μm diameter) form a perforated film. The weak CL intensity and small grain size in some of these films precluded a detailed correlation of microstructure with CL as has been demonstrated previously in CVD-grown diamond.[4] However, a general correlation with overall film structure is described below.

The emissions listed in Table I are identified as follows. The bands at 431 and 436 nm are known as band *A* and are due to closely spaced donor-acceptor (*D-A*) pairs. This emission is normally associated with natural, rather than synthetic, diamonds[5] but has often been observed from CVD-grown material[6–11] and has been correlated with dislocations.[4] The bands at 586 and 607 are probably also band *A* but are due to widely separated *D-A* pairs and are more typical of synthetic diamond, although the peak of the band at 607 nm is at the low-energy limit for band *A*. The intense peak at 737.8 nm is the same, within experimental error, as that observed previously in CVD-grown diamond and is due to di-Si interstitial impurities.[4,11–13] The origins of the emissions at 464, 484, and 503 nm are unknown although they have been observed previously in dilute CH_4 CVD-grown diamond.[8] The 534 nm peak has also been observed in CH_4-grown material and may be due to a nitrogen-vacancy-related complex.[8,9,12] For the CH_4-grown film, the 428 nm band is again due to closely spaced *D-A* pairs. The very broad band on which this is superimposed is probably also due to *D-A* pairs although it has an uncommonly large full width at half maximum (FWHM) of over 1100 meV and peaks at a higher energy than is usually encountered in *D-A* emission. For the CF_4-grown material, the band at 540 nm is typical of band *A* emission from widely separated *D-A* pairs in synthetic diamond. The small FWHM (7 meV) of the small peak at 737.8 nm confirms that this is again due to Si interstitials.

The *D-A* pair bands are due to nitrogen and boron impurities which presumably exist as contaminants of the source gases, vacuum system, and reactor components. Secondary-ion mass spectrometry (SIMS) of the films confirms the presence of these impurities. The interstitial Si impurity is believed to originate from the etching of either the Si substrate or silica reactor walls by the plasma. No new CL emissions from the CO- or CF_4-grown films were observed, suggesting that neither O or F are present as optically active impurities, although certainly F is incorporated in the CF_4-grown film during growth, as revealed by SIMS. In natural diamond, O has been found to exist at the 30–90 ppm level,[14] as elemental or mineralogical inclusions or possibly as a substitutional or interstitial impurity.[15] No optical activity has been documented which is consistent with our observations. No information about the presence of F in diamond was found in the literature.

The details of the CL emissions and film microstructure are, however, dependent on the growth gases and we now attempt to correlate the two. Dealing first with band *A* luminescence, all specimens, except the CF_4-grown films, show emission at around 430 nm due to closely spaced *D-A* pairs. Previous studies, which show that this emission is correlated with dislocations in CVD-grown diamond,[4] suggest that dislocations are present in these films. Potentially, other defects, e.g., stacking faults, nondiamond inclusions, may also allow *D-A* pairs to exist in the closer proximity normally associated with defect-free natural diamonds. This may account for the extremely broad band *A* observed in the CH_4-grown material where such defects in single crystals abound and to a lesser extent the CO-grown film on sapphire. However, if the density of other defects becomes too high resulting in poor crystallinity, increased nonradiative recombination reduces the overall CL intensity, as seen in the CO-grown films. Significantly, the CF_4-grown material was the least defective at a microscopic level, i.e., excluding microtwins, and showed no such band due to closely spaced *D-A* pairs. All films showed some degree of band *A* due to widely separated *D-A* pairs normally seen in synthetic diamond. In the CF_4-grown films this was the only peak of any significant intensity and the slightly higher peak energy, 2.3 eV compared with about 2.1 eV for the CO-grown films, suggests a smaller mean *D-A* pair separation. Faster growth rates have been observed when O is added to dilute CH_4,[14] which might result in *D-A* pairs being incorporated in even more random lattice sites resulting in larger mean *D-A* pair separation and a band *A* peak at lower energy.

The CO- and CF_4-grown films all showed some degree of interstitial di-Si impurity which is believed to originate from etching of Si-containing materials by the plasma in the growth zone. Although absent in the CH_4-grown film

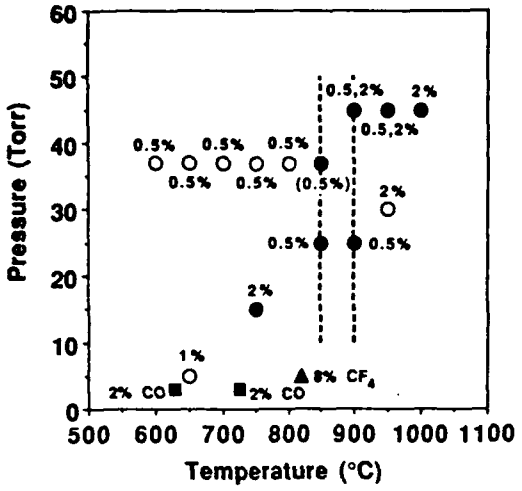

FIG. 2. Incidence of the di-Si interstitial defect, as observed by CL (1.681 eV peak), CVD-grown diamond on Si substrate as a function of growth temperature and pressure with the concentration of CH_4 used indicated; ● = peak observed, ○ = peak not observed, data from Refs. 4, 8–11, 13, and this work. For comparison, films grown using dilute CF_4 and CO (on Si and sapphire) which show the 1.681 eV peak are also represented (▲ = dilute CF_4, ■ = dilute CO). Broken vertical lines indicate range of pressures used for films shown as grown at 25 Torr, since exact pressures were not given. For the data point in parentheses, the peak in the CL spectrum was identified as GR1 due to neutral vacancy defect rather than di-Si (Ref. 9). Similarly, the peak in Ref. 10 was identified as GR1 but subsequently attributed to di-Si by the same workers (Ref. 13).

here, this has been observed in similar material by other workers.[4,11–13] The reason for this probably lies in the details of the growth conditions; previous observations by CL of the di-Si interstitial defect shown graphically in Fig. 2 suggest that it only occurs at higher growth temperatures and pressures and/or CH_4 concentration, although the limited number of data points, the different growth methods and other reactor-dependent variables make such a generalization only tentative. Intense peaks in the CO-grown films, grown under similar conditions to the CH_4-grown material, indicate that CO enhances the etching potency of the plasma resulting in higher levels of di-Si impurity. Conversely, the small size of this peak in the CF_4-grown film shows that little of this impurity has been incorporated as the optically active di-Si interstitial form during growth. This is surprising since CF_4-based plasmas are known to be very reactive; even visible etching of a glass viewport in the reactor occurred during previous runs. In addition, SIMS shows the Si content to be higher in this film than in the CO-grown films. This suggests that Si is also being incorporated as an optically inactive form and so implies that the nature of incorporation of Si depends on the gaseous species used and formed during the CVD growth process.

The source of the Si impurity has also been the subject of recent investigation. The spectra from the CO-grown material on the Si and sapphire substrates show the same basic emissions inspite of large differences in film microstructure. However, relative to band *A* and other emissions, the peak due to the di-Si interstitial defect was much more intense when the substrate was Si, indicating that much of this impurity originates from the substrate. The persistence of this peak when a sapphire substrate is used indicates that at least some of the Si originates from the reactor which contrasts with recent studies by Ruan *et al.*[13] who found that this peak only when a Si substrate was used during growth with dilute CH_4. This could be explained by the apparently enhanced etching properties of the CO-containing plasma as previously discussed. The potential for reactor "memory" due to deposits on the reactor wall from earlier depositions on Si substrates also exists.

In conclusion, use of dilute CO and CF_4 does not introduce any optically active impurity or defect states not previously observed in dilute CH_4-grown CVD diamond. The different gases do, however, result in different film microstructures and concomitant CL spectra. Dislocation-related band *A* CL is observed from CO- and CH_4-grown films but only widely separated *D-A* pairs exist in the CF_4-grown material. The di-Si interstitial impurity was most readily incorporated in CO-grown films, with both the Si substrate and reactor walls believed to be the source. In comparison, the CF_4-grown film contained a higher concentration of Si, but only a small amount as the optically active di-Si form.

We are pleased to thank G. C. Hudson and D. P. Malta for their technical input and helpful discussions. This work was supported by the Facility for High Resolution Electron Microscopy at Arizona State University, supported by NSF Grant No. DMR-89-13384. JBP, RAR, and RJM gratefully acknowledge support of this work by the Strategic Defense Initiative Organization/Innovative Science and Technology through the Office of Naval Research (Contract No. N000014-86-C-0460).

[1] See, for example, "Diamond and Diamond-like Materials," special section of J. Mater. Res. **5**, 2273 (1990).
[2] R. A. Rudder, G. C. Hudson, J. B. Posthill, R. E. Thomas, and R. J. Markunas, Appl. Phys. Lett. **59**, 791 (1991).
[3] S. H. Roberts, Inst. Phys. Conf. Ser. **61**, 51 (1981).
[4] R. J. Graham, T. D. Moustakas, and M. M. Disko, J. Appl. Phys. **69**, 3212 (1991).
[5] P. J. Dean, Phys. Rev. **139**, A588 (1965).
[6] H. Kawarada, K. Nishimura, T. Ito, J-i. Suzuki, K-S. Mar, Y. Yokota, and A. Hiraki, Jpn. J. Appl. Phys. **27**, L683 (1988).
[7] A. T. Collins, M. Kamo, and Y. Sato, J. Phys. **1**, 4029 (1989).
[8] A. T. Collins, M. Kamo, and Y. Sato, J. Phys. **22**, 1402 (1989).
[9] L. H. Robins, L. P. Cook, E. N. Farabaugh, and A. Feldman, Phys. Rev. B **39**, 13367 (1989).
[10] W. D. Partlow, J. Ruan, R. E. Witkowski, W. J. Choyke, and D. S. Knight, J. Appl. Phys. **67**, 7019 (1990).
[11] A. T. Collins, M. Kamo, and Y. Sato, J. Mater. Res. **5**, 2507 (1990).
[12] V. S. Vavilov, A. A. Gippius, A. M. Zaitsev, B. V. Deryagin, B. V. Spitsyn, and A. E. Alenksenko, Sov. Phys. Semicond. **14**, 1078 (1980).
[13] J. Ruan, W. J. Choyke, and W. D. Partlow, Appl. Phys. Lett. **58**, 295 (1991).
[14] H. W. Fesq, D. M. Biddy, C. S. Erasmus, E. J. D. Kable, and J. P. F. Sellschop, in *Physics and Chemistry of the Earth*, edited by L. H. Ahrens, J. B. Dawson, A. R. Duncan, and A. J. Erlank (Pergamon, Oxford, 1975), Vol. 9, p. 817.
[15] J. Walker, Rep. Prog. Phys. **42**, 1605 (1979), and references therein.